Influence Of The Plastic Zone On The Peak Stress Profile At A Round Hole In A Fiber Metal Laminate

Master Of Science Thesis

by

Ahmad Shahier Amierie

Student number: 4152506
Faculty of Aerospace Engineering

TU Delft

Abstract

Fiber Metal Laminates needs to be seen as a construct of its individual constituents rather than a material on which the industry has capitalized on. Therefore, analytical models must be made in order to predict the mechanical behavior of the laminates which would reduce the big test matrix for defining empirical values for design allowables.
An analytical model made to predict the mid-section stress distribution of Fiber Metal Laminate plate with a centre round hole under uni-axial tension. The $\sigma'\varepsilon$-curve of the laminate is defined by the Metal Volume Fraction. Assuming that the elasto-plastic energy of a small strip is equal to the uni-axial imaginary elastic energy, the $\sigma'\varepsilon$-state of these small strips can be calculated. The elastic peak stress profile at the midsection is defined by a decreasing exponential equation with three parameters. The centre of the small strips are the points where the value of interest are determined.
Predicting the net-section stress distribution under elasto-plastic loading is determined iteratively by using the Finite Width Correction Factor as a convergence factor between the applied and net-section load. The analytical model gives quite good and accurate results far into the plastic regime validated by DIC experiments and strain gauges. One of the major findings was that indeed it is possible to have delamination and fiber-bridging beneath the plastic zone, which had implications for determining accurately the Blunt Notch Strength.

Contents

Nomenclature

List of Acronyms

ARALL	Aramid Reinforced Aluminum Laminate
BNS	Blunt Notch Strength
CLT	Classical Laminate Theory
COD	Crack Opening Displacement
DIC	Digital Image Correlation
FEM/A	Finite Element Method/Analysis
FML	Fiber Metal Laminate
GLARE	Glass Laminate Aluminium Reinforced Epoxy
HM	Hagenbeek Model
LEFM	Linear Elastic Fractur Mechanism
LT	Lekhnitskii Theory
MVF	Metal Volume Fraction
OHT	Open Hole Tension
PA	Proposal Alderliesten
SCF	Stress Concentration Factor
SERR	Strain Energy Release Rate
SIF	Stress Intensity Factor
SSCP	Stress-Strain Calculation Program(HM)
SYM	Stress Yield Model
TR	Tresca
VM	Von Mises

List of Symbols

α	Angularity of the Laminate	[-]
γ_{xy}	Shear Strain	[-]
δ_{ij}	Kronicker Delta	[-]
∇^4	Biharmonic Operator	[-]
ϵ^0	In-plane Strain vector	[-]
ε_e	Elastic Strain	[-]
ε_{ep}	Elasto-plastic Strain	[-]
$d\varepsilon_{ij}$	Total Deformation Increment	[-]
$d\varepsilon_{ij}^{el}$	Elastic Strain Increment	[-]
$d\varepsilon_{ij}^{pl}$	Plastic Strain Increment	[-]
ε_{nom}	Nominal/Net Section Strain	[-]
ε_{peak}	Peak Strain	[-]
ϵ_x	Strain in x-direction	[-]
Σ_i	Deviatoric/Volumetric Stress Invariants	[-]
ϵ_y	Strain in y-direction	[-]

θ	Angle around the Hole	[Deg]
κ	Bending/Torsional Strain Vector	[-]
ν_{ii}	Poison Ratio	[-]
ρ	Notch Radius	[mm]
σ_θ	Tangential Stress Distribution	[MPa]
σ_{ep}	Elasto-plastic Stress	[MPa]
σ_{nom}	Nominal/Net Section Stress	[MPa]
σ_{peak}	Peak Stress	[MPa]
σ_x	In Plane Normal Stress	[MPa]
σ_y	In Plane Normal Stress	[MPa]
σ_y	Yield Strength	[MPa]
$\frac{\partial \sigma_y}{\partial x}_{y=0}$	Gradient Of The Peak Stress Profile	[MPa/mm]
τ_{xy}	In Plane Shear Stress	[MPa]
ϕ_i	Holomorphic Function	[-]

A	In-Plane Laminate Stiffness Matrix	[N/mm]
A_e	Imaginary Elastic Area/energy	[J]
A_{ep}	Real Elasto-Plastic Area/Energy from The Stress-Strain curve	[J]
A_{ii}	In Plane Laminate Young's Modulus	[N/mm]
A_k	Effect of Force Resultant on the Stress Field	[-]
a	half Major Axis Ellipse	[mm]
a_{ii}	In Plane Laminate Compliances	[mm/N]
B	In-plane and Out-of-Plane Coupling Matrix	[N]
b	half Minor Axis Ellipse	[mm]
db	Delamination Border	[mm]
D	Laminate Bending Stiffness matrix	[Nmm]
D	Diameter of Hole	[mm]
E_{0°	Single Ply Young's Modulus Prepreg 0° direction	[GPa]
E_{90°	Single Ply Young's Modulus Prepreg 90° direction	[GPa]
E_{FML}	Young's Modulus FML	[GPa]
E_M	Young's Modulus Metal	[GPa]
F_z	Complex Form of the Airy's Stress Function	[-]
G_i	SERR of a Specific Delamination MODE	[J]
G_T	Total SERR	[J]
g_n^k	Disturbed Stress Field	[-]
h_k	Homogeneous Stress Field	[-]
K_ε	Plastic Strain Concentration Factor	[-]
K_σ	Plastic Stress Concentration Factor	[-]
L	Plastic Zone Coutour	[-]
M	Applied Moment Vector on Laminate	[Nmm/mm]
N	Applied Load Vector on Laminate	[N/mm]
dN	Delamination Load Cycle	[-]
P_{FML}	Property of Interest FML	[-]
P_M	Property of Interest Metal	[-]
P_{pre}	Property of Interest Prepreg	[-]
Q	Reduced Stiffness Matrix(Single Ply)	[MPa]
r	Directionality of the Laminate	[-]
r_{pl}^{TR}	Plastic Zone Radius Via TR Yield Criterion	[mm]
r_{pl}^{VM}	Plastic Zone Radius Via VM Yield Criterion	[mm]
S	Compliance Matrix	[m/N]
S_{BN}	Blunt Notch Strength	[MPa]

S_{max}	Gross Stress Applied	[MPa]
S_{nom}	Nominal/Net Section Stress	[MPa]
S_{peak}	Peak Stress	[MPa]
s_i	Complex Roots of the Biharmonic equation	[-]
$\mathbf{T}$	Rotation Matrix	[Deg]
t_{0°	Thickness Prepreg 0° direction	[mm]
t_{90°	Thickness Prepreg 90° direction	[mm]
t_M	Thickness Metal	[mm]
$U(x,y)$	Airy's Stress Function	[-]
u	Displacement in x-direction	[mm]
u_k	Complex Function for determining Displacements	[-]
v	Displacement in y-direction	[mm]
v_k	Complex Function for determining Displacements	[-]
W	Width of Laminate	[mm]
w_{fix}	Minimal/Fixed Width of the Yield Strips	[mm]
w_i	Width of the Yield Strips	[mm]
$X(\theta)$	Applied Load on the Hole Edge	[MPa]
x	x-axis Reference	[mm]
$Y(\theta)$	Applied Load on the Hole Edge	[MPa]
y	y-axis Reference	[mm]
z_k^n	Complex Variable	[-]

List of Figures

Preface

To my dearest daughter,
Nayra

Fiber Metal laminates(FML) are the future building blocks of Aerospace structures. The increase in toughness, strength, stiffness, resilience and many more, while reducing the weight is the main pillar for future design en development. FMLs has it all. In order to make it more competitive compared to other materials and being the main structure for aerospace design application, FMLs needs to be standardized more. FMLs needs to be seen as a structure which is described by its individual constituents and not as a material.
Following the courses of Dr.ir. R.C. Alderliesten on Stress Concentration Factor, elastic and plastic analysis, fatigue and many more on metals and composites, it became clear that combining these materials into a structure would benefit greatly the mechanical design processes. But then the question remained. Why are there almost complete composite or metal airplanes, but no airplane that consist almost completely out of FMLs.
Reading through the history of FMLs, it was because the industry capitalized on a material and put their patents on, such as the ARRALL and Glare FML-type families. In order to have a better future for the FMLs in the Aerospace Industry the gap between work done by academics and implementation done by commercial aerospace industry must be closed. This can be done by considering FMLs as a structure and not as a material and having analytical model predicting the mechanical behavior of FML influenced by their individual constituents.

I'm extremely grateful and like to recognize the invaluable assistance of my supervisor and professor, Dr. Ir. R.C. Alderliesten. A great figure of invaluable knowledge and insight on the matter. Who was always there to help and advice on the research, but also in personal and private matters. Thank you for your guidance.
I would like to express my gratitude towards my wife, parents and brothers who supported me through the ups and downs in this stage of my life. I would like to thank and acknowledge the help of my colleagues and lab assistance for their contributions and assistance that made this research possible.

Executive Summary

The historical problem using Fiber Metal Laminates(FML) in design arose when producing company's such as Dutch chemical company AKZO and others, capitalized on a new material, while research showed that this combination of fiber epoxy layers in conjunction with aluminum plate is a delicate interaction between the different constituents. So it needs to be seen as a structure. Different groups made their own fiber-metal combinations and filed in for patents. This tendency to see a FML such as ARALL or GLARE as a material by the commercial market restricted the research for standardization of FMLs by engineers compared to full composite structures. After two decades of work by many researchers on different types of FMLs, there is still an enormous gap between work reported by academics and work done by commercial institutes on FML applications.
When FMLs are implemented into the design of a structure, the global mechanical behavior and properties of the FML is determined via large test matrices. Which are very expensive and time consuming. Therefore, it is much better to only determine the properties of the FML constituents via empirical methods and having analytical models to determine the properties of the FML. Such a path would lead to more standardization of FMLs. The FML would then be considered as a structure.

The phenomena that is considered in this report is the Blunt Notch Strength(BNS). Because the BNS is influenced by the peak stress profile, the objective of the research is to relate the peak stress profile linear elastically to the net-section stress. An important factor in converging the analytical model would be the finite width correction factor.

The analytical model that has been made follows the Proposal of Alderliesten(PA). It relates the peak stress profile linear elastically to the net-section stress of a center blunt notch in a FML plate under elastic and elasto-plastic conditions, considering that the Neuber Postulate is true.
A constrain on the model was that it wouldn't make use of any empirical data, except for the mechanical properties of the individual constituent of the FML material. Therefore the Hagenbeek model(HM) which makes use of the Metal Volume Fraction(MVF) was implemented to create the σ'ε-curve of the FML.
For the incremental calculation of the net section stress during elastic and plastic loading until failure, the Strip Yield Model(SYM) was implemented. The SYM divided the mid-section of the plate in small strips. The point at the center of each strip is where the values of interests are determined.
Saff's paper provided the data to make an analytical formula for the peak stress profile in the elastic regime for the FML samples, suggesting a decreasing exponential equation with three parameters α, β and γ.

The FML that is used for the model and DIC experiments is the Glare 2A-4/3-0.3, because it was widely available. 3D DIC experiments with strain-gauges applied onto the samples has been done to validate the Matlab analytical model. The strain-gauges were used to validate the DIC experiments and the Matlab analytical model. The Vic 3D DIC software was used to perform the DIC experiments.

The Research proves that indeed the peak stress profile can be related linear elastically to the net-section stress. The DIC experiments and the strain gauges are in agreement with the analytical model far into the plastic regime even without implementing delamination and fiber bridging. The main difference is the influence of when the plastic zone widens outwards. The plastic Stress Concentration Factor(SCF) becomes constant. Before failure the plastic SCF and the mid-section strains determined via the DIC experiment increases dramatic. Since the DIC equipment observes only the surface of the

aluminum layer, delamination and fiber bridging must have occurred. This can be observed much better from the in-equilibrium between the far field load and the mid-section load at these stages of the experiment.

Although great results has been achieved, far better than expected, there is still much to be done. No general formula has been found to determine the Finite Width Correction factor the inaccurately cases considered in this research. The analytical model determines the Finite Width Correction factor for convergence numerically. The plastic zone size and growth needs be determined during each loading increment in order to capture the observed constant value of the SCF far into the plastic regime. In order to comply with the experiments and reality, delamination and fiber bridging must be incorporated into the analytical model. Consequently, this will solve the significant deviations between the BNS of the analytical model and the DIC experiments.

1

Introduction

The introduction of FMLs can be traced back to the destruction of the Fokker facilities during second world war. The company had to start from scratch, and they were low on funds for special type of equipments, such as large milling machines for the production of stiffened panels. Rob Schliekelmann, one of the engineers at Fokker company, who graduated at Delft University, introduced to bond the aluminum layers. This technique was then used to make laminate structure for the Fokker F-27. Further research at Delft University by Schijve and Vogelsang[4] showed that laminated structures(without fibers) had increased fatigue properties. The crack growth on the surface layer would be restraint, because the crack tip didn't penetrate the epoxy layer. When the crack tip would grow, the redistribution of the stress onto the the subsurface layer would reduce the stress intensity at the crack tip in the first layer. Further research on to locally improvement of the properties leaded to the addition of aramid fibers. And the ARALL(Aramid Reinforced Aluminum Laminate) was born. When reinforcing of fibers are considered, the intact fibers in front of the crack would restrain the crack tip from opening significantly. This phenomena is called fiber bridging. A broad aspect of the history and the early research and development of FMLs is well documented by Vlot [4].

The historical problem using FMLs in design arose when producing company's such as Dutch chemical company AKZO and others, capitalized on a new material, while research showed that this combination of fiber epoxy layers in conjunction with aluminum plate is a delicate interaction between the different constituents. So it needs to be seen as a structure. Different groups made their own fiber-metal combinations and filed in for patents. This tendency to see a FML such as ARALL or GLARE as a material by the commercial market restricted the research for standardization of FMLs by engineers compared to full composite structures. After two decades of work by many researchers on different types of FMLs, there is still an enormous gap between work reported by academics and work done by commercial institutes on FML applications; As mentioned in the book Fiber Metal Laminate: An introduction[4]. And further emphasized by Alderliesten[2].

Although it would be perfect to manufacture an airplane in one go, still there would be always a need for junctions and cut-outs, joints, windows and doors. Therefore an important design parameter is the blunt notch strength, also called open hole tension(OHT) strength. Metals, specially aluminum, and mostly ductile alloys have low notch sensitivity. The reduction of strength when introducing a hole or a notch would be limited, as stated by Alderliesten. It is still a key parameter in design against fatigue. The introduction of composite plies in a laminate with a metal makes the FML more sensitive to stress concentrations, because a higher strain hardening is induced due to that the fibers only deform linear elastically[2]. Furthermore failure modes in the composite plies is much more complicated. Therefore

all aspect of the OHT-strength needs to be thoroughly taking into consideration when using FMLs. Generating enormous data, it is possible to have an empiric solution, but it would only apply to one specific laminate of FMLs. This is the way how the industry were convinced launching the FMLs into the commercial market.

Since not every aspect and behavior of a material or structure is fully known as a closed form solution, or there are to many unpredictable factors on which the structure depends. Therefore all material design allowables need to have a statistical basis. Such a statistical basis is the result of either a direct or an indirect computation of a one sided lower tolerance limit for one set of data points. The indirect computation is based on a ratio (to another established property, e.g. Volume Fraction). If the property of interest is a function of a fixed factor, such as corrosion, then knock down factors or a regression will be used. In either cases a large test program need to be set up in order to generate enough data to guarantee the material properties in terms of their design allowables. The direct method needs many more test results to get the statistical basis for the design allowables than the indirect method. Because of the large amount of combinations that are possible with FMLs, these test programs are very time consuming and expensive. Each specific combination would require their own design allowables, thus also their own big test program[4].

Because of the economic advantages it is much better to have an analytical model in order to predict the behavior of the Blunt Notch Strength(BNS) in FMLs. Other objectives are defining the net-section stress gradient and the influence of plasticity in the aluminum layer on the net-section stress gradient. Of course test experiments would always be needed for validation, But at least it would require less time and costs on big test programs in order to guarantee the material properties in terms of their design allowable. This subject is chosen, because first of all, such an analytical model doesn't exist and is considered a challenge to do. Secondly, it is well known that the fiber-resin layers are quite sensitive to blunt notches and cut-outs. The mechanical behavior of small hole such as a rivet hole cannot be ignored. The aim of this research is to show the world that Fiber Metal Laminates(FML) are the best materials for future lightweight airplanes, because it combines the best of the two worlds, namely metallic and/or composite designs.
This research will greatly benefit the scientific community and specially, the aerospace industry itself because of the economic advantages. Many materials can be used for many designs. Having analytical models instead of using empirical data will push FMLs toward a more attractive material when doing a cost-benefit analysis for a part or structural design. Hopefully, The scientific community will be persuaded to focus more on having closed solutions for other problems/behaviours than the BNS considering FMLs. Although for experimental validation of the model, Glare will be used, the model itself could be used generally for all type of fiber-resin and metallic layers.

In order to create a useful analytical model and a experimental setup, the literature on the subject will be consulted. The questions to the literature are,

- Which methods exist for predicting the influence of the plastic zone and the stress/strain field around a blunt notch? With emphasize on the orthotropicity of the material and without the need for empirical values.
- Which failure phenomena, such as fiber bridging and delamination, are included in the methods considered and to what extent?
- How does a hole influences the mechanical behavior in FMLs?

A more elaborated and detailed description on the research questions is given in chapter 2.4.2 Research Questions.

The literature review in chapter 2, presents the methods and models that are found to be useful. A general overview is given on the BNS and the net-section stress gradient. Consideration on implementing the chosen model and DIC experiments for validation are given.
The MATLAB software will be used to create the analytical model. The implementation of the model is described in Chapter 3. The research paper follows up with the experimental procedures which includes the experimental setup using the Vic 3D DIC and the MTS 250kN. The chosen geometry of the samples and sample preparation for inserting in the MTS bench are given.
The results of the analytical model(Matlab) and the DIC experiments are presented in chapter 5. The research paper follows up with the discussion, conclusion and future recommendations.

2

Literature Review

Although during the early stages of the history of FMLs, various scientist and engineers found out great improvements in damage tolerance than in conventional metal structures. Soon it became clear that, when combining two materials, the adverse part of the properties of the constituents must also be taken into account. Since the use of fiber materials in engineering, the BNS became increasingly important, because research showed that the brittle character of composite material is behind the high sensitive behavior towards cut outs(e.g. hole or notch). Unlike composites, metals have low notch sensitivity. It implies that the strength reduction could be less than the difference in the yield and ultimate strength as stated by Alderliesten[2]. An application of metals in the design industry is that permanent deformations are not allowed, this in turn reduces the necessity of determining the BNS for metals. Because the yield strength is considered sufficient for structural sizing, thus often the reduction in strength due to a notch was considered less important.
Since the rise of FMLs, the BNS cannot be ignored in engineering fields. Extensive research is done by various scientists, in order to have a much better understanding on the phenomena influencing the BNS.

The focus of the literature study was how plasticity in the metal layer of a FML laminate will influence the peak stress at a blunt notch. When the metal is strained above its elastic limit, a plastic zone develops near the notch. The locally plastic flow of the metal layer causes the peak stress to relax. As a result, the increasing strain in the prepreg layer in conjunction with high shear strains at the interface between the metal and the prepreg layer, may cause delamination. The aim of the literature study was to develop a theoretical model, that can predict how the peak stress relax when plastic zone grows at a blunt notch in a FML laminate.

The MVF method is a first approximation on predicting mechanical properties such as, stiffness, yield-strength and ultimate-strength. Although it is shown that the predicted properties has an accuracy of 95% with B-values that suggest that 98% of the properties used are above the lower limit values, it doesn't take into account the complex behavior of the laminate when high stress points are considered.

The Lekhnitskii model is good in predicting mechanical behavior at a round hole of an orthotropic laminate. It calculates the solution in the complex domain. The Lekhnitskii model predict the stress components at the edge of the hole in laminated structures. For the plastic regime analytical and approximated solution have been found for certain boundary conditions. But the analytical solution are initiated at high applied load far ahead the elastic limit.

The Lekhnitskii theorem is of interest,because it can solve the peak stress at the notch at any moment in the elastic regime. Furthermore it has the potential to solve the plastic zone around a notch. This can also be used to get stresses further away from the notch, though is limited. If the stress/strain field in and around the plastic zone is known at any given moment, then derivations can be made on how the peak stress gradient changes when the material locally is in the plastic regime.

The metal can plastically deform and harden beyond yield-point. That is a main property of metals which engineers find very useful. This mechanism is essential in fatigue properties at a blunt notch. This theorem can also be used to calculate stress concentration factor(SCF) on the hole edge as function of the radial angle, since also the solution is only valid on the boundary of the geometry of interest[13].

The Strip Yield Model(SYM) is of interest, because, it has shown its potential. With the SYM, the plastic zone, fiber bridging as well as delamination processes can be modeled. It is based on dividing the material at the notch root in small strips. For each strip the elastic as well as the plastic deformations can be calculated. So if the stress can be calculated in this manner at the notch, then it can be solved for the change in the peak stress gradient.

Chapter 2.1 explains the blunt notch strength and the behavior of materials and structure consisting of a round smooth hole. A general overview is given on the phenomena that is taking place during loading in the elastic and plastic regime. Chapter 2.3 explains the models that were considered. The research questions are written in more detail in chapter 2.4. In chapter 2.5 the methodology is given. Here-in the steps to be taken for answering the research questions can be found.

2.1. Blunt Notch strength

The blunt notch strength of FMLs is discussed with various influences of phenomena such as, metal plasticity, multiple types of failure in the composite layer and delamination at the interfaces. First a definition is given for the Blunt Notch Strength(BNS). The use of the BNS in conjunction with a FML is discussed. Furthermore some analytical equations are given for determining Stress Concentration Factors(SCF).

2.1.1. Stress Concentration Factor(SCF) and (Blunt)notch sensitivity

The BNS has been defined as the net or nominal strength of a rectangular plate including a center hole as given by,

$$S_{BN} = \frac{W}{W-D} S_{max} \tag{2.1}$$

where, S_{max} is the gross stress applied when failure occurs at the hole. 'W' and 'D' is the width and diameter of the center hole respectively. For engineering matters, the S_{BN} can be an important parameter to be considered when using notch sensitive materials. Common are brittle materials. Metals having high ductility with relative low yield strength are known for their notch insensitive behavior. A beneficial factor to this is the almost perfect plastic behavior above yielding. The S_{BN} is used mostly as an empiric parameter, although under some conditions in can be determined exact or approximated. Furthermore because of the consistency the S_{BN} provides during experiments with only metallic materials, it can be almost regarded as a material constant for the same $\frac{D}{W}$-ratio.

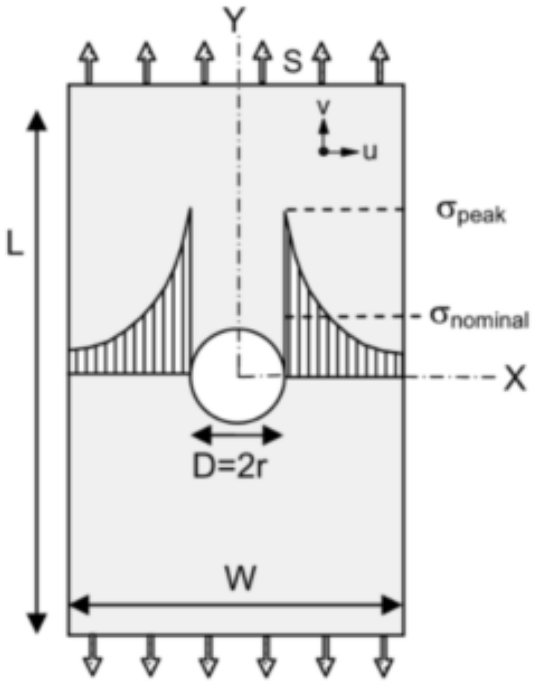

Figure 2.1: A visual presentation of an Open Hole Tension(OHT) experiment[1].

Definition of SCF

In order to determine the S_{BN} of a panel, experiments had been done as illustrated in figure 2.1. The nominal strength is illustrated and given as a dependency on the geometry of the plate. Without the hole, and considering the panel material is isotropic, the stress distribution under loading will be homogeneous. When introducing a hole in the plate, the stress will redistribute, and find other ways to go through the material. This in turn cause the near stress field at the hole to become inhomogeneous. As a consequence, stress concentrations at certain locations at the hole may cause stress peaks greater than the failure stresses considered while the nominal stress S_{nom} is significantly lower than the yield stress[1]. For the OHT experiment as shown in figure 2.1, an analytically solution for the peak stress for an infinite plate has not been obtained, though there are accurate numerical method which do converge quite well to the real solution. Surprisingly, the peak stress for an infinite plate containing an ellipse has been solved, in terms of the major axis of the ellipse and the notch root ρ[13][14]. For an elliptical hole in an infinite plate the peak stress can be calculated by;

$$S_{peak} = \left[1 + 2\sqrt{\frac{a}{\rho}}\right] S_{nom} \tag{2.2}$$

Equation 2.2 can be manipulated, using $\rho = \frac{a}{b^2}$. Setting the axis of the ellips $a = b$, defines a circle. Then as conclusion can be made that in an infinite plate with a circular hole the peak stress S_{peak} is three times higher than the nominal stress S_{nom}. The Stress Concentration Factor(SCF) is defined as the part between the brackets of equation 2.2. Do Note that these equations are only valid for isotropic materials. For an anisotropic material, the orthotropicity must be taken into account. An exact solution can be derived by creating and solving the biharmonic equation given in B.3. More recently a more compact solution is made, though it is an approximation. The SCF of an infinite plate containing an ellipse can be approximated by [2],

$$SCF_{inf,ellipse} = 1 + \frac{a}{b}\sqrt{\frac{2}{A_{22}}\left(\sqrt{A_{11}A_{22}} - A_{12} + \frac{A_{11}A_{22} - A_{12}^2}{2A_{66}}\right)} \tag{2.3}$$

where A_{ij} terms representing the in-plane stiffness of the composite laminate.

For an orthotropic infinite Glare sheet with a round hole, calculation of SCF are given by[3],

$$SCF_{o,inf} = \frac{\sigma_{peak}}{\sigma_{nom}} = 1 + \frac{a}{b}\frac{i\left(\mu_1 + \mu_2\right)}{\mu_1\mu_2} \tag{2.4}$$

with,

$$\begin{gathered} \mu_1 = \sqrt{\frac{g-h}{2}} + i\sqrt{\frac{g+h}{2}} \quad \mu_2 = -\sqrt{\frac{g-h}{2}} + i\sqrt{\frac{g+h}{2}} \\ g = \sqrt{\frac{E_{11}}{E_{22}}} \qquad\qquad h = \frac{E_{22}}{2G_{12}} - \nu_{12} \end{gathered} \tag{2.5}$$

where the subscripts '11' and '22' stands for the loading direction and perpendicular to the loading direction respectively. For the SCF in an orthotropic finite width specimen the SCF can be caculated by

$$SCF_{Glare} = \frac{SCF_{o,inf}}{SCF_{i,inf}} SCF_{i,fin} \tag{2.6}$$

Where the subscript 'o' and 'i' stands for orthotropic and isotropic respectively. The $SCF_{i,fin}$ are taken from the handbook results of Petterson[3].

The influence of plasticity on stress gradient.

In this section, the elasto-plastic response and the peak stress gradient will be discussed. First some detail are explained about the elasto-plastic response of an OHT experiment. Some approximation will be given in order to come to an understanding how this behavior is and possibilities to predict it. At the end the elasto-plastic response of a FML will be discussed.

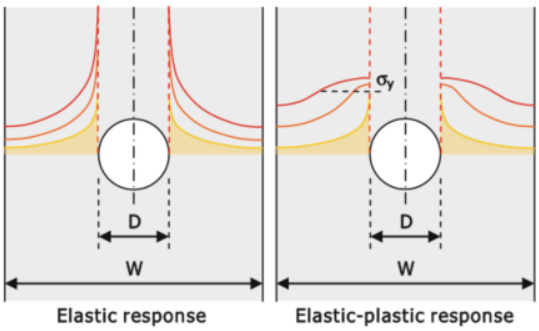

Figure 2.2: Visualisation of the elastic stress distribution and the elasto-plastic stress redistribution[2].

In figure 2.2, three stress lines concerning the peak stress gradient is illustrated. Assuming an isotropic material such as metals, when the peak stress reaches values higher than the yield stress of the material, the metallic material yields, and a plastic zone will form near the hole. The plastic zone forces the

stresses that are concentrated near the hole to redistribute over a large surrounding area. In turn the peak stress gradient relaxes, as can be seen in the elasto-plastic response of figure 2.2.

A better understanding on the change in the peak stress gradient can be beneficial in design, if knowing what the extent and implication of the elasto-plastic response is. Specially when it is expected that during some specific critical operation of the aircraft the material could expect loads higher than design load. Then the question remains, to what extent is a elasto-plastic response allowable. In order to have responsibility and be able to design in the elasto-plastic regime, the design philosophy must have a more concrete understanding of the fundamental aspects of the behavior in this regime.

2.1.1.2.1 Plasticity using FMLs in OHT experiments

When plasticity is locally induced in the material, LEFM is not valid anymore. Complex phenomena such as dislocation movements influences the mechanical properties of the metal in the plastic zone. First, some boundaries need to be set when considering plasticity in a phenomenological manner. Although when working with metals, in the plastic regime, when considering metal with low yield strength and high ductility, often these metals are assumed to be perfectly plastic. That means that there is no work hardening, or the work hardening is negligible. In reality, there is always work hardening. This work hardening could make the metal more susceptible to stress concentrations during future cycles. The strain hardening of the metal can be accounted for by using the Ramberg-Osgood equation with the change of the yield surface. Work hardening is more evident in FMLs due to the influence of the linear elastic behavior of the fibers.
The FMLs respond linear elastically to the applied load, which increases the strain hardening in the FML. This higher strain hardening makes the FML even more sensitive to the occurrence of stress concentrations than monolithic aluminum[2]. Do note that the SCF may differ from ply to ply in a laminated structure.
Because of a plastic zone formation, the deformation between two layers may not be in compliance. And if the inter-laminar shear stresses at the interface is too high to compensate for the elasto-plastic deformation of the metal layers, delamination will occur. Although a plastic zone formation could be beneficial to some extent, delamination is considered often as damage that is never allowed. On the other hand, close to final failure, delamination can be beneficial, because it can postpone fiber failure. Therefore the fibers can still take some loads after delamination has occurred.
The elasto-plastic response shown in figure 2.2 may also differ from ply to ply. This will be more evident after delamination has occurred.
Other factors which influences the stress gradient, such as the finite width will be discussed more in the next section.

Effects of notch geometry on the SCF and notch sensitivity.

For a circular hole in a finite(1) and infinite sheet(2), the peak stresses and the SCF will be the same. This is because of geometric similarities of the specimens shown in figure 2.3. That means that the dimension ratios such as D/W is the same. The Length of the specimens is usually not considered because in the finite sheet, if the length is more than two times the width, the influence on the SCF is negligible.
The peak stresses and the SCF are the same, because while in the bigger sheet the deformation are greater, the relative deformation will be the same. Therefore the strains are the same. As a result the stress distribution seems quite similar, but the stress gradient does differ. This can be related to the fact that the gradient is inversely proportional to the root radius ρ and not a dimensionless variable. On the other hand it can be said that, if D/W becomes larger, the net section will be smaller area over which the stress gradient can decay, resulting in different gradients.

The size effect on the SCF can be accounted for using equation 2.7, which in reality is an approximation made by Heywood on the SCF-curve based on calculation of Howland[1]. For increasing D/W-

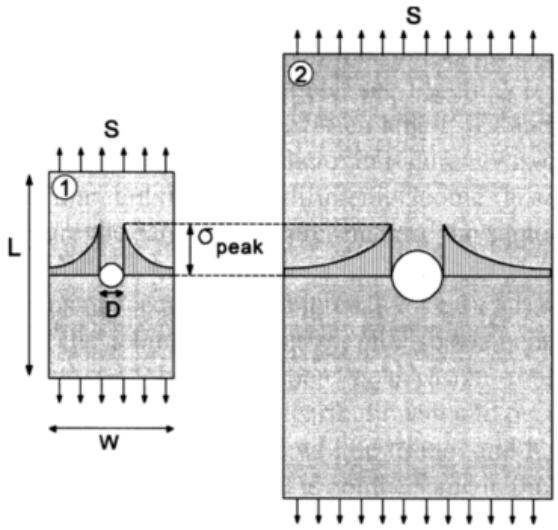

Figure 2.3: Although these 2 specimen are geometric similar, the stress gradient differs[1].

ratios the SCF for an isotropic material converges to $SCF = 2$.

$$SCF_{finite} = 2 + \left(1 - \frac{D}{W}\right)^3 \tag{2.7}$$

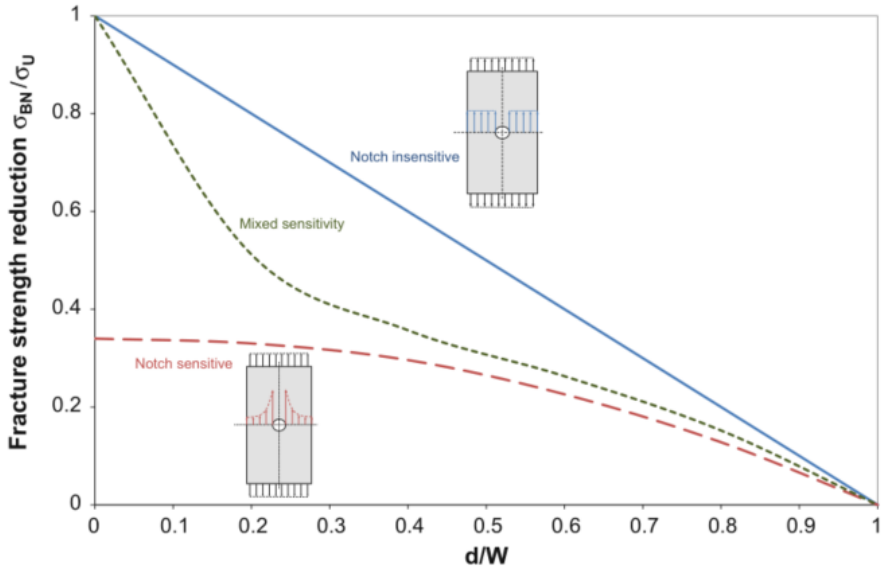

Figure 2.4: Although these 2 specimen are geometric similar, the stress gradient differs[2].

Because the SCF as stated previously is dependent on the diameter of the hole, The hole-plate geometry influences the notch sensitivity as well [2]. In completely notch insensitive materials, the plate does not feel that there is a hole. In turn, there are no peak stresses and net-section stress is constant and some what higher than the gross stress.
It becomes more interesting when using notch sensitive materials or a combination of the two type of materials considered. The notch sensitive materials including even a small hole, already starts with a strength reduction of $\sim \frac{2}{3}$ in comparison with insensitive materials. But when combining the two type

of materials(FMLs) resulting in mixed sensitivity, the start of the strength reduction for tiny holes is almost same as the notch insensitive materials(an advantage of FMLs in comparison to full composite structures). For increasing hole diameter, there is a rapid reduction in strength for $\frac{d}{W} < 0.3$, while beyond this point strength reduction follows more or less the curve of notch sensitive materials. This can be seen in the graph of figure 2.4.

The results of the experiments of Roebroeks and Vermeeren[3] are given in figure 2.5. The results shows that for Glare, the $SCF > 3$ does not have any influence on the BNS. This another reason why crack initiation is faster in FMLs.
The BNS is an ultimate design load for static load cases. The elastic yield limit is a limit design load. Because the ultimate load is to be equal to 1.5 times the limit load, it means that the BNS becomes critical when $\frac{S_{BN}}{\sigma_y}$ decreases below 1.5[3].

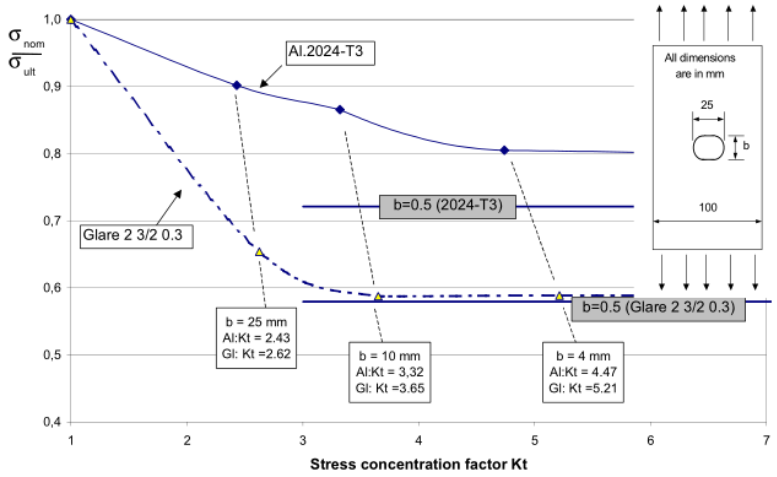

Figure 2.5: Relative nominal strength for different notch geometries[3].

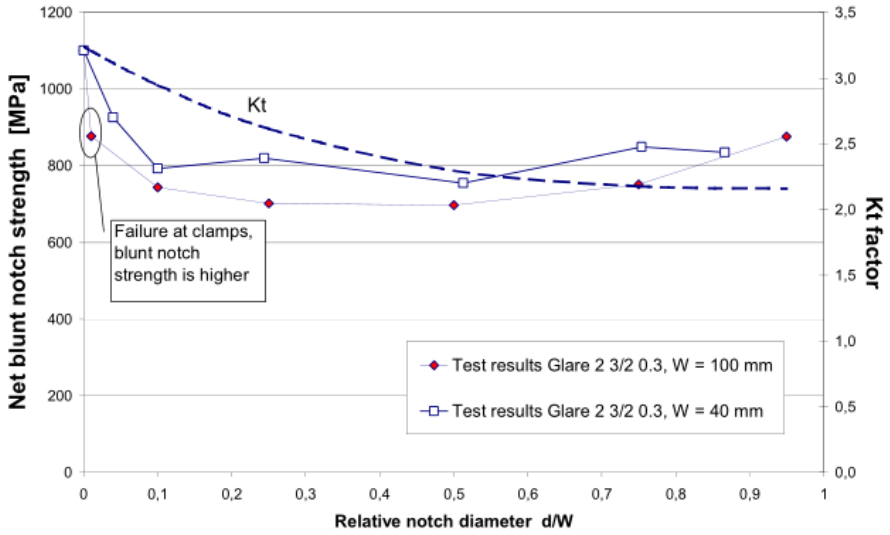

Figure 2.6: Glare BNS results for different $\frac{D}{W}$-ratios[3].

The BNS increases for decreasing hole diameter and constant width, resulted from experiments done by Roebroeks[3]. He explains that this is because the stress gradient increases for smaller holes and that the plastic zone in the metal layer is small. This in turn results in significant shear stresses which

cause delamination.
In figure 2.6 the results on two different Glare specimen width(40 and 100mm) are plotted as function of $\frac{D}{W}$. Along the right secondary axis the SCF is given. From the experiments, the main conclusion is that if SCF values should describe the BNS of Glare laminates, a higher SCF would resulted in a lower BNS. However this was not confirmed[3].

2.2. Conclusion

As stated in this chapter, complex phenomena influences the blunt notch strength S_{BN}. Although great improvements are made in order to predict these phenomena, a concrete general method is not yet made. Various solution have been made for infinite plates. Sometimes from these, it is possible to deduce the solution for a finite plate. The plastic zone formation in the metal layer has the most influence on the relaxation of the peak stress gradient. Fibers locally will strain more. Stresses can by-pass the metal onto the composite layer. But still there is no compact analytical solution for the peak stress for FMLs, even in the elastic regime. Though an exact solution for the stress gradient of an elliptical hole in an infinite plate has been accomplished as function of $x > a$[1]. As stated in the previous section, The geometry of the OHT experiment is of great significance when solving for the SCF as well as for the peak stress gradient. During the experimental set up the boundaries considering the geometry of the OHT experiment must be taken into account carefully. Especially when considering FMLs.

2.3. Current Methods in predicting stress-strain field around a hole.

Although the Blunt Notch Strength S_{BN} is seen as a material property, determining it for materials sensitive to cut-outs, especially for FMLs, as an closed form solution has not been found. The S_{BN} for various aluminum grade FMLs are within the plastic regime of the aluminum constituent[3]. Most volume of the FML consist of the metallic part and assuming that a plastic zone will form before the occurrence delamination and fiber bridging, the initial change in the peak stress profile is highly dependent on the metallic layer. Thus the behavior of the metal layers will dominate the FML OHT-specimen from elastic into elasto-plastic behavior.
Suggestions are made to develop a theory/model which can predict the change of the peak stress profile $\frac{\partial \sigma_y}{\partial x}_{y=0}$ in the metallic layer, which should be solely based on the stress and strain curve of the considered material. This in turn should be, together with the influence of bridging of the fibers and delamination on the stress-strain curves of FMLs, incorporated into an analytical model which can solve for the S_{BN} of FMLs. Last but not least, the method/models considered must not consist of empirical variables.

During the literature study, the models/methods that were found to be usefull are.

- Proposel Alderliesten(PA)
- Lekhnitskii theory(LT)
- Metal Volume Fraction(MVF)
- Hagenbeek Model(HM)
- Strip Yield Method(SYM)

These methods are chosen, based on their specific qualities proven in the literature. The MVF method is used to calculate overall final laminate properties of FMLs. The MVF determines the FML material

properties by means of a weighed average of the properties of the individual constituent proportional to their volume used in the FML plate. The metallic contribution has been determined with experiments, which implies that the method can only be used for FMLs with specific constituents for which the values have been determined[5]. In section 2.3.1 the MVF method will be treated as well as the Hagenbeek model and the proposal of Alderliesten.
Hagenbeek et al[15] made a numerical model in which they used the MVF together with the Norris Failure criteria in order to predict the Blunt Notched Strength(BNS) of a couple of Glare grade FMLs. It can account for plasticity, But delamination and fiber bridging is not incorporated.
Alderliesten(PA)[5] proposes developing a methodology that is mathematical generic of nature of predicting the metallic contribution for arbitrary metal/alloys solely based on their stress and strain curve. In the elastic regime the choice can be made to determine the FML properties with the MVF or the Classical Laminate Theory(CLT). Both have reliable outcomes. In the elasto-plastic regime it determines the deformation energy based on the stress-strain curve. The Ramberg-Osgood relation can be used as first approximation for the plastic part of the stress-strain curve[2].

The Lekhnitskii theory is an old model, dated before WW2, is later on improved and used by various scientist to predict the behavior of orthotropic/anisotropic plates including a hole. The Lekhnitskii theory only accounts for plasticity. This model maps conformal the boundary of interest onto a unit circle on the condition that the region of interest is continuous smooth function with a continuous changing tangent. The region of interest may be one or the other side of the function considered. The laminate constants are determined with the CLT. Solving is done in the complex domain. In the elastic regime the solution is only valid on the region of interest. In the plastic regime the size and shape of the plastic zone can be determined. This model is of interest because it has proven that it is possible to calculate the SCF. It is different in its mathematical build up than the other models considered. Analytical solution are made for various cut-outs in an anisotropic plate[16][13].

The SYM is made in the 1960. The SYM model is specially used for sharp notches and crack growth. The SYM model does account for delamination and fiber bridging as well as plasticity of the metallic layer. It divides the region of interest in strips with smaller width. For each increment of the load applied the equilibrium conditions for the strips are solved. This literature study looks into whether it is possible to use this model for the case of BNS. The LT and the SYM will be discussed in section B.3 and 2.3.2.1

2.3.1. The models MVF, HM and PA

The MVF approach

The MVF method uses the fraction of volume of the individual constituents in order to predict the property of interest of the final laminate. The volume fraction method is a weighted average of the different constituents in terms of their properties. Other properties has shown similar dependance on the volume fraction of the constituents.
If GLARE3 is used with fiber orientation of 0° and 90° degrees in the composite ply, then the property of interest of the composite layers will be calculated via the rule of mixture for each single ply using the Reuss and Voigd model dependent on the orientation of fibers in the FML. The FML stiffness for example would then be given as;

$$E_{FML} = E_M t_M + E_{0^\circ} t_{0^\circ} + E_{90^\circ} t_{90^\circ} \tag{2.8}$$

In which, the E_{0° and E_{90° stands for the stiffness of the composite plies. The subscript 'M' stands for the metal constituent and the 't' is the thickness of each layer. For Glare FMLs the properties of the composite plies is ussually already determined by other means for the 0° and the 90°-orientation of

the fibers. Therefore the formula to calculate the property of interest in FMLs is given as;

$$P_{FML} = P_M MVF + P_{pre}(1 - MVF) \tag{2.9}$$

P is the property of interest of the specific constituent. the subscript FML, M and pre stands for Fiber Metal Laminate, Metal- and prepreg-ply respectively. The Prepreg-ply could be all different variety of fiber-resin combinations or only pure resin to enhance delamination properties as mentioned by Alderliesten[2].

The MVF approach is validated by test experiments and conclusion are layed down in the book Fiber Metal Laminate: An Introduction[4]. The MFV-method assumes a linear relationship between the properties of the metal layer in correspondence to their thickness and the average of the experimental tested laminate. The line is then extrapolated to the point of $MVF = 0$, which stands for a pure composite laminate. $MVF = 1$ stands for properties of the monolithic metal, in this case that is the aluminum. In figure 2.7 the graph show the extrapolation line from pure metal to pure composite and there in between the FML volume fractions taken into consideration.

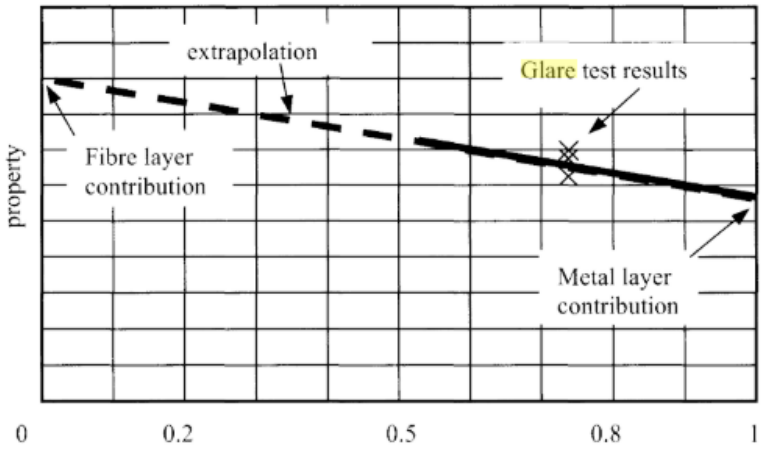

Figure 2.7: A visual presentation of the MVF-method described in equation 2.9[4].

The MVF method is proved to be valid for the range of 0.45 < MVF < 0.85. Current used Glare laminates are designed with the use of this margin. Do note that this approach is only valid for dictating the mechanical properties of laminate subjected to a static test. These are the in-plane mechanical properties(e.g. tensile, compressive, Young's modulus and shear strength calculations). This method can be used as a general approach to any FML-design considering the limitations of course[4].

OHT-strength using the MVF approach

A Tool is developed by Hagenbeek et al[15], namely the 'Stress-Strain Calculation Program(SSCP)'. The SSCP is used to calculated the bi-linear stress-strain curve of an arbitrary (Glare) laminate. It is an easy and effective method for fast and preliminary investigation of the effects of pre-straining and plasticity. Furthermore they used the MVF-method in combination with an open hole tension model using the Norris failure criteria in order to predict the OHT-strength for a couple of Glare laminates. Hagenbeek et al[15] have proven that the Norris failure criteria can be combined with the MVF-method to calculate multi-axial(bi-axial + shear component) Blunt Notch Strength.

Proposal Alderliesten

The motive of this proposal is to relate the change of the peak stress profile $\frac{\partial \sigma_y}{\partial x}_{y=0}$ linear elastically to the net section stress. The input should be the stress-strain curve of the material or laminated structure. The $\frac{\partial \sigma_y}{\partial x}_{y=0}$ is more dynamic of nature in the plastic regime. The $\frac{\partial \sigma_y}{\partial x}_{y=0}$ is dependent on the influence of the plastic zone, fiber bridging and delaminations. If the stress-strain curve of the metallic constituent in the FML laminate is known, the elasto-plastic strain energy, which is defined by the area under the stress-strain curve, can be used to determine how much the pure(imaginary) elastic strain induced in the material would be if the material(e.g geometry/structure) behaved full elastic according to the initial elastic constants(Young's modulus) used.
Determining this imaginary elastic strain or energy, knowing the 'real' elasto-plastic deformation/energy calculated via the elasto-plastic stress-strain curve, the difference of energy could be used to relate the change of the peak stress profile $\frac{\partial \sigma_y}{\partial x}_{y=0}$[5] with the net section stress. Because the Neuber postulate agrees with the elastic prediction according to Schijve[1];

$$\sigma_{peak}\varepsilon_{peak} = SCF^2\sigma_{nom}\varepsilon_{nom} \tag{2.10}$$

in which the subscription 'peak' and 'nom' stands for the peak stress and the nominal/net section stress-strain respectively.

Consider the elastic stress-strain curve in figure 2.8. The deformation energy given as the blue area A_{ep} can be used to determine the imaginary elastic stress and strain in figure 2.8 or the imaginary elastic energy A_e. As a first approximation, assumptions are made that $A_e = A_{ep}$.

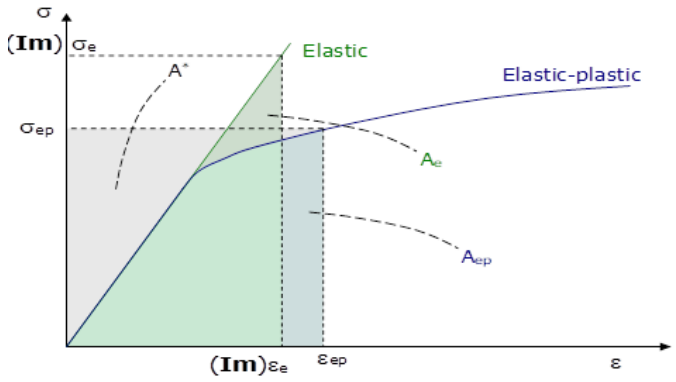

Figure 2.8: Energy consderation using the stress-strain curve of the material(e.g. structure)[5].

The real elasto-plastic stress strain curve is determined via the Ramber-Osgood equation. Suggestion here is that the smaller green area given above the stress-strain curve in figure 2.8 can be used to relate the change of the peak stress profile $\frac{\partial \sigma_y}{\partial x}_{y=0}$ with the net section stress.

The suggestion to relate the change of the peak stress profile $\frac{\partial \sigma_y}{\partial x}_{y=0}$ to the change of the net section stress can be better clarified using the Neuber postulate[1].
As long as plastic deformations does not occur, all deformation are proportional to the applied load(Hooke's Law). As soon as plastic deformations occurs(initialization of the plastic zone formation) S_{peak}, at the edge of the hole, is lower than the elastic prediction $SCF * S_{nom}$, and ε_{peak} is greater than the elastic prediction $SCF * \varepsilon_{nom}$. According to Neuber postulate the product of $S_{peak}\varepsilon_{peak}$ still agrees with the elastic prediction given as equation 2.10.

The change in the stress and strain profile relating the nominal values to the peak values during the plastic zone formation is shown in figure 2.9.

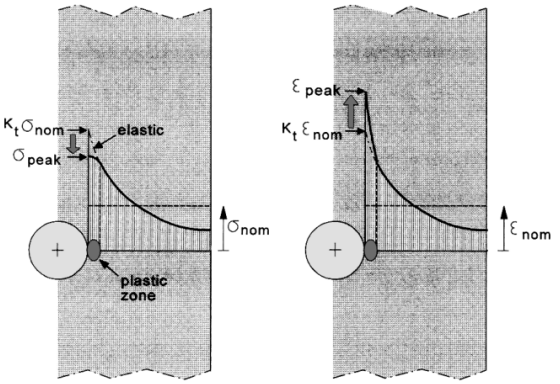

Figure 2.9: Illustration of redistribution of the stress(left) and strain(right) caused by plastic zone formation[1].

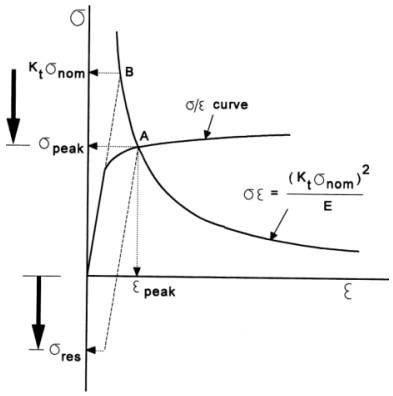

Figure 2.10: Graphical method for determining the peak stress at the edge of a hole in a OHT-specimen[1].

Neuber proved that the postulate is correct for hyperbolic notch under shear loading and assumed that the postulate would also be correct for other types of notches and applied loading. Providing the plastic zone size is small, the assumption of Neuber was somewhat confirmed empirically[1].
This means that, considering figure 2.10, at the intersection of point A both relations are satisfied for the peak stress and strain. Furthermore point B in figure 2.10 is the imaginary S_{peak} when no plasticity would have occured, assuming the equality of $A_e = A_{ep}$ shown in figure 2.8. The difference of point A with B gives the reduction of the peak stress[1][5]. Increasing incrementally the applied load would suggest , the platic zone size grows, the graph of the product '$\sigma\varepsilon$' given in figure 2.10 moves along the stress-strain curve.

2.3.2. Stress Concentration around a hole

The MVF approach is mostly used as a rough estimation which can be quite close to reality. Often it is used to predict the overall laminate properties. The MVF approach is based on idealized assumption as mentioned in section 2.3.1. Therefore, if there is a hole in the laminate, or the stacking sequence of the fiber layers consist of multiple fiber direction, the MVF method could deviate more from reality. Because the stress and strain field in this case deviates more than the simple case using only uni-directional fiber layers.
A much better method is the Classical Laminate Theory(CLT) explained in appendix B. The CLT emphasizes that the properties of a layer stacked hybrid structure should be a function of the properties of the individual layer with their specific stacking sequence. The CLT is used when dealing with orthotropic laminated structures such as composites and FMLs. It is possible to calculate the in-plane and out-of-plane stiffness, but also the in-plane and out-of-plane coupling effects induced by the stacking sequence of the laminate. Furthermore it will be the foundation on which the elasto-plastic calculations,based on the Lekhnitskii theory, is build on. In this section the Lekhnitskii theory will be explained and how it can be used to determine the stresses on the boundary of the hole and inside the plastic zone.

Strip Yield method(SYM)

A commonly used model in the elasto-plastic fracture mechanics is the strip yield model. The Strip yield model was first introduced in the 1960 by Dugdale[7]. Since stress singularities makes it difficult to find a near crack tip solutions for stresses en strains. Dugdale divided the material near the crack tip in small strips as can be seen in figure 2.11. In the 80's, Theocaris[7] solved the plastic zone in between two cracks that grow to each other. The solution was based on the Dugdale concept of yield strips, with the assumptions that, the material is homogeneous, isotropic and elastic-perfectly plastic. Recent developments on the SYM of Dugdale in the first decade of 21's century encompasses all three modes of crack growth and delamination, as wel as mixed mode phenomena. Various improvements are made on predicting the plastic zone size and many more[7].
Yi et al[17] and Rodi[6] accomplished in 2012 an analysis on elasto-plastic fracture mechanism of Mode 1 crack in a dissimilar material. In both models the Strip Yield Model of Dugdale is extensively used in order to determine the plastic zone size and the influence on crack growth under uniform loading.
In the present research the SYM model will be limited to the analysis of the influence of the plastic zone on the peak stress distribution at a round center hole.
In this section the working principles of the SYM is layed down, when considering a plastic zone, delamination and bridging stresses.

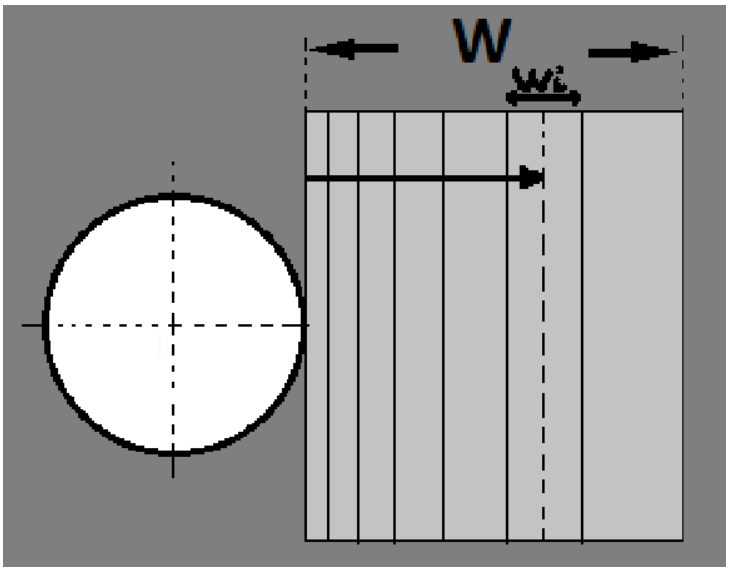

Figure 2.11: Illustration of yield strips near a hole.

Modeling of the plastic zone size using SYM.
As can be seen in figure 2.11, the notch geometry of interest will be divided into smaller elements of variable width w_i. In order to have enough accuracy in describing the stress gradient, the elements with the smallest width is placed near the hole edge. Because the greatest change in the peak stress profile is known to take place near the hole edge. Thus a requirement of the model would be to find out, by iterative means, the total amount of bars needed. The aim of this procedure is to minimize the smallest bar element to a value w_{fix}.
After the initial number of bar elements are defined, the half width of the bar element(from the hole edge) is used as the reference position for the bar elements. Rodi[6] used in his work a value of $w_{fix} = \frac{1}{2}mm$. He mentioned that it is important to define a proper value of w_{fix}, because if the stress calculated at the crack tip based on an equation, that has the form of a fraction or an inverse

square root where-in the depended coordinates are included, will predict a peak stress that might be too large. This occurs when the center line of the bar element is too close to the crack tip. Thus the value w_{fix} is not allowed to be too small. Otherwise prediction of failure on fiber bridging and delamination border growth may be premature.

Delamination using SYM

In this section delamination is considered when occurred during elasto-plastic conditions. During plastic zone formation at a hole, the prepreg layer in a FML can strain significantly. High shear stresses can accumulate at this zone in the interfaces between the metal and prepreg layer. Its highly likely that delamination may occur, specially mode II and to some extent mode I. After mode II delamination, the fibers in the prepreg layer can strain over a longer distance, which in turn reduces locally the stress. This research will focus only on quasi-static delamination of mode II.

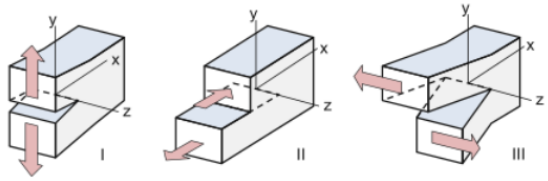

Figure 2.12: Visualization of three delamination opening modes; Mode I(tension), Mode II(shear) and Mode III(transver shear)[6].

In figure 2.12 the different delamination modes are illustrated. In order to describe and predict the delamination growth, often the Strain Energy Release Rate(SERR) is used. SERR is based on Linear Elastic Fracture Mechanism(LEFM). Because it is difficult to describe locally the stress at or near a hole at the interface of two completely different and inhomogeneous materials, therefore the energy dissipation is considered. In a linear elastic system, there is no interaction between the different modes of delamination. Thus for a given system in the elastic regime, the total SERR can be obtained by;

$$G_T = G_I + G_{II} + G_{III} \tag{2.11}$$

When considering superposition of the same delamination mode influenced by different factors, SERR is obtained by;

$$\begin{aligned} G_I &= \left[\sqrt{G_{I(1)}} + \sqrt{G_{I(2)}} + \sqrt{G_{I(3)}} + ...\right]^2 \\ G_{II} &= \left[\sqrt{G_{II(1)}} + \sqrt{G_{II(2)}} + \sqrt{G_{II(3)}} + ...\right]^2 \\ G_{III} &= \left[\sqrt{G_{III(1)}} + \sqrt{G_{III(2)}} + \sqrt{G_{III(3)}} + ...\right]^2 \end{aligned} \tag{2.12}$$

The delamination growth rate $\frac{db}{dN}$ is related to SERR by;

$$\frac{db}{dN} = C_d G^{n_d} \tag{2.13}$$

In which, 'b', 'N' and 'G' are the delamination border, cycle and SERR respectively. The parameters 'C' and 'n' material are coefficients defined by the laminated structure used.

In most cases, static delamination growth in FML is driven by load transfer from metal to composite layer through the interface. Due to the development of a plastic zone near the hole, it may occur that

the deformation of the metal and the composite layer is no longer in compliance. The strains induced locally cannot be followed by the composite layer, hence high shear stresses will develop at the interface due to the load transfer from metal to composite. This in turn will cause delamination, when the critical conditions are met. When there is different delamination lengths comparing the different interface between the laminate layer, out-of-plane deformations could arise, inducing mixed-mode delamination. It is very common that delamination at different ply interfaces does not grow at the same rate. This should carefully be taken into account. A possibility is to create some averaging approaches.

In case of delamination, first the delamination increment 'db' given in equation 2.13 for every load increment will be calculated. When the delamination borders are known for that increment, then the yield strip will be used to determine the fiber bridging stresses, by solving the compatibility equation for every strip.

Bridging stresses
An important and very useful property of FMLs is the great resistance induced by the fibers against failure. Because of the high stiffness and failure stress of glass fibers under tension, the glass fibers can be used as a bypass to the loads when plasticity or even failure occurs in the metallic layers. After the elasto-plastic stresses and strains are known of the particular bar element of interest, the bridging stress can be calculated by solving the compatibility equation for each strip. The bridging stress are the stresses that bypasses the metal and are carried by the fibers.

Failure Criteria
Shapes of the plastic zone will be highly influenced by the failure criteria assumed. Although the failure criteria below is used for a sharp notch, it does shed some light on the differences of using plane stress and plane strain. Two common known yield criteria in use for metals are Tresca- and Von Mises Yield criteria. With these failure criteria, the elasto-plastic contour can be obtained[18]. The plastic zone shapes are shown in figure 2.13 and 2.14 based on their respective failure criteria.

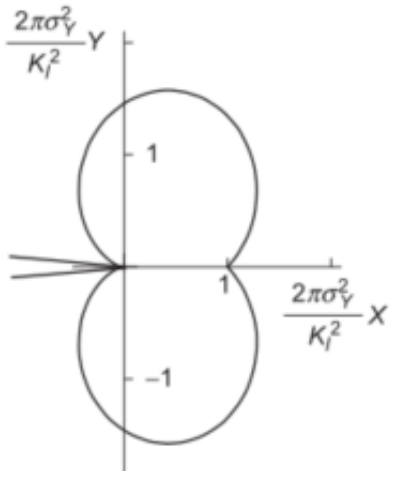

Figure 2.13: Plastic zone shape determined using Tresca Yield criterion[7].

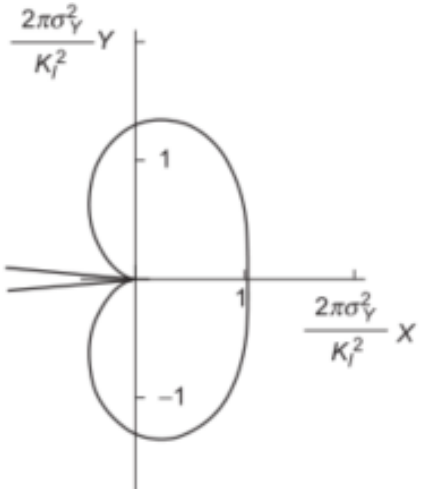

Figure 2.14: Plastic zone shape determined using Von Mises Yield criterion[7].

These plastic zone sizes are half the estimate used by Irwin's plasticity, though it is believed to be closer to the actual size of the plastic zone. The Irwin's plasticity prediction based on assumption that the small scale yielding during crack initiation still follows LEFM criterion. He adjusted the stress intensity factor(SIF) due to the crack tip plasticity[18].

$$r_{pl}^{TR} = \frac{K_{SIF_I}^2}{2\pi\sigma_Y^2} cos^2\frac{\theta}{2}\left[1+sin\frac{\theta}{2}\right]^2 \tag{2.14}$$

$$r_{pl}^{VM} = \frac{K_{SIF_I}^2}{2\pi\sigma_Y^2} cos^2\frac{\theta}{2}\left[1+3sin^2\frac{\theta}{2}\right] \tag{2.15}$$

Equation 2.14 and 2.15 are used to calculate the plastic zone considering Tresca and Von Mises Yield Criteria respectively, under plane stress conditions[18].

$$\begin{aligned} r_{pl}^{TR} = \frac{K_{SIF_I}^2}{2\pi\sigma_Y^2} cos^2\frac{\theta}{2}\left[1-2\nu+sin\frac{\theta}{2}\right]^2, \quad & \nu \leq \frac{\sigma_{yy}}{\sigma_{xx}+\sigma_{yy}} \\ r_{pl}^{TR} = \frac{K_{SIF_I}^2}{2\pi\sigma_Y^2} sin^2\theta \quad & \nu \geq \frac{\sigma_{yy}}{\sigma_{xx}+\sigma_{yy}} \end{aligned} \tag{2.16}$$

$$r_{pl}^{VM} = \frac{K_{SIF_I}^2}{2\pi\sigma_Y^2} cos^2\frac{\theta}{2}\left[(1-2\nu)^2+3sin^2\frac{\theta}{2}\right] \tag{2.17}$$

Equation 2.16 and 2.17 are used to calculate the plastic zone considering Tresca and Von Mises Yield Criteria respectively, under plane strain conditions[18].

Solving equation 2.14 to 2.17 for $\theta = 0$, shows that the estimation under plane strain condition is 16%[18] of the corresponding plane stress value. This is because the shape of the plastic zone under plane strain conditions is more dependent on the poison ratio than under plane stress conditions. The reason is that the poison ratio effects the stresses tri-axiality under plane strain conditions . This in turn restricts the plastic deformation. Thus restricting plastic yielding to some degree.

2.3.3. Conclusion

Revision has been done on couple of methods considered useful on how to predict the elasto-plastic fracture mechanism at a hole. The first method considered was the MVF approach. The MVF approach is quite limited, but still very useful for having a rough estimation on the properties of FMLs. As said in previous section of this chapter, these properties in turn can be used to estimate the stress concentration factor at the edge of the hole, assuming the properties estimated by the MVF approach is constant through the thickness and taking into account the mixed sensitivity of FMLs. On the other hand, since the S_{BN} is defined as a material property, the S_{BN} for metal and pre-preg can be filled in equation 2.9 in order to determine the S_{BN} of the FML directly. Alderliesten[2] states that this prediction applies to uniaxial loading in which the fibers in the pre-preg layer is in that particular direction. Furthermore it is assumed that the fibers perpendicular to the applied load does not contribute to the BNS.
Hagenbeek et al[15] have proven that the Norris failure criteria can be combined with the MVF-method to calculate multi-axial(bi-axial + shear component) Blunt Notch Strength. The SSCP made, can be used to construct the stress-strain curve of FMLs for the elastic and plastic regime.
The method proposed by Alderliesten(PA)[5] is most promising for relating the change in peak stress profile to the net section stress. Because it uses only elasto-plastic stress-strain curve defined by the material(e.g. structure) constants. These constants can be determined via the MVF or the CLT. This approach could be used in conjunction with the SYM model. Using the principles of the SYM model, and applying the method of PA, the elastic and plastic strain for each strip can be determined. The small finite width yield strips can be used as a superposition to determine incrementally the influence

of the plastic zone initialization and growth on the change of the peak stress profile. Using the energy considerations explained in section 2.3.1.3, it might be possible to relate the change of the peak stress profile to the net section stress.

The first method considered to predict the plastic zone near a hole in section B.3, was the rigorous math solving in the complex domain, referred to as Lekhnitskii theorem. While it shows very promising, and indeed it is possible to estimate plastic zone sizes and many more, the math it self is quite difficult, with steps need to be taken very carefully. An advantage of this approach is, that it is completely analytical, excluding any iterative processes. The possibilities ranges from, calculating stress concentration factor(SCF) and stress intensity factor(SIF) at only the hole edge, to the near field solution at positions of interest and even stress fields inside and outside the plastic zone. This approach has a stronger basis in the orthotropicity than all the other methods discussed.

The second method discussed in section 2.3.2.1, was the Strip Yield Model(SYM) proposed at first by Dugdale[7]. This model is previously only implemented for sharp notches. During recent development, improvements are made on the use of the SYM for prediction of variety of problems inside the boundary of elasto-plastic fracture mechanism. Though it is an iterative process, it is simple enough to solve the problems of an open hole tension(OHT) experiment in much lesser time than a severe time consuming Finite Element Analysis(FEA). This is also because the solution will be made only on the mid-section of the plate aligned with the center of the hole. This is also the place were the peak stress profile of interest lies. By the work of various scientist in the field, the SYM can encompass almost all elements of elasto-plastic fracture mechanism at the edge of a notch, such as delamination, fiber bridging and the plastic zone at the hole edge.

2.4. Research Question

It is almost eighty years ago, when the engineers at Fokker company made their decision on using laminated structures. The history and the steps that where taken as written by Vlot[4] and furthermore emphasized by Alderliesten[2], shows an image of why it took such a long time for FMLs to be incorporated in the commercial industry. Although great achievements were made in obtaining the overall material constants and behavior of a FML-laminate, major elements in the design philosophy using the FMLs, which conventional aerospace materials were not considered critical, couldn't anymore be ignored.
This research is about the change of the peak stress gradient during occurrence of plasticity in the metal layer and the influence of the induced orthotropic nature of the composite layer. Therefore key elements of the solving the problem will lie in how properly can the models considered, predict the shape,size and influence of the plastic zone of the metal layers. Of course, in conjunction with the behavior of the composite layer.

2.4.1. Discussion

After lots of empirical research for some grades of FML, enough proof have been presented in order to convince aviation industry for a more promising future using FMLs. After lots of work by great people, Glare was accepted to be used on the A380. Glare panels were used in the upper part of the fuselage for their endurance against fatigue cycles and Glare panels were used for the leading edge of the horizontal and vertical tale section, because of its improved impact resistance. In order to have a full FML laminated airplane, all the structural elements considered during design, must have their proper models of prediction with great accuracy. This research is limited to the peak stress gradient of an OHT-specimen. The challenge is to account also for the orthotropic nature of composite layers.

Two mathematical models that are considered, are the Lekhnitskii theory and the Strip Yield model of

Dugdale. Both models have their own implications. The advantage of the Lekhnitskii theory is that it is analytical. Their are no iterative processes, but consideration in solving in the imaginary domain must be done carefully. Various scientist in the field, such as Lekhnitskii, Muskhelishvili, Kolosov and Westergaard, have shown great possibilities of this method. Later on, they have extended the solution from only at the boundary to the overall plate geometry in some cases. With this method it is possible to solve the stress and strain field over the whole laminate.
The second model is the strip yield method. It divides the material near critical position in strips with dimension small enough to have a convergence. This gives a near field solution. That is fine, since the plastic zone forms near the notch root. By various experiments it is shown that the important part of the stress gradient to be understood is near the hole edge. The position were the plastic zone will form. This position is also where the change in the peak stress gradient has the greatest range, depending on the size of the plastic zone.

Besides these two models, other proposals and methods which might be useful to consider for the MSc thesis has been taken into account as well. These are the MVF, HM and PA.

Since it is known which specific phenomena are influencing the peak stress gradient near the notch root, the focus of this research must lay down on the interaction of these phenomena with the peak stress gradient. As mentioned before, these are the plastic zone, fiber bridging and delamination of the plies. Therefore the research question is chosen such, that the priority on the models is to encompass all the phenomena influencing the behavior of interest in an analytical manner.

2.4.2. Research Questions

The research question as well as the sub-questions of this project is formulated as:

1. How does the peak stress profile near the notch root changes when the metal layers of the laminate are beyond their yield limit? Specially, when the compatibility of the fiber layers are considered in conjunction with the plastic zone.

    (a) What are the possibilities to determine analytically the stress and strain fields in a OHT experiment, and what are the extent of these models to take account for the various phenomena of influence considered? Most importantly to what extent is it possible to change these models for the benefit of this research?

    (b) Is it possible to relate, the peak stress profile or the SCF at the notch root, linear elastically to the net section stress? If, so what are the implications or benefits for the plastic regime?

    (c) Is possible to have delamination underneath the plastic zone before any crack growth at he hole edge?

    (d) Which finite width corrections needs to be considered in order to describe the peak stress profile properly? And what are the limits?

2.5. Methodology

In this chapter, the extent of the use of the methods considered will be discussed. An overview will be given including the necessary steps that needs to be taken in order to come to a conclusion. First the models will be discussed. Afterward the steps to be taken in the MSc thesis is given. At the end of this chapter, consideration on experimental steps is given, which can be used for validation of the Msc thesis model made or to get more insight on the phenomena influencing the peak stress profile. A rough estimation on time-planning is included in the last section.

The models considered
The Lekhnitskii theory(LT) constitutes a mathematical model, but is not very compact. For the plastic zone, this model has lots of variations. Some great names that have gotten their signatures on solutions of this problem are Lekhnitskii, Westergaard, Muskhelishvili and Kolosov. All have set their own assumption and chosen failure criteria. Each have their own limits that needs to be weighed first, in order to construct the algorithm in MATLAB for solving the problem. The general equations that are considered are already given, while the specific details of the mathematical model to be used in the MSc thesis still needs to be determined. This method has proven its use, especially for calculating SCF. A major obstacle of this model is, finding contour L, which separates the elastic and plastic regime and the shape of contour L. Muskhelishvili[19] and also Savin[13][16] have used for several cut-outs an elliptical shape which surrounds the cut-out completely[13]. These can be seen in appendix C in figure C.1, C.2 and C.3. Maybe this is the case when solving for very high loads. The interest of this research is close to or just when plasticity is taken place. It is known for this case that the plastic zone does not encompass the whole hole. The plastic zone will start from a point on the hole edge and grow against the hole edge. This is illustrated in appendix C in figure C.4. The solution of the case mentioned in figure C.4 has not yet been found, but an approximation has been made by Fayerberg[13]. Do note that this approximation is made with the use of an empirical value.

In the beginning, the Strip Yield Model(SYM) was only considered for sharp notches. This is still the case to this day. For sharp notches, the crack opening displacement(COD) is used to calculate the length of the yield strips. For blunt notches or a round hole, like in an OHT-specimen the length of the yield strips must be defined in such a way, that it will encompass at least the whole disturbed stress field near the hole. Another consideration might be how much and how far the yield strips should be layed down for an efficient model, considering the length of material from the hole till the side edge that can be used. Taking into account the illustration of the peak stress profile and S_{nom} in figure 2.1 and 2.9, suggestion is made that the position till the yield strips will be layed down, would be from the hole edge till the intersection of the peak stress profile and the constant function S_{nom}. Because the area left and right of the intersection between the peak stress profile and S_{nom}, should be equal. On the other hand this intersection may move sideways when plasticity occurs. If it becomes to difficult to determine the stresses left of the intersection, then its always possible to lay down the yield strips from the hole- til the plate edge. Thus using SYM for a round hole, some geometric implication may need to be considered. Again, also for this model there are various failure criteria, and many more.

On the time-line at the end of this chapter, Lekhnitskii model got only a small portion. This is because it needs to be verified to what extent the Lekhnitskii model can be used in the plastic regime, while for sure the SCF can be calculated via LT in the elastic regime[13][16]. Thus the SCF determined via the LT can be used as an input or verification in the model made in the MSc thesis. If it is shown that the LT can be implemented in the plastic regime as this literature study suggests, then this model might be considered to use it as a comparison with the SYM.

The main proposal of this literature study is to analytically relate the change of the peak stress profile with the net section stress using only the material or laminated constants. Therefore determining stress-strain curve of the material or structure considered is essential. The stress-strain curve can be made via the MVF or the CLT in the elastic regime. In the plastic regime approximations can be made using the Ramber-Osgood relation or the SSCP of Hagenbeek et al[15]. The PA suggests using the energy consideration with the stress-strain curve in order to relate the change of the peak stress profile to the net section stress in the plastic regime.

The main line that the MSc thesis project will take, is the SYM with the mathematical implementation of the PA. The SYM model is considered for this purpose because it has been achieved and proven that it is possible to build in the fiber bridging mechanism and delamination[6][17]. Other methods reviewed could be used as input or verification for the main model considered in the MSc Thesis project. These are methods used for the construction of the stress-strain curve of the material or lami-

nated structure and the Kirsch's equation[8] in comparison to the equation considered by Alderliesten for the tangential stresses at the hole edge given in appendix A[5].

While a lot of the theory will be checked and equations calculated by hand, a computer software come quite handy for faster and longer calculations. It has also nice features for keeping track of the data made. This is essential when using iterative math processes. A part of the MSc thesis will be building a code in order to generate the data needed for answering the research questions. Further more it will be used to manipulate the result in order to make graphs and conclusion during writing of the thesis report and for the presentation of the results.

Experimental Setup
While the bulk of the research is building mathematical models and finding out analytical solutions for the stated problem, a careful considered experimental setup within the boundary of the stated problem might give some insight. At first, the boundaries of the stated problem will only confine to a uni-directional fiber FMLs as shown in figure 2.15. If the research goes well, some small or big angels of the fibers could be considered as shown in figure 2.16. An experimental setup, using DIC measurement of the induced plastic zone could show the difference in size, shape and the stress-strain field in using different fiber angels. Using the DIC equipment, it is possible to track points on the laminate and determine the stress/strain over the whole specimen. The complete peak stress profile as well as the change of it can be determined dependent on the spacial resolution of the camera used.

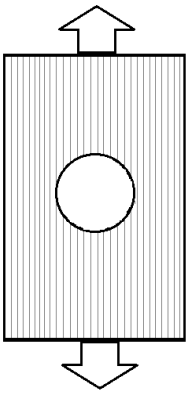

Figure 2.15: Illustration of an OHT-specimen with uni-directional fibers under tension.

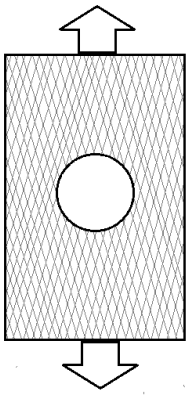

Figure 2.16: Illustration of an OHT-specimen under tension with fibers under an angle.

In figure 2.18 the DIC results are graphically shown used with geometry given in figure 2.17. In figure 2.18 on the back of the color gradient the speckle pattern can be seen. The positions of these speckles is tracked by the camera during loading. With this information the displacements of the speckle pattern can be defined and the strain field. Using high spatial resolution camera with the right parameters it is possible to capture the regions of high strain gradients surrounding stress concentrations at the edge of a hole.

The peak strain gradient has been determined by different feature-based DIC algorithms near a blunt notch. Tension and four point bending tests with blunt notch samples has been done. The tension experiment is shown in figure 2.17 and 2.18. The results of DIC tension experiment has been verified with an FEM model. The results correlate good as can be seen in figure 2.19 [8].

Schwinn et al [9] have used DIC method in order to determine the BNS of Glare3 under various biaxial loading. The experiments are done on Glare3 plate with a five-hole pattern. The experiments are motivated by the strength reduction of fuselage owed due to riveting. Figure 2.21 shows the DIC results

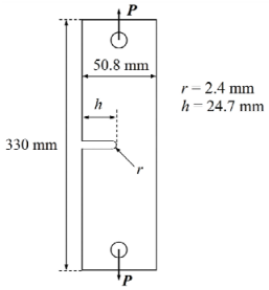

Figure 2.17: Specimen geometry used in the DIC experiment by Gonzales[8].

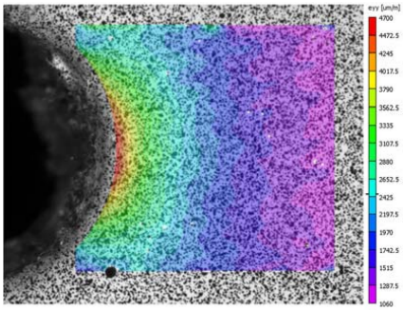

Figure 2.18: DIC results loaded at 100N[8].

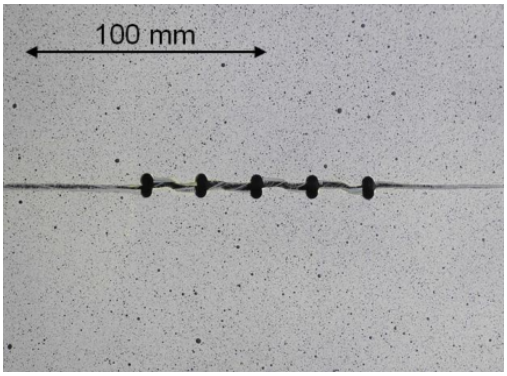

Figure 2.20: Failure of Blunt Notch with fibers direction less than 30° applied load[9].

of only tension applied of $\sigma_{xx} = 298MPa$ with fibers under 45°. The blunt notch failure of this experiment was at $\sigma_{xx} = 304MPa$. Most experiments failed similarly as shown in figure 2.20. For the off-axis angles greater than 30° used for the fibers, the experiments were aborted, because failure occurred at the clamps.

In order to use the DIC experiments for this MSc thesis, some considerations need to be made. Since the OHT-experiments mentioned in this literature study will be loaded vertically, a 2D DIC setup should be sufficient. While using a 2D DIC setup, it must be certain that no torsion, bending or other out of plane deformations should occur. Otherwise the results of the DIC might not be correct and a 3D DIC setup is advised.
Specific positions should be chosen in order to place some strain gauges. The data of the strain gauges will be used to verify the results of DIC experiments.
The DIC experiments are such that after a loading step, a picture is made by the camera and saved. If possible, it is advised to configure the DIC setup such that it makes continuous pictures of the experiments.

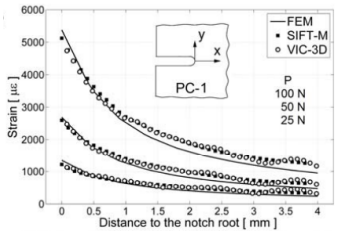

Figure 2.19: Results of FEM-model and the two different DIC mesh algorithms used in tension experiments[8].

A second experiment that might be considered is, the plastic zone induced delamination. In this experiment the delamination and the growth underneath the plastic zone will be investigated. Because the question remains whether the plastic zone will first induce a crack at the hole edge or whether it is possible to have delamination underneath the plastic zone before any crack initiation. This experiments may be essential in having data to compare with the analytical models. Thus these experiments will be used to correlate with analytical models explained in section 2.3. On the other hand, there are

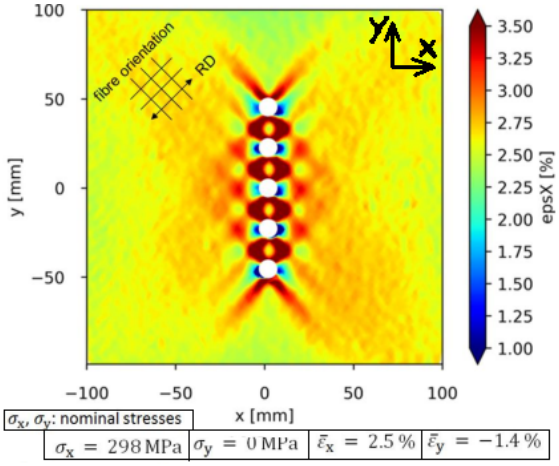

Figure 2.21: DIC results of the laminate with multiple holes[9].

a lots of data on empirical researches done for FMLs with a blunt notch. During the implementation of the said models, it will become more clear to what extent these experiments could be useful.

The optimum specimen geometry for the BNS of Glare has been determined by an experimental study performed by Bosker[20]. He concluded from the experiments on the effect of different $\frac{D}{W}$-ratios on the Glare grade 4A, that the optimum $\frac{D}{W}$-ratio for conclusive BNS specimens using in phisical experiments should be above 0.1. Because lower $\frac{D}{W}$-ratio would show neglegible change in the BNS if the diameter of the hole becomes smaller for the same net sample section.

2.6. Conclusions

The two models considered for this research are the Lekhnitskii- and the Strip Yield Model. In chapter 2 it is shown that the Lekhnitskii model is completely analytical. It doesn't consist of any iterative processes. Other scientist in the field, such as Westergaard, Kolosov, Muskhelishvili and Savin have made analytic solution for a variety of cut-outs in an infinite plate. In these solutions high loads are applied which in turn implies that the plastic zone encompasses the hole completely. The Westergaard function can be used if small scale yielding is assumed, but it is limited to calculating the plastic zone radius at a sharp notch.
Howland[21] solved the stresses in a strip including a hole under tension, only if the immediate neighborhood of the hole was considered. He achieved his by solving the biharmonic equation. He concluded from the results that the mathematical model is in good agreement with the experimental results. The mathematical model is only made for the elastic regime.
The main question of this research is how the peak stress profile changes when a plastic zone just starts at the edge of the hole. This is illustrated in appendix C in figure C.4. For the stated problem of this research, the solution has not yet been found, but a close approximation within an interval of loads applied has been made by Fayerberg[13]. He did have used an empirical variable to calculate the elasto-plastic contour L shown in figure C.4.
An issue is that not all the failure phenomena, such as fiber bridging and delamination, has been included in the Lekhnitskii model at this moment. A promising feature of the lekhnitskii model is that slip zones can be incorporated in the model. This represents also the reality of the plastic zone initialization. The Plastic zone initialize as small local slip zones in the crystal lattice, but this is beyond the boundary of the MSc thesis.

The Strip Yield Model is by definition an analytical model. Although it uses an iterative process to find the width of the yield strip in order to have convergence. It is possible to incorporate fiber bridging and delamination[6]. The issue with this model is, finding what is the best way to calculate the initial length of the yield strip. Yield strips must be long enough to capture the entire disturbed stress field due to the round hole. Thus the plastic zone. The SYM uses the concept of placing yield strips onto the location of interest. These yield strips can then be used as a superposition next to each other in order to determine stresses and strains at the midsection of the plate as well as the plastic zone shape and size.
For each yield strip the equilibrium and the compatibility equations need to be solved. For initialization and input of the model, the Proposal of Alderliesten(PA) will be used.
For the calculation of the laminate constant, the MVF and the CLT can be used. The SSCP and the Ramberg-Osgood equation can be used to determine the stress-strain curve of the laminate in the plastic regime. The numerical method for calculating the plastic stress and strain concentration factors[22], K_σ and K_ε, also mentioned in the Neuber postulate, can be used as verification for PA.

The analytical models will be validated by using DIC-experiments. The DIC experiments will be verified using strain gauges at specific positions of interest. Gonzales[8] used the Kirsch and the Creager-Paris equation for determining the distribution of strain concentration factor. He made a closed form solution fitted by a sinusoidal function. This in turn was used to correlate with the DIC results. Gonzales[8] concluded that with errors less than 3% the validity of DIC experiments has been confirmed.

The analytical model will be based on the Proposal of Alderliesten(PA). The proposal is that the imaginary elastic energy should equal the actual elaso-plastic energy of the material in its stress state. The PA makes use of Neuber's Postulate in conjunction with the SYM model to determine the change of the peak stress profile.
The σ'ε-curve of the FML laminate will be made using Hagenbeen model(HM) wich includeds the MVF.

3

Implemented Theory

In chapter 2 multiple options are given for some mechanism for the build up of the MATLAB model. These mechanisms are the input data, determining the SCF, plasticity etc. This chapter explains how the theorie is implemented. It will give some insights on the MATLAB code performing the calculations. In section 3.2, the σ'ε-curve of materials and laminate is explained. In section 3.3, the construction of the tangential stress distribution at the mid-section of the plate is discussed. At the end of this chapter, the determination of BNS is discussed as well as explaining the MATLAB code function and a code-diagram.

3.1. input

One of the boundaries set for this project, is that the input should only consist of the material/laminate properties. This section explains all the input needed for the MATLAB model. These inputs are the σ'ε-curve of the laminate, where the the rule of mixture is used for the fiber-resin layer and Ramberg-Osgood(RO) equation 3.3 for the metal layers. The MATLAB code has also the possibility to insert parameters for a prepreg given by the manufacturer. The MVF is used in conjunction with the Hagenbeek model in order to combine these σ'ε-curve into the σ'ε-curve of the FML. The tangential stress profile at the mid-section of the plate is constructed using Saff's method[11].

Matlab Code
The partial diagram in figure 3.1, shows the initial path taken for the BNS analysis. The numbers on the diagram follow each other in the Main MATLAB file. In order to initialize the BNS analysis the constituent of the FML plate needs to be chosen as mentioned in point 1. in the diagram. The ellipses are functions outside the the Main file. After choosing the materials, the function in the diagram labeled also point 1. will run the function 'FML-Buildup'. This function generates the constituent material properties of the FML. It is a database for the constituent materials of the FML. Other metals, fibers and resins can be added. The properties of the fiber-resin layer can be calculated via the rule of mixture or inserting data given by the manufacturer of the prepreg.

Following the main file, the thickness of the metallic and composite layers needs to be defined for each layer individually as well as the orientation of the fibers in degrees. This is shown as point 2. which also will run a function 'ABD-matrix'. As the name suggests, it will generate the ABD-matrix of the FML. The ABD-matrix will be used to calculate SCF_{inf} in point 6.

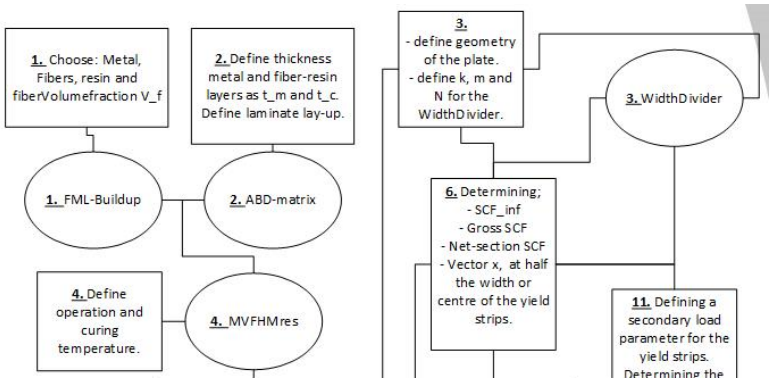

Figure 3.1: Partial diagram of the Matlab Model and the route taken.

In point 3. of the Main file, the geometry of the plate is defined, such as gross and nominal width and diameter of the hole. This section of the main file also consist of a function point 3. 'WidthDivider'. This function will divide the nominal width W_h of the plate into small strips for the use of the Strip Yield Model(SYM). Other parameters that need to be defined are k, m and N. These parameters are needed for the function 'WithDivider'. It uses the integral of the kwadratic function $y = k * x^m$ to divide the nominal width into small strips. The integral of this function is set equal to the nominal width and solved for the variable x. for example, $x = b$ shown in figure 3.2. The x-axis is then divided in N sections of equal length. Integrating $y = k * x^m$ with x_{n-1} and x_n as the integral boundaries gives the width w of the yield-strips. The integral boundaries are defined as,

$$x_{n-1} = \frac{(n-1) * b}{N} \tag{3.1}$$

$$x_n = \frac{n * b}{N} \tag{3.2}$$

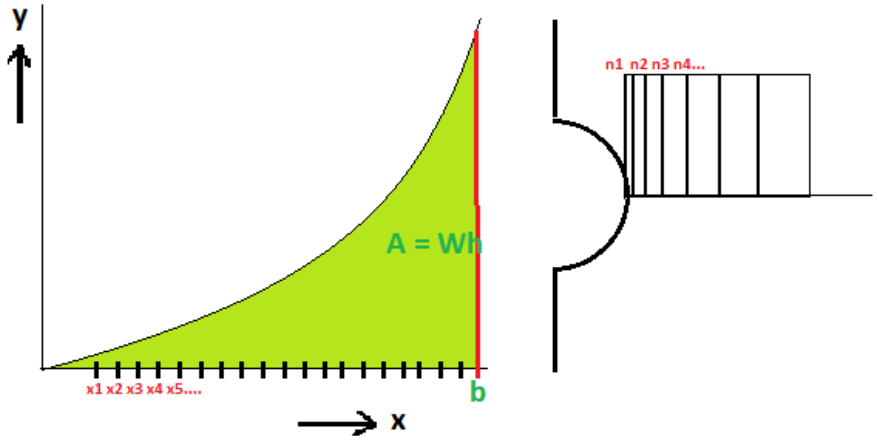

Figure 3.2: Division of the nominal width into yield strips.

At point 4. of the Matlab diagram, the curing and operational temperature of the laminate needs to be defined. The functions 'MVFHMres' determines the residual strength after curing and other mechanical properties of the laminate. The next section will explain this further in details.

3.2. Constructing the σ'ε-curve of the FML

The σ'ε-curve of the FML can be considered as a superposition of the σ'ε-curves of the constituent of the FML. The FMLs are usually divided into metallic and composite layers. But one can also divide the composite layer into the fibers and the resin layer or having various metal combination for the metallic layers, which each having their own σ'ε-curves. These σ'ε-curves can be combined using the MVF to determine the σ'ε-curves of the FML considered.
The σ'ε-curve of the laminate is needed for determining the strain energy at each load increments for each yield strip. In section 3.2.1, an analytical equation for the σ'ε-curve of the metal is presented. The research done by Pourhassan et al[10] is used to construct the σ'ε-curve. They did 2D and 3D DIC experiments on dogbone specimens loaded in tension. The DIC data correlates well with the extensometer. The graph data is digitalized as stress and strain vectors which consist of the full envelop of the elasto-plastic σ'ε-curve of various metals. One can load the σ'ε-curve of any metal into the MATLAB model. The Ramberg-Osgood equation is used to fit the data of these stress and strain vectors in order to have a continuous analytical equation for the σ'ε-curve of the metallic layer. The Ramberg-Osgood fit that is used for the final model is presented in figure 3.3.
The fiber-resin layer is considered as a brittle constituent defined by its Young's modulus determined using the rule of mixture. Thus the σ'ε-curve of the fiber-resin layer is assumed to be linear, although the specific σ'ε-curve of the resin layer is not linear for all the applied load. The MVF is used, as well as the coefficient of thermal expansion inducing the residual stresses combining the specific material layers, in order to construct the σ'ε-curves of the FML. In section 3.2.2, the construction of the bi-linear curve of the FML is explained.

3.2.1. Construction of σ'ε-curve for the metallic constituent

When the σ'ε-curves of the metallic layer is known from experimental data, an analytical expression for the σ'ε-curve of the metallic layer can be made using the research of Ramberg and Osgood[23]. There is a lot of σ'ε-curve data available on various tensile, compression and bending tests, on all kind of metals. The data is usually provided in graph like σ'ε-curve, and sometimes as stress and strain vectors.

The Matlab model works, when it is provided with an analytical expression for the σ'ε-curve of the material. Since test-data is always provided incrementally, the Ramberg-Osgood equation is used to fit the data and have an continuous analytical expression for the σ'ε-curve of the metal.

A proposed expression for obtaining an analytical function for the σ'ε-curve of a typical metal such as aluminum and steel alloys is given as,

$$\epsilon_{ep} = \varepsilon_{el} + \varepsilon_{pl} = \frac{s}{E} + K\left[\frac{s}{E}\right]^n \tag{3.3}$$

where, n is the strain-hardening parameter and K is the strength coefficient,

$$K = \epsilon_y \left(\frac{E}{s_y}\right)^n \tag{3.4}$$

Having the parameters K and n as a constant, equation 3.3 concurs with the expression suggested by Nadai[] as,

$$\epsilon = s/E + \epsilon_y \left(\frac{s - s_p}{s_y - s_p} \right)^n \tag{3.5}$$

On the condition that the proportional limit $s_p = 0$ and that the yield strain ϵ_y doesn't have to correspond with the yield stress s_y. In equation 3.5, The ϵ, s, ϵ_y and s_p are the elasto-plastic strain, applied stress, yield strain corresponding to the yield stress, yield stress s_y and the proportional limit respectively.

The proposed expression for the σ'ε-curve of metallic material is given as,

$$\epsilon_{ep} = \frac{s}{E} + a \left(\frac{s}{s_y} \right)^n \tag{3.6}$$

which is theoretically more convenient for plasticity. because in this equation, the yield strain ϵ_y does not correspond to the yield stress s_y. And the parameter a in the Ramberg-Osgood equation 3.6, can be seen as the 0.2% yield off-set when the applied stress is set equal to the yield stress s_y. The parameter a is then defined as

$$a = \alpha \frac{s}{E} \tag{3.7}$$

Accordingly, at the start of plasticity,

$$\epsilon_{el} = \frac{s}{E} \tag{3.8}$$

$$\epsilon_{pl} = \alpha \frac{s}{E} \tag{3.9}$$

Setting the Young's Modulus E and the yield strength of the aluminum as 72400 MPa and 345 MPa respectively, which is applicable to aluminum 2024-T3. The power law $x_1 y^{x_2}$ is used to fit the plastic part of the data, where 'x_1' will coincide with a and 'x_2' with $\frac{1}{n}$ in equation 3.6. Note that the second term becomes dominant when $\frac{s}{s_y} > 1$. But also when $\frac{s}{s_y} < 1$, the proposed expressions still implies small plastic strain, although the plastic strain would be insignificant.

As a first approximation α = 0.0091 and n = 9.4787 was obtained. A trial and error method is used for convergence. The values for the parameters are determined to be α = 0.0045, n = 14 and s_y = 345MPa. The blue graph in figure 3.3 presents the data for aluminum 2024-T3, taken from the research of Pourhassan et al[10]. And the red graph in figure 3.3 is the Ramberg-Osgood fit that has been made.

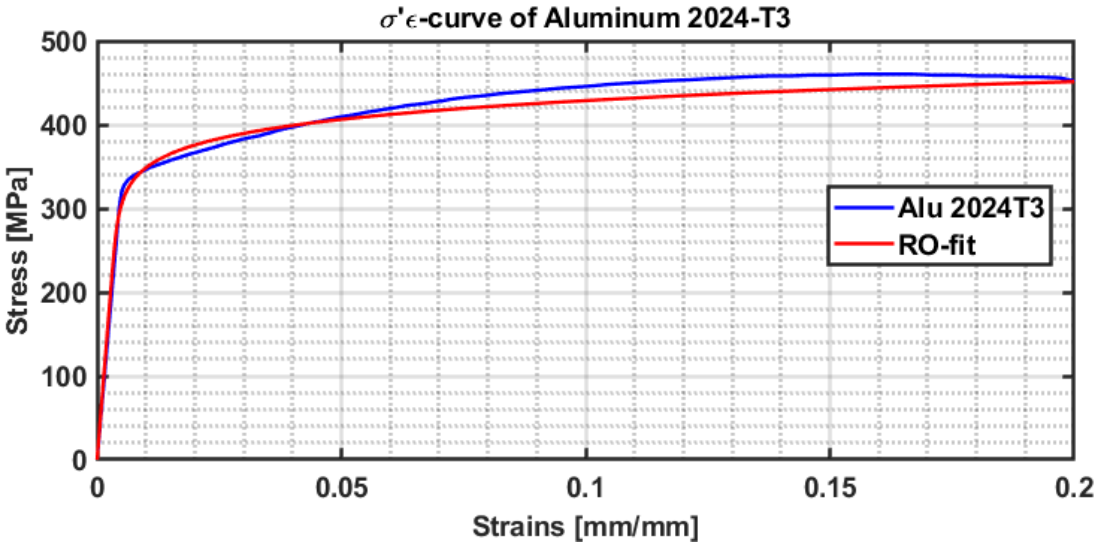

Figure 3.3: Stress-strain curve of aluminum 2024-T3[10] and the Ramberg-Osgood fit used.

3.2.2. Contructing the bi-linear curve of FML

the σ'ε-curve of the FML is made using the research of Hagenbeek et al[15]. The model will determine the σ'ε-curve of an arbitrary FML. First it will calculate the residual stresses after curing, using the curing and operational temperature of the constituents. Combining the σ'ε-curve of the constituents into the σ'ε-curve of the FML is done by implementing the MVF. In comparison to the SSCP of Hagenbeek, the stiffness of the aluminum in the plastic regime is not assumed to be constant. Therefore the bi-linear σ'ε-curve of the FML is not absolutely linear. The model that has been made, does not approximate the elasto-plastic curve of the FML as two linear curves. Though the variation is small.

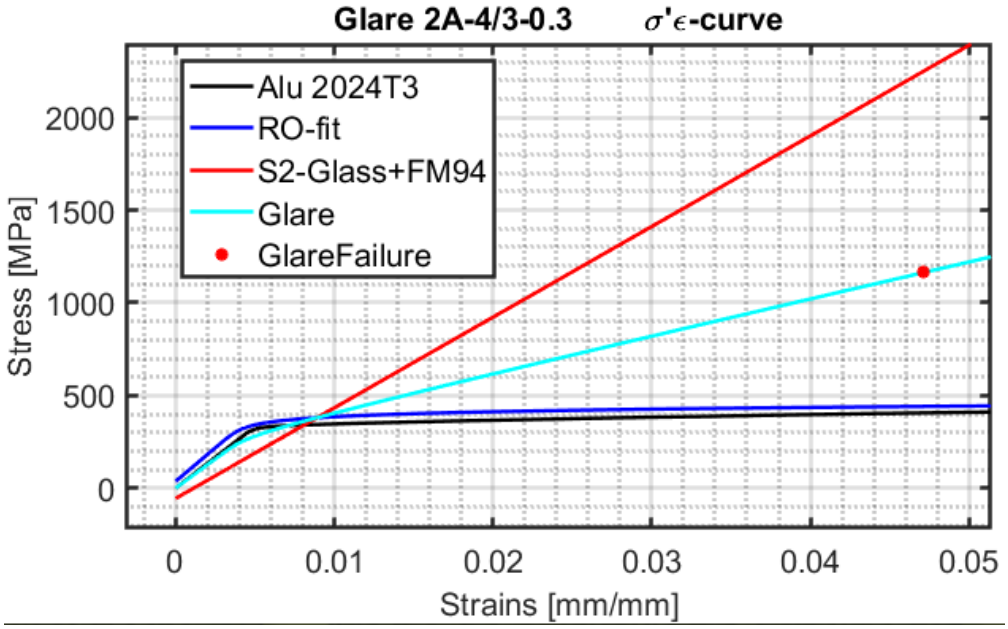

Figure 3.4: The σ'ε-curve of the FML and its constituents with and without the additional residual stresses.

The Young's modulus of the fiber-resin layers in the loading- and transverse directions can be calculated via the rule of mixture, or taken from the data-sheet of the manufacturer.

The residual stresses are determined with the curing and operating temperature, T_c and T_o respectively, and the coefficient of thermal expansion α of the constituents. Commonly the Coefficient of thermal expansion α of the metal is larger, which results in that the metal layers are loaded in tension and the fiber layers in compression after curing. The Glare 2A samples used for the experiments are not post-stretched. Therefore post-stretch is not taken into account, when developing the MATLAB code. With post stretching-procedures, the residual stress state of the metal en fiber-resin layers can be reversed. This is beneficial for fatigue loadings[2], but this is beyond the scope of the current research.

The residual stresses σ_r are defined as,

$$\sigma_{rX} = [E_m t_m (\alpha_m - \alpha_X) + E_{0^o} t_{0^o} (\alpha_{0^o} - \alpha_X) + E_{90^o} t_{90^o} (\alpha_{90^o} - \alpha_X)] E_X \frac{T_0 - T_c}{E_{lam} t_{lam}} \tag{3.10}$$

where X stands for either the property of the metal, the 0^o fiber- or 90^o fiber layer. The thickness of the layers are given by 't' with its respective index. The index 'lam' stands for the laminate property. Do note that the properties with index 90^o, means that the fibers are perpendicular to the direction of the loading, but the residual stress of this layer is defined parallel with the direction of the loading.

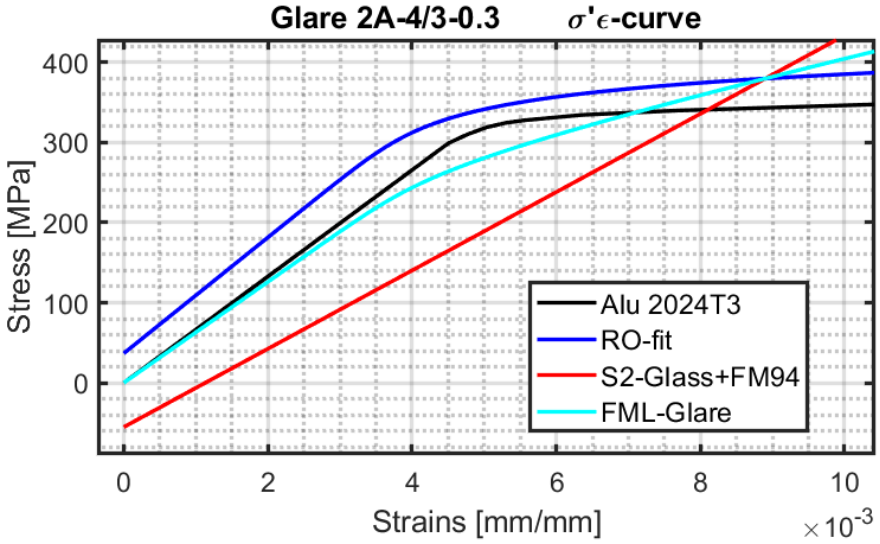

Figure 3.5: Close up on the elastic regime of the σ'ε-curve of figure 3.4

The residual stresses are added to their individual σ'ε-curve. Therefore, the blue graph representing the RO-fit of the aluminum 2024T3 is shifted vertically. In order to obtain the σ'ε curve of the FML, the individual σ'ε-curve are added together with the use of the MVF. It can be seen from figure 3.5 that after curing the fiber-resin layers are in compression and the metal layers in tension, when the strain is zero.

Matlab Code
The elasto-plastic σ'ε-curve of the metal is added in thee Matlab main file as a vector at point 5. 'Insert elasto-plastic σ'ε data...'. Using 'graph to data digitizer'-software, one could make a stress vector and its corresponding strain vector out of any graph. σ'ε-graphs of aluminium 2024-T3 presented by Pourhassan et al[10] is used for the Glare-type FML tests in this research.

The RO-equation consist of two parts. The second term is the plastic part. The powerlaw ax^b fits only the plastic part of the σ'ε data of the metal that is used. After adding the elastic and the plastic part of the RO-equation together, manuel tweaking and adjustment of the parameters are advised for a better fit.
Since the fiber-resin layers are assumed to behave elastic, only the stiffness modulus in the loading direction is needed for defining the σ'ε-curve of the prepreg layer. After the residual stresses and the MVF is determined, which is done at point 4. 'MVFHMres' as a function in the main Matlab file, The σ'ε-curve of the FML can be made. Also at point 5. the strain is defined when the fibers break, which is usually much lower than the metallic and resin constituents, is the point at which the Matlab software will determine BNS of the FML. Finally at point 5. 'Construction: σ'ε-curve of the FML'. The metallic and the fiber-resin σ'ε-curve are added together using the MVF.

3.2.3. Determining the SCF

The SCF_{tg} for a blunt notch in a finite width plate is the stress concentration factor, based on the gross area stress. This SCF is related to the SCF_{net} defines as the net-section area stress concentration factor by,

$$SCF_{tg} = \frac{SCF_{net}}{1 - \frac{2a}{W}} \tag{3.11}$$

The SCF_{net} is defined as a fit to the elliptical hole results in Peterson's handbook[11]. The fit is defined as,

$$SCF_{net} = 2 + f_1 f_2^2 + f_1 f_2^4 + 0.643 f_3 \left(1 - f_4^2\right) + 0.167 f_3 \left(1 - f_4^4\right) + 0.109 f_3 f_5 \left(\frac{2a}{W}\right) \tag{3.12}$$

where,

$$\begin{gathered} f_1 = \frac{SCF_\infty}{2} - 1 \\ f_2 = 1 - \frac{2a}{W} \\ f_3 = \frac{a}{b} - 1 \\ f_4 = \frac{4a}{W} - 1 \\ f_5 = 1 - \left[\frac{2a}{W}\right]^{100} \end{gathered} \tag{3.13}$$

And the SCF_∞ is the gross stress concentration factor for orthotropic infinite plates, which is the exact solution derived by Lekhnitskii[19]. The SCF_∞ is defined in terms of the ABD-matrix as,

$$SCF_\infty = 1 + \frac{a}{b}\sqrt{\frac{A11}{A66} - 2\nu_{12} + 2\sqrt{\frac{A11}{A22}}} \tag{3.14}$$

In order to determine the ABD-matrix of the FML, CLT is used, The CLT is explained further in appendix B.

Matlab Code
In point 6. of the Matlab diagram which coincide with point 6. in the Main Matlab file, the stress concentration factors are determined. In point 6. of the Main Matlab file there are various calculation on the SCF_∞ and SCF_{net} which is also often called SCF_{tn}. for further calculations the SCF_{net} and

SCF_∞ is used, because the difference was small. Furthermore the mid-value x-coordinates of the yield strips are defined as the position of interest for further stress and strain calculations. At point 7. the experimental data from the experiments on the Glare plates are loaded and in point 8. the applied load- as wel as the applied(gross) and nominal stress vectors are defined. In the elastic imaginary regime the applied load and stress must be far greater than what the material can expect. This can also be seen from the energy consideration of figure 3.9.

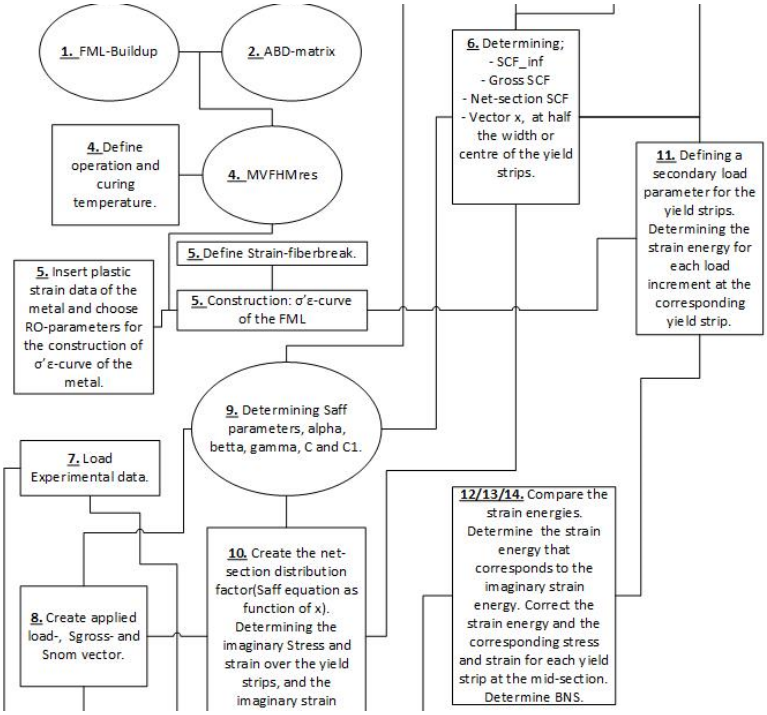

Figure 3.6: Partial diagram of the Matlab Model and the route taken.

3.3. Construction of SCF gradient over the mid-section area

Elastic tangential stress distribution at a circular hole in an infinite plate
The tangential stress distribution in an infinite plate can be represented by[1][14]

$$\frac{\sigma_\theta}{\sigma_{\text{inf}}} = 1 + \frac{1}{2}\left(\frac{r}{x}\right)^2 + \frac{3}{2}\left(\frac{r}{x}\right)^4 \tag{3.15}$$

At the notch root. i.e. $\frac{r}{x} = 1$, this equation simplifies to

$$\frac{\sigma_\theta}{\sigma_{\text{inf}}} = 3 = SCF \tag{3.16}$$

The SCF in a finite isotropic plate can be approximated by the equation of Heywood[1] given as equation 2.7. The derivation of the tangential stress distribution is presented by Howland[21] and approximation is given by Saff[5].

Elastic tangential stress distribution at a circular hole in a finite plate
For the construction of the distribution of the stress over the mid-section, the theory and equations

presented by Saff[11] is used. All research in various literature have concluded that the stress distribution at the mid-section has an exponential decay[11][2], starting from the SCF at the hole edge.

The form of the stress distribution from the hole edge over the mid-section is assumed to be,

$$\frac{\sigma_y(x, y=0)}{S_{nom}} = \alpha + \beta \left[1 + \frac{x-a}{\rho}\right]^{-\gamma} \tag{3.17}$$

where, $\rho = \frac{b^2}{a}$. The hole parameters can be seen in figure 3.7. The form is derived such, that it matches the following three boundary conditions;

1. SCF, The net-section stress concentration factor at the edge of the hole.
2. $C\frac{K_t}{\rho}$, The stress gradient at the edge of the notch[24].
3. The load across the net-section must equal the applied load.

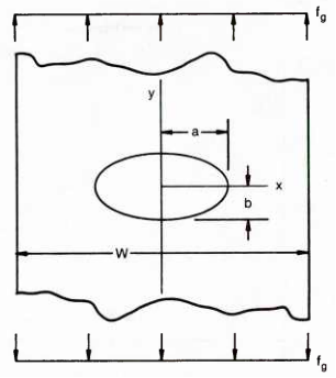

Figure 3.7: Open hole in a finite width plate.[11]

From condition 1,

$$\frac{\sigma_y(x=a, y=0)}{S_{nom}} = SCF = \alpha + \beta \tag{3.18}$$

From condition 2,

$$\frac{d\sigma_y(x=a,y=0)}{dx} = \frac{-CSCF}{\rho} \quad or \quad \gamma = \frac{CSCF}{\beta} \tag{3.19}$$

The parameter C in equation 3.19 is bounded to the finite width of the plate. Condition 3 is used to determine β and γ. Because β and γ are bound by the 2^{nd} condition, they should be solved iteratively as stated by saff[11].

The α defines the stress at the end of the plate considering equation 3.17. Subtituting for $x = inf$, results in that the second term in equation 3.17 goes to zero. This means that for the infinite case $\alpha = 1$, because the stress far from the hole edge must equal the nominal stress in the infinite case.

In order to start the iterative process, a vector for the parameter β is made. The parameters of Saff's equation needs to be all positive, since the net section stress distribution is known to be an exponential decay in the first quadrant of the graph. The net section SCF is defined in the previous section.

When the SCF is known and assuming that the SCF does not change under elasto-plastic loading, the parameter α can ben calculated by rewriting equation 3.18 as,

$$\alpha = SCF - \beta \tag{3.20}$$

Afterward, equation 3.19 from the second condition is used to calculate γ, which also will satisfy the stress gradient at the edge of the hole $C\frac{K_t}{\rho}$, given by Seely and Smith[24].

Condition 3 is used for convergence of the parameters. For every β, an α and γ is calclulated and the net-section load is compared with the load applied. The convergence is found when the applied load and the net-section load are equal.
This convergence depends also on the parameter C in equation 3.19. The expression for C is chosen to be,

$$C = \left(\frac{1}{2} + \frac{5}{3}\sqrt{\frac{b}{a}}\right)\sqrt{1 - \frac{2a}{W}} \tag{3.21}$$

For the infinite case, only the term between the brackets in equation 3.21 is to be used. Where b/a is the aspect ratio of the hole. The term $\sqrt{1-2a/W}$ is the finite width correction factor of Koiter [25]. As a first estmination equation 3.21 can be used to find C, which is quite close to the real solution. For greater D/W and orthotropicity, C in equation 3.21 will deviate more from the real solution. Therefore a variation of C is used for the calculation of the parameters α, β and γ. For each value of C, the net-section stress of the matlab solution and the DIC experiments is compared. The value of C which gives the lowest mean deviation in percentage will be used as the final solution for C.

Matlab Code
Point 9. of the Main Matlab file is the function which determines Saff-parameters. The function 'saff-parameters' will use the conditions mentioned, in order to calculate the parameters α, β and γ. This solution is still done only using equation 3.21 to calculate the value for C.

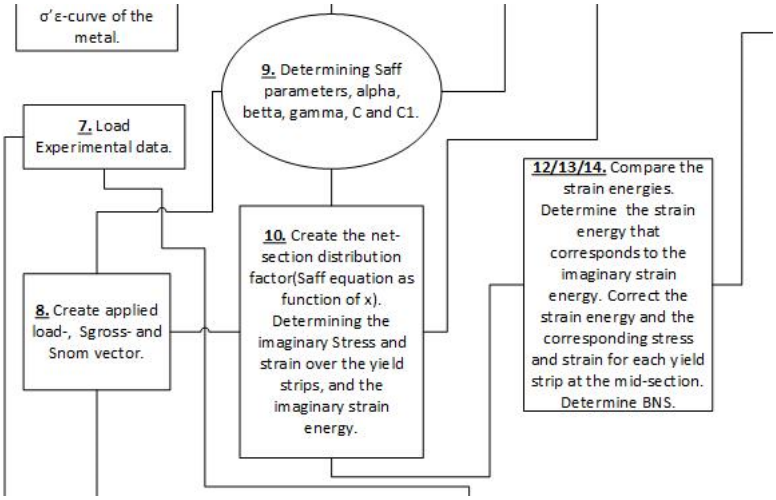

Figure 3.8: Partial diagram of the Matlab Model and the route taken.

3.4. Elasticity, Plasticity and BNS failure

In the previous sections, the inputs are given. In this section, it is further explained how these inputs is used to calculate BNS failure. This calculation is based on the method proposed by Alderliesten[5] mentioned in the literature study.

First, the mid-section of the plate is divided into strips. The quadratic function $k * x^m$ is used for this purpose, but any quadratic function could suffice. The integral of the quadratic function is used for the division of the mid-section in such a way, that the strips with smallest width are layed down at the hole edge and the largest at the end of the plate. The mid-point of each strip is the point at which the value's of interest are determined.

The SCF gradient over the mid-section is multiplied by the S_{nom}, and so the mid-section stress distribution is determined for each load increment. At first this is done elastically. Using the laminate Young's modulus E_{lam} in the loading direction, the strain for each strip is calculated. This is done for all load increments. These stresses and strains are further called the imaginary stresses and strain of the yield strips. From these, the imaginary strain energy can be determined.

At the same time, the imaginary strain energy is compared with the real strain energy from the σ'ε-curve of the laminate for each yield strip. This comparison is used to correct the stress and strain of the yield strips. During the elastic part, up to the yield point of the aluminum, the correction is minor. Because the E_{lam} follows the elastic part of the σ'ε-curve of the laminate. As can be seen in figure 3.9, each imaginary load increment shown in green, is compared to the real elasto-plastic curve by comparing the area under the curves in order to find the real stresses and strains of the yield strips.

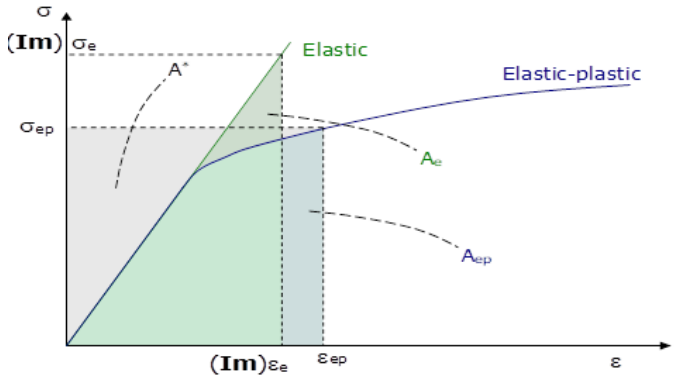

Figure 3.9: Energy consderation using the stress-strain curve of the material(e.g. structure)[5].

The BNS is taken as, when the first strip at the edge of the hole hits the failure point of σ'ε-curve of the laminate, defined by the break strain value of the fibers. In this manner, the whole mid-section stress distribution, from the hole edge, can be determined for each load increment.

Do note that during plastic deformation of the yield strips, there is no equality anymore between the far field load and the mid-section load. In order to achieve equality, the mid-section stresses are integrated over the mid-section of the laminate. A factor 'r1' is determined between the far field load and the mid-section load for each load increment. The factor 'r1' is then multiplied with the mid-section stresses in order to ensure equality between the far field load and the mid-section load.

Matlab Code
Point 10. of the Matlab diagram and also in the Main Matlab File, the imaginary stresses, strains and the imaginary elastic strain energy is calculated. This is done for all the applied load increments. This will make the matlab code faster and more efficient. At point 11. a secondary load is defined. This

secondary load should have smaller increments than the previous applied load, in order to have a better convergence for the comparison of the imaginary deformation energy and the real deformation energy. The secondary load is used to calculate the real elasto-plastic deformation energy from the analytic σ'ε-curve of the FML laminate. Again, for all the secondary load increment, the real elasto-plastic deformation energy is calculated, in order to have a better and efficient Matlab software.

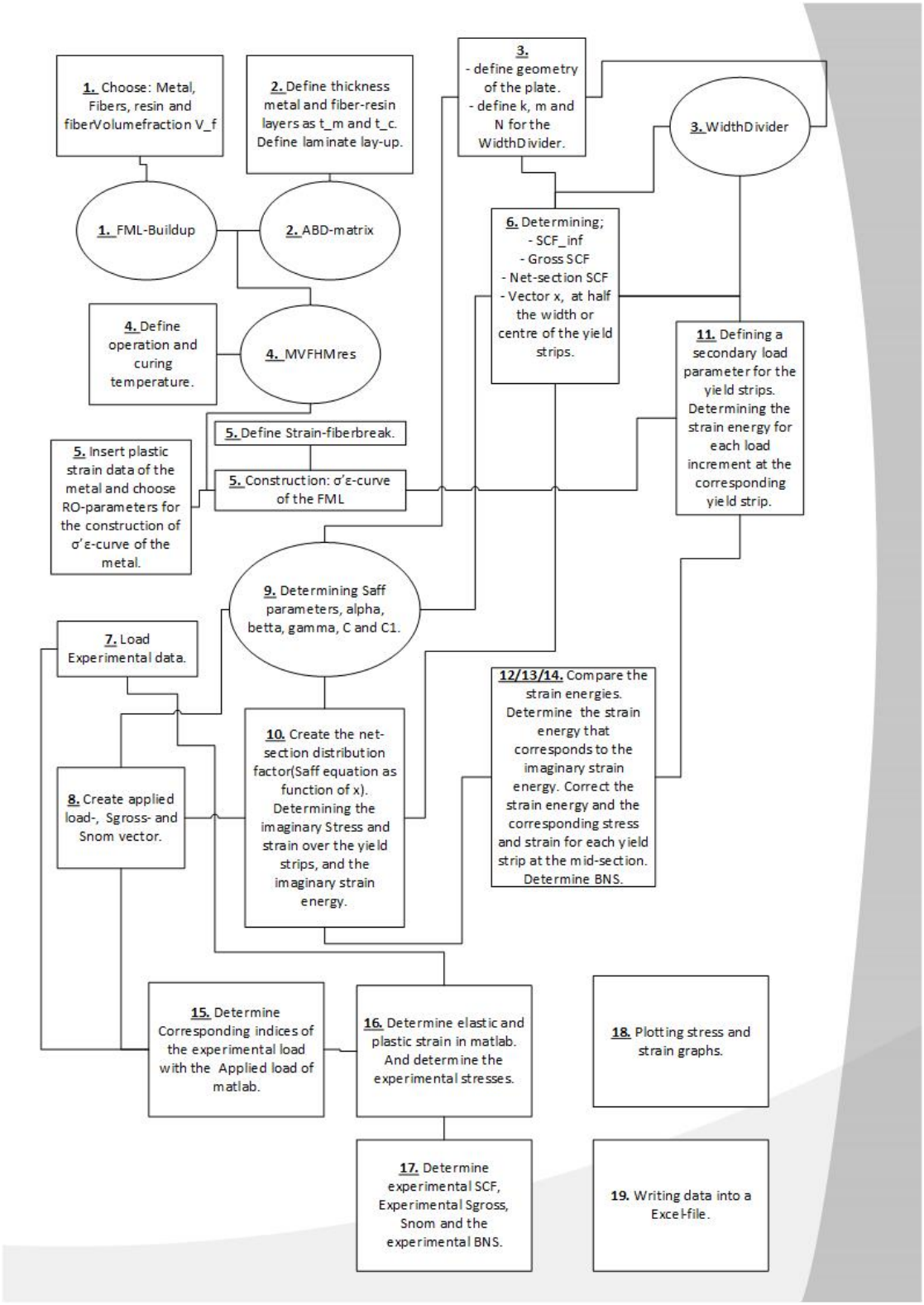

Figure 3.10: The route taken by the Matlab algorithm.

4

Experimental Procedures

In order to validate the analytical solution, experiments has been done on Glare samples with various hole diameters. In this chapter the experimental procedures are explained. There were some setbacks in the first batch of samples. From these, a new batch was made, which have taken the problems and their solution into account for the second batch.

4.1. Specimen and fixture design

The specimens are made from Glare $2A-4/3-0.3$ with geometric specifications given in table 4.1. All the specimens have round hole with smooth edges. The specimens are cut $1cm$ larger on all sides. Then they are machined till the right size. So that means that each sample is cut to a witdh of $180cm$ from a larger Glare plate. This is done because during cutting, an out-of-plane bending/rotation is applied on the specimens edge, which causes small delamination and damage to the fibers and aluminum layers at the edge.

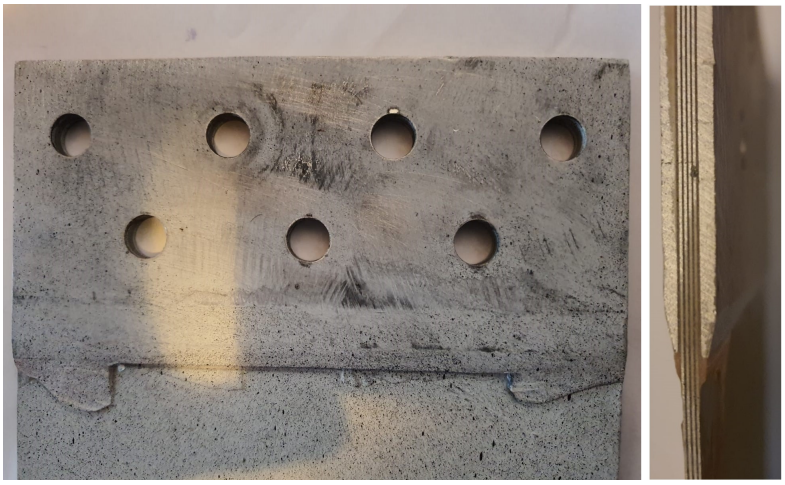

Figure 4.1: Aluminum tabs on the specimens.

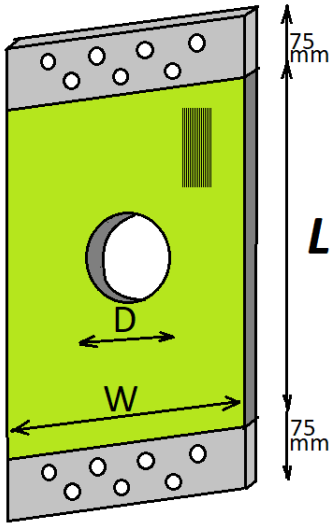

Figure 4.2: Sample geometry and dimension. The fibers are aligned with the loading direction

The specimens are loaded only in tension. The available static tensile testing machines had clamps which uses oil pressure to grab and hold the specimens. For good clamping of the specimens, the inside of the clamps have rugged surfaces. In this manner, the load is transferred via shear onto the specimen. This would work fine when testing metals or composites. But problems arise when testing Glare specimens. Using not enough pressure, the clamps will slide of the Glare specimen. Using too much pressure will crush the fiber-resin layers. Even when using large clamping area of 100mm by 150mm, The problem was not solved. Therefore it was chosen to load the specimens in tension via bolts. Since the bearing strength is relative low compared to the overall strength of the Glare specimens, aluminum tabs were adhered to the Glare specimens. Consequently this increases the bearing strength of the hole. And the aluminum tabs together with the adhesive provides a better load transfer from the bolts onto the Glare specimens. The Glare specimens are also loaded much more homogenous from the clamps.

	D	W	L
1	45	150	370
2	60	150	370
3	75	150	370
4	90	150	370

Table 4.1: This table shows the four different hole diameters for Glare $2A-4/3-0.3$. The length of the aluminum pads are not included.

The size of the aluminum tab were chosen to be $75x150mm$, with a thickness of just under $2mm$. The horizontal and vertical pitch of the bearing holes are 40mm and 25mm respectively. With more than 15mm clearence from the edges. This would provide sufficient strength against bearing failure at the holes, but also the surface area's were sufficient against shear failure at the bonds. In figure 4.1 and 4.2, the hole pattern of the clamps can be seen. For a better performance and loading, the second row of the grid holes are chosen to have an offset of half the pitch length of the first row. The side view of the aluminum tabs and the bond-line can be seen in figure 4.3. The bond-lines are quite equal in thickness over the bond area. In order to reduce the stress concentration, the edges of the aluminum tabs er made at an angle. This can be seen on the left side of the tabs in figure 4.3.

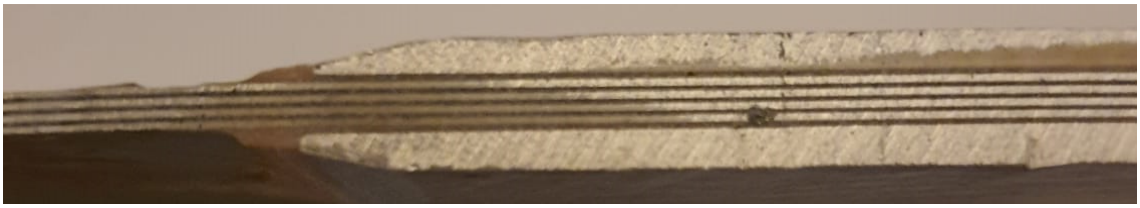

Figure 4.3: Side-view: Aluminium tabs on the specimens.

4.2. Specimen Fixture

For the experiments, the MTS-250KN fatigue bench was used. In order to use it for static tensile test, the loading parameter is set as a ramp with a displacement rate of $0.01\frac{mm}{s}$. The loading process is displacement controlled. Figure 4.4a shows how the specimens are inserted in the MTS bench. The bolts at the clamps are loose. So in doesn't transfer any shear force. This means that the load transfer from the clamps to the specimens are only through bearing, which makes it much more simple to determine the amount of boltholes needed en the geometry of the aluminum pads.

(a) This picture shows how the speciment is inserted in the MTS-250kN bench.

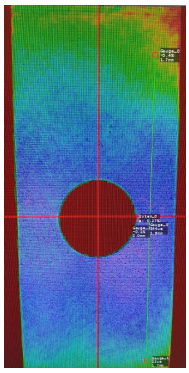

(b) Field of uncertainty due to the focus, lighting and aperture settings of the camera and the chosen speckle pattern.

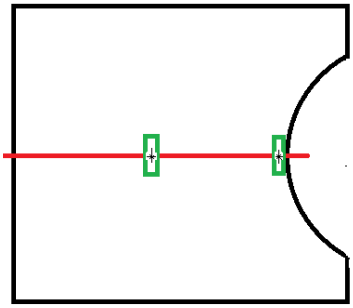

(c) Positions of the strain gauges

Figure 4.4: Specimen fixture in the MTS 250kN bench, DIC camera showing the red cross-head onto the field of uncertainty, and the positioning of the strain gauges for each sample.

In front of the specimens, at the same height of the hole in the middle, the cameras and lighting are set up. The red cross-head shown in figure 4.4b is used to center the cameras onto the center of the specimen.
After calibration of the DIC cameras, the field of uncertainty can be determined. It is a measurement of how well the cameras can follow the reality. The field of uncertainty depends on the experimental setup and image acquisition.

The experimental set-up is based on the positioning of the sample, camera and lighting. The positioning of the sample should be in the field of view of the cameras and the depth of view of the lenses. The target on the samples, which is the mid-section of the glare plate, should be in focus of the lenses. The aperture must be optimized relative to the lighting and the exposure time.
The quality of the image acquisition depends on the speckle size en contrast, which consequently could reduce the noise. The light source can also be considered as a heat source. Heating up the environment surrounding the experiment, may distort the images taken by the cameras. Therefore, it is advisable to have the lighting at an obligue angle relative to the specimen. After calibration of the camera, the field of uncertainty was determined by the Vic 3D software, which can be seen in figure 4.4b. The field of uncertainty depends on the camera settings and the speckle pattern. It is used by the software to advise or suggest a appropriate subset and step size. The bluish purple color means that the chosen DIC setup is sufficient for the target of interest.

For all the specimens two strain gauges are used. They are adhered on the back of the specimens. The position of these strain gauges are, one strain gauge right next to the hole and another one at the middle of the mid-section of the plate. Furthermore, Using the Vic-Gauge 3D DIC software, it was possible to apply virtual strain gauges and a virtual extensometer. With this option, one could follow real time strain measurements of the real and virtual strain gauges when the experiments are on going.

5

Experimental Results

5.1. Material properties of Glare and its constituents

OHT-experiments have been done on $GL2A-4/3-0.3$ samples to validate the MATLAB model. The input of the MATLAB model consists of the mechanical properties of the constituents. These are shown in table 5.1. The mechanical properties of the fiber-resin layer is shown in table 5.2. The values in table 5.2 are from the pre-preg given by the supplier. The mechanical properties can also be calculated from the rule of mixture for the fiber-resin layer, but that gives usually an overestimation on the mechanical properties. Therefore, the values for the mechanical properties of the pre-preg layer is implemented as given by the manufacturer due to the DIC experiments would be done on Glare plates provided by Airbus. If the rule of mixture would be chosen, then it is also advisable to use the knock-down factors for manufacturing of the pre-preg.

	Young's Modulus[MPa]	Poison-ratio	G[MPa]	CTE [m/mK]	S_{yield}[MPa]
Aluminum 2024-T3	7.24e4	0.3	2.8e4	2.34e-5	345
Glass S2	86900	0.23	3.7e4	2.88e-6	
FM94	2000	0.33		10e-5	

Table 5.1: FML-constituents

	ELc [MPa]	ETc [MPa]	GLTc [MPa]	ν-LTc	S_{ult} [MPa]	$\varepsilon_{ult}[\frac{mm}{mm}]$	CTE_0[m/K]	CTE_{90}[m/K]
Fiber-resin layer	48900	5.5	2900	0.27	2200	0.0472	6.15e-6	2.62e-5

Table 5.2: Data used for the fiber-resin layers.

The FML-properties calculated for the Glare $GL2A-4/3-0.3$ are shown in table 5.3. The $\varepsilon_{ult} = 0.0472$ is the strain at which the S2-glass fibers will break. This is also taken as the failure mode at the edge of the hole for the BNS. The ABD-matrix of the laminate shown in equation 5.1 is made by using CLT. Dividing the A_{11} by the thickness of the laminate t_{lam} gives 6.7e4 MPa, which is much higher than E_{lam} from table 5.3 determined via the MVF. Therefore it was chosen to use E_{lam} from table 5.3 for further calculations, since this value is much closer to the values found in the literature on Glare FMLs.

FML-properties	MVF = 0.601		Residual stresses			
Glare 2A-4/3-0.3	E_{lam}[MPa]	t_{lam}[mm]	Sr_c[MPa]	Sr_m[MPa]	S_{ult}[MPa]	ε_{ult}
	6.30e4	1.998	-55.3	36.8	1164	0.0472

Table 5.3: FML-Properties

$$ABD = \begin{bmatrix} 134495 & 28642 & 0 & 0 & 0 & 0 \\ 28642 & 95476 & 0 & 0 & 0 & 0 \\ 0 & 0 & 64371 & 0 & 0 & 0 \\ 0 & 0 & 0 & 47511 & 11684 & 0 \\ 0 & 0 & 0 & 11684 & 38948 & 0 \\ 0 & 0 & 0 & 0 & 0 & 25823 \end{bmatrix} \tag{5.1}$$

5.2. Data collected

In this section the result of the matlab model and the experimental result of the DIC will be discussed. Table 5.4 shows the parameters determined for the four samples used.

Saff's Parameters					
Sample	SCFt	α	β	γ	C
D45	2.35	0.5601	1.7924	2.4150	1.84
D60	2.24	0.2920	1.9444	2.2313	1.94
D75	2.15	-0.3776	2.5285	1.7183	2.02
D90	2.09	-1.5271	3.6167	1.3635	2.36

Table 5.4: The four samples and their parameters for the mid-section stress distribution. The sample name D45 stand for the 45mm diameter hole. All the plates have a width of 150mm.

Figure 5.1 the the global $\sigma'\varepsilon$-curve of the four samples. The distribution of the SCF_t over the mid-section is made via Matlab and the global $\sigma'\varepsilon$-curve is taken from the DIC-experiments. The distribution of the SCF_t over the mid-section are shown in figure 5.2. The increase in the hole diameter results in a smaller SCF_t at the edge of the hole but also the distribution of the SCF_t over the mid-section of the plate becomes less steep. The global $\sigma'\varepsilon$-curve of the laminate has a more gradual transition from elastic onto the plastic regime. The plastic regime is more or less linear as expected, due to the almost typical bi-linear $\sigma'\varepsilon$-curve of the FMLs.

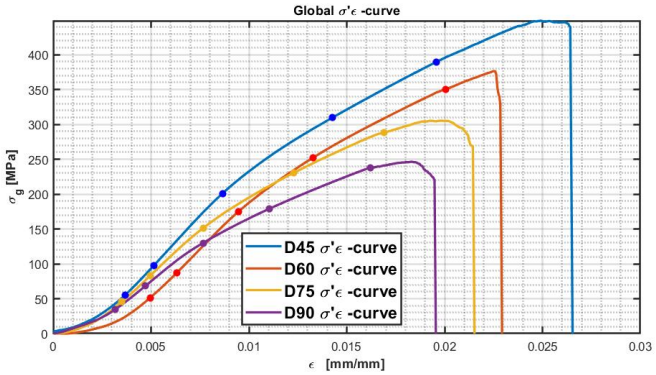

Figure 5.1: Global $\sigma'\varepsilon$-curve provided by the MTS250.

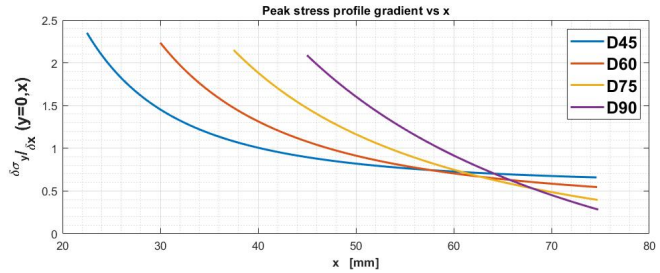

Figure 5.2: Net-section stress gradient.

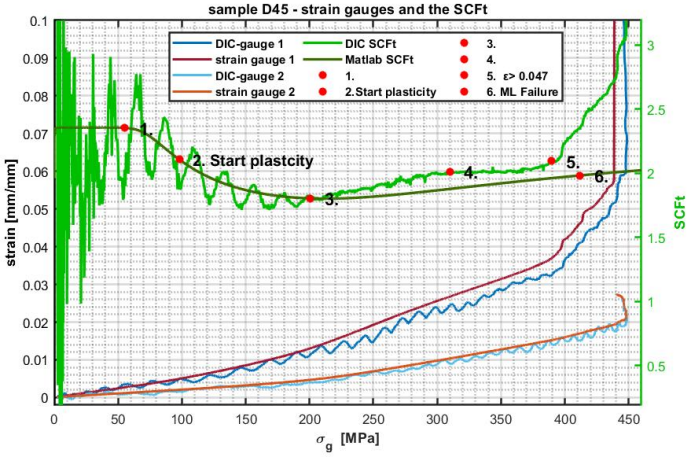

Figure 5.3: DIC and Matlab SCF_t including the data of the physical and digital strain gauges of sample D45.

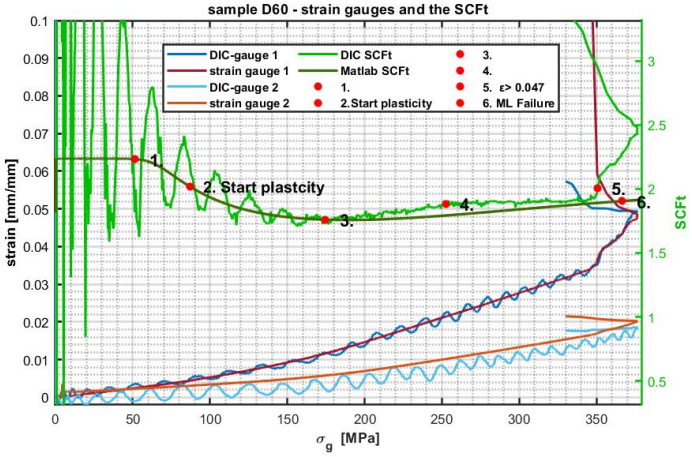

Figure 5.4: DIC and Matlab SCF_t including the data of the physical and digital strain gauges of sample D60.

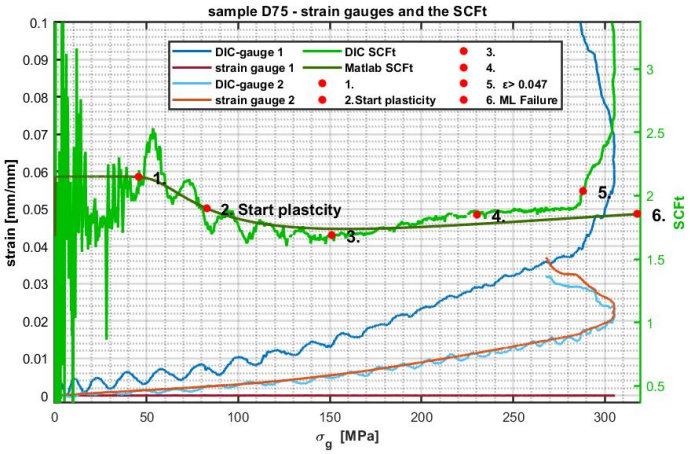

Figure 5.5: DIC and Matlab SCF_t including the data of the physical and digital strain gauges of sample D75.

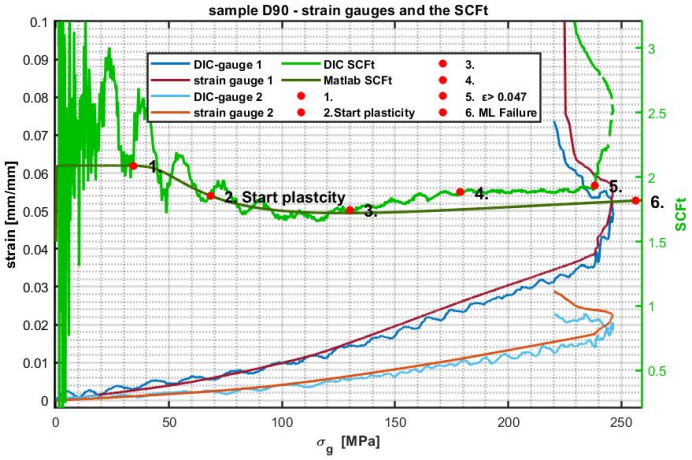

Figure 5.6: DIC and Matlab SCF_t including the data of the physical and digital strain gauges of sample D90.

In figure 5.3 till figure 5.6, the experimental SCF_t taken from the DIC experimental data, the SCF_t determined by the MATLAB model and the data of the digital and physical strain gauges, are shown.

In the elastic regime there is a lot of noise. Though near the plastic regime the noise dampens out. Further more in the plastic regime the noise isn't visible anymore. It could be that due to high tensions of the plate in the MTS-bench, the vibration caused by the ambient factors, such as external lights or other experiments done nearby, doesn't have any influence on the plate at higher applied load increments. Another explanation could be that the sensitivity and resolution of the cameras used, is not enough at lower applied load.

All SCF_t graphs shows a large curvature in the plastic regime like a minimum. For example seeing figure 5.3, the graph rises from point 3 till point 4. After that it stays more or less constant. The experimental load differences shown in figure 5.7 stays more or less constant at a zero value, which it is suppose to be, until around point 5 of the SCF_t graphs. After that, the load difference becomes greater and the SCF_t also increases, while the global $\sigma'\varepsilon$-curve of the sample D45 still is increasing, but at a decreasing rate till $S_g = 450$. The global $\sigma'\varepsilon$-curve has then a more or less constant value, while the load difference between the applied load and the net-section load becomes very high. The same trend can be seen in all the experimental SCF_t graphs.
The Matlab SCF_t coincide well with the DIC results in the elastic and the early part of the plastic regime. But the constant value of the SCF_t at the second part of the plastic regime between point 4 and 5 is not observable. Near failure, the DIC and the Matlab SCF_t diverge completely.

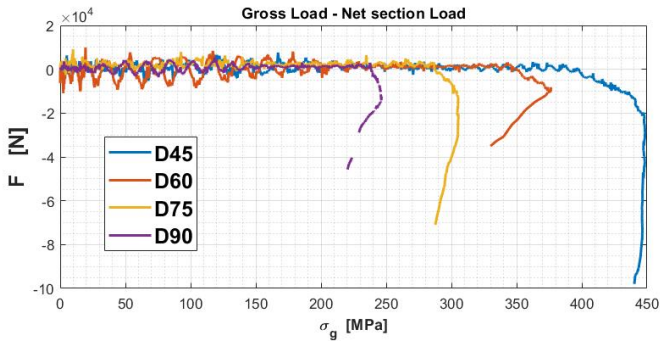

Figure 5.7: DIC Load differences between the applied and net-section load of the four samples.

The six red dots or points from the SCF_t graphs are also shown in the $\sigma'\varepsilon$-curve of the FML made with the MATLAB model in figure 5.8 and 5.9. Point 1 at around 0.3% is when the cyaan $\sigma'\varepsilon$-curve of the Glare diverges from the linear elastic Young's modulus of the FML in figure 5.9. Point 2 is taken as the onset of plasticity which is close to the 0.2% offset strain. from point 2 to point 3, the SCF_t graphs has a small curvature like a minimum. This is due to beginning of strain hardening of the aluminum, that causes the decreasing rate of the SCF_t graphs after point 1 to increase. Due to significant strain hardening the SCF_t graphs increases from point 3 to point 4. The constant value from the graph between point 4 and point 5 may be due to widening of the plastic zone towards the edge of the plate, while the plastic zone near the hole edge doesn't grow significantly anymore. The cluster of data point of the samples in figure 5.8 and 5.9 are from the 5 red points in the SCF_t graphs. The last dot in figure 5.8 is actually the 0.047 strain taken as the failure for the BNS experiments, which is shown as point 6 in the SCF_t graphs. The one data point is actually the four failure points of the four samples on top of each other.

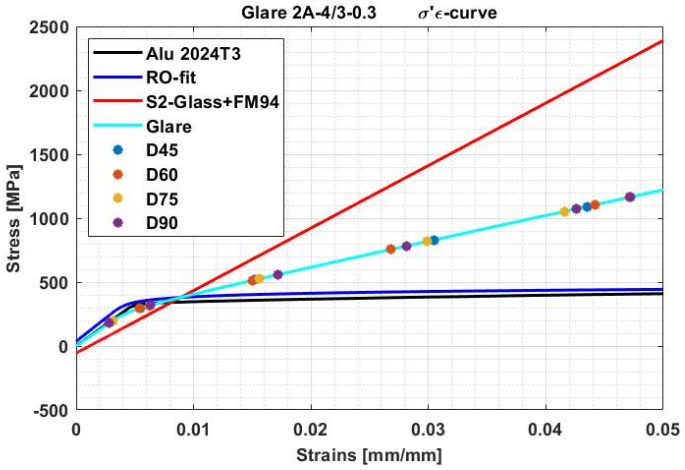

Figure 5.8: Global $\sigma'\varepsilon$-curve of the FML from the MATLAB model.

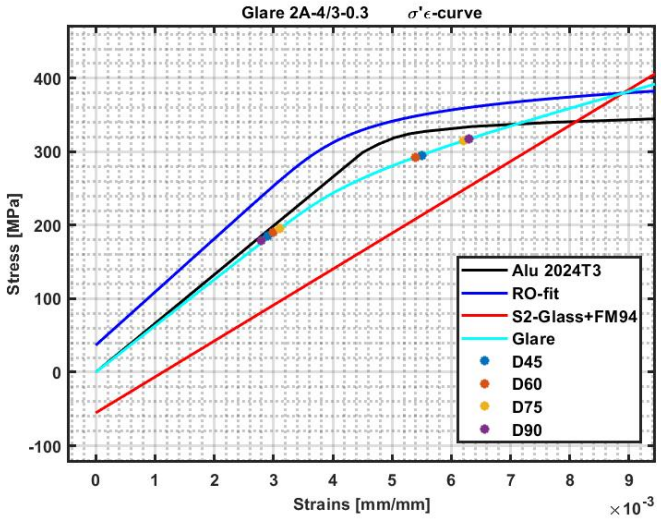

Figure 5.9: Elastic part of the Global $\sigma'\varepsilon$-curve of the FML from the MATLAB model.

In the the SCF_t graphs of figure 5.3 till figure 5.6, the digital DIC and the physical strain gauges are shown. During the experiments it was possible to add real time digital strain gauges. These were used to compare with physical strain gauges. As can be seen from the graphs, they follow each other very close. The first strain gauges are attached at or close to the edge of the hole, while the second strain gauges are attached at the center of the mid-section of the plate. They all show the same trend. The first strain gauges have a more or less linear elastic part. At the onset of plasticity the graphs is increasing. Far into the plastic regime, the graphs are still increasing but at a decreasing rate. Near the end of the DIC experiments, when the global $\sigma'\varepsilon$-curve from figure 5.1 goes more or less horizontal just before failure, the strain gauges shows a strong increase in strain. That is when the material shows no load caring capability. The second digital strain gauges shows noise at all the load increments, while the noise of the first strain gauges dampens out at higher load increments.

The mid-section stress or the peak stress profile for the samples used are presented in appendix A. These are from the DIC experiments and the Matlab model as well as the data from the physical strain

gauges. In the elastic regime, the DIC-curves shows unusual behavior in all the samples. It has some unpredictable bumps. At higher load increments, these bumps fades away. These may be due to low measurement resolution and accuracy of the DIC cameras in the elastic regime. As can be seen from the graphs, the DIC and MATLAB curves as well as the strain gauges, which follows each other very well. Close or near the end of load increments, the first strain gauge becomes zero it seems. That is because the strain gauge can't take the high deformation induced and gets broken.

Close to failure, when the DIC-curves hits the $\varepsilon = 0.047$(shown in the title of the graphs), the DIC and the matlab curve diverges, while the strain gauges still follows the DIC-curves. An interesting phenomena is that all the DIC-curves decreases curvature downward near the edge of the plate.

5.2.1. The blunt notch strength

The net-section stress concentration factor determined using the elliptical fit from Peterson[11][26] coincide well with the equation of Heywood. There is a small divergence between the Heywood equation 2.7 and the elliptical fit as can be seen in figure 5.10. This is due to the orthotropicity of the laminate using the CLT together with the analytical solution of Lekhnitsky for gross SCFtg in an infinite orthotropic laminate.

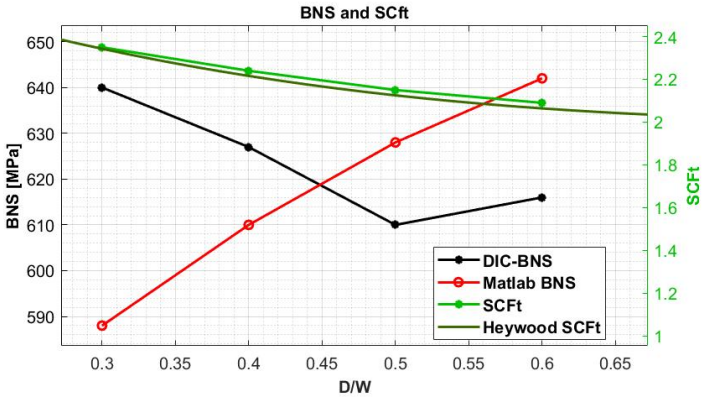

Figure 5.10: The calculated net-section stress concentration factor via equation 3.12, the Heywood equation 2.7 and the BNS results.

The BNS of the samples determined via the DIC-experiments and calculated via Matlab model are shown in figure 5.10. The blunt notch strength of Glare 2A-3/2-0.3 is 694MPa[2]. The increase of the aluminum layer would result in an increase in the BNS. Therefore, the BNS of the Glare 2A-4/3-0.3 should be at least 694MPa or higher[2]. Although the curve of the DIC results are in a decreasing trend as expected. Though, using the same range as in figure 2.6, the DIC result would seems to be almost constant with a small decrease for the same d/W-ratios till $D/W = 0.5$. The DIC results for the BNS of Glare 2A-4/3-0.3 is below the 694MPa and the results in figure 2.6[3].

Interestingly, it does seems that a greater $D/W > 0.5$ results in increase in the BNS, which is in agreement with the results of figure 2.6. But this cannot be confirmed, since there is only one data-point above $D/W > 0.5$ as can be seen from figure 5.10.
As mentioned by Roebroek[3], assuming that the net-section SCFt describes the BNS, a higher SCFt would result in a lower BNS or a lower SCFt would result in a higher BNS, which is not in agreement with his experimental results in figure 2.6. This means that the BNS does not completely depend on the SCFt for all the D/W-ratios considering FMLs. The DIC results shown in figure 5.10 agrees with the experimental results of Roebroeks[3].

For small hole diameter, the SCFt is higher resulting in a lower BNS. But a smaller diameter also results in a steeper mid-section stress gradient near the hole edge as can be seen from figure 5.2. The higher stress gradient for smaller hole diameter would show a smaller plastic zone. The significant shear stress between the metal and the fiber-resin layers are most likely to create much sooner local delamination and therefore postpone failure due to the fiber bridging mechanism resulting in a higher BNS.

For large D/W-ratios above 0.5, the BNS increases. While the decrease in SCFt is minor for greater D/W-ratios, the increase in BNS is much stronger. Roebroeks[3] explained that due to plasticity in the metallic layer and the inward movement of the ligaments the SCFt decreases even more near failure which would result in a higher BNS. Thus, it can be concluded that the term (W-D/W) has a much stronger influence on the BNS than the SCFt at higher D/W-ratios. This is better shown in the Matlab result for the BNS in figure 5.10. The Matlab model only accounts for plasticity of the aluminum and not delamination and the fiber bridging mechanism.

Saff's paramters

Figure 5.11 shows the values determined for the parameters used for determining the mid-section stress concentration distribution. Note that C increases, while if C would be determined using equation 3.21, it will have a decreasing trend. But a lower C-value for higher D/W-ratios will result in greater mean deviation of the mid-section stress distribution between the Matlab model and the DIC experiments. The mean deviation of all the mid-section stress distribution of each sample is only taken from the onset of plasticity till the onset of divergence between the Matlab and the DIC experiments. The divergence starts when the Matlab model hits $\varepsilon \equiv 0.047$ at the edge of the hole. The start of the data for the calculation of the mean deviation is taken at the onset of plasticity, because in the elastic regime the DIC data shows doubtful and unexpected behavior for all the samples as can be seen in appendix A. The C-value that gave the lowest mean deviation in percentage is used for further calculations. Parameter C can be seen as finite correction factor, a higher value for C results in a lower mid-section stress gradient.
Because of equation 3.18, when the β is greater than the SCFt, the α becomes negative, as can be seen in figure 5.11.

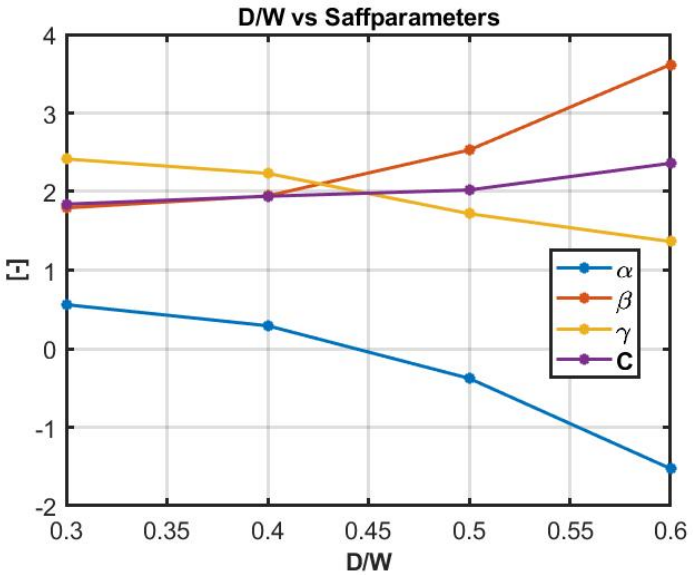

Figure 5.11: Saff's parameters determined for the samples used.

5.3. Samples after testing

The four sample geometry used for the DIC experiments are presented in figure 5.12, the red lines on the samples are the dynamic delamination boundaries after failure. Great warping can be observed around the hole and at the net-section geometry. Due to plastic displacements the round smooth hole become a oval shaped close to failure.
The failure surfaces, delamination and fiber breakage are presented in figure 5.13, 5.14, 5.15 and 5.16.

Figure 5.12: The four glare samples used and their delamination boundaries.

Figure 5.13: Failure surface of sample D60.

Figure 5.14: Failure surface of sample D75.

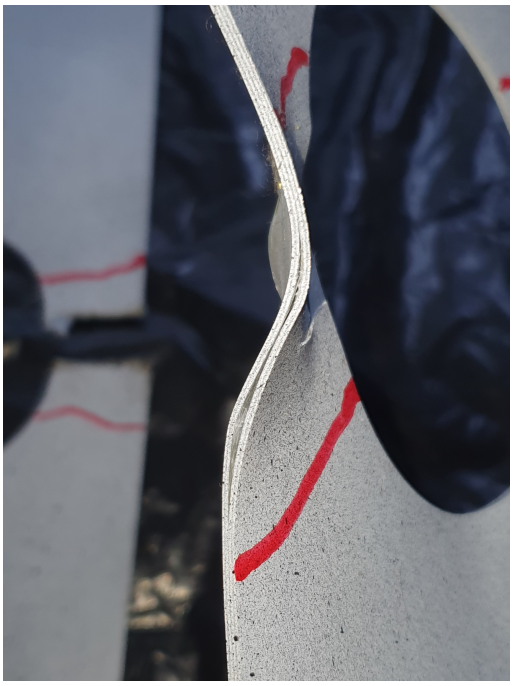

Figure 5.15: Delamination in sample D90.

Figure 5.16: Longitudinal crack in de applied load direction. Failure surface and delamination in sample D60.

6

Discussion

The objective of this research was to find an analytical method/models for the calculation of the mid-section stress distribution in a FML materials with a center blunt notch. The Models should take into account the various phenomena taking place considering FML's and to relate the peak stress profile linear elastically to the net-section stress. An important factor in converging the analytical model would be the finite width correction factor.

The analytical model that has been made follows the Proposal of Alderliesten(PA). It relates the peak stress profile linear elastically to the net-section stress of a center blunt notch in a FML plate under elastic and elasto-plastic conditions, considering that the Neuber Postulate is true.
A constrain on the model was that it wouldn't make use of any empirical data, except for the mechanical properties of the individual constituent of the FML material. Therefore the Hagenbeek model(HM) which makes use of the Metal Volume Fraction(MVF) was implemented to create the σ'ε-curve of the FML.
For the incremental calculation of the net section stress during elastic and plastic loading until failure, the Strip Yield Model(SYM) was implemented. The SYM divided the mid-section of the plate in small strips. The point at the center of each strip is where the calculations are made.
Saff's paper provided the data to make an analytical formula for the peak stress profile in the elastic regime for the FML samples, suggesting a decreasing exponential equation with three parameters α, β and γ.

3D DIC experiments with strain-gauges applied onto the samples has been done to validate the Matlab analytical model. The strain-gauges were used to validate the DIC experiments and the Matlab analytical model. The Vic 3D DIC software was used to perform the DIC experiments.

The analytical model has its limitation, but it predicts the results of the DIC experiments closely. The results of the strain-gauges follows the DIC experiments and the analytical model almost exactly. The mid-section stress distribution and the results of the strain-gauges for the applied gross stress S_g can be found in appendix A and the net-section SCF_t is given in section 5.2.

The SCF_t as function of the S_g can be divided small section, namely the elastic regime, onset of plasticity, plastic zone growth at he center hole, the widening of the plastic zone toward the edge of the plate, delamination and failure. Although the onset of plasticity is taken as the 0.2% strain, the model predicts the onset of plasticity much earlier and is in agreement with the DIC results. The transition from elasticity towards plasticity is more gradually than for pure metals.
The mid-section stress distributions, as function of x for the applied gross S_g determined by the Mat-

lab model and the DIC experiments, proves that Neuber's Postulate can be used to relate the peak stress profile linear elastically to the net-section stress of a center blunt notch in a FML plate under elasto-plastic conditions.

The model does have its limitations. It can be best observed from the SCF_t graphs. Although the SCF_t results of the DIC experimental shows a lot of high cycle behavior in the elastic regime which dampens out in the plastic regime, the SCF_t results of the Matlab model in the elastic regime can be validated by strain-gauges 1 from the mid-section stress distributions in appendix A.

It is well known that a plastic zone formation relaxes the stress and would result in a decrease in the SCF_t. When the $\sigma'\varepsilon$-curve of the material starts to diverge from the linear elastic E_{lam}, The SCF_t decreases as was stated by Alderliesten[2] and Roebroeks[3]. Hammouda[27] states that the plastic SCF_t decreases due to the plastic zone and increasing applied stress until it reaches a constant value. Of course, this should be the case, since S_{peak} decreases due to plasticity and the S_{nom} has the same value as it is defined by the S_g with the correction of the net-section width.

When the plastic zone starts to grow and the strain hardening becomes more significant, the plastic SCF_t ought to increase. Both the model and the DIC results shows this behavior, but the SCF_t results of the DIC experiments has significantly a greater increase than the Matlab model as can be seen from point 3 till point 4 in figure 5.3, 5.4, 5.5 and 5.6. From here the Matlab model and the experimental results starts to diverge. The results of the strain-gauges en the SCFt proves that the notch sensitivity is depended on ductility and strain hardening capacity as is suggested by Alderliesten[2], Schijve[1] and Agogino[28].

After some growth of the plastic zone at the hole, the plastic zone starts to widen more towards the edge of the plate. because of the stress relaxation and the strain hardening that is taken place at these new locations, there is a gradually redistribution of the load through the mid-section of the plate. The plastic zone at the hole edge doesn't grow much anymore and the SCF_t stays almost constant. This behavior can only be seen from the results of the DIC-experiments. The plastic zone of the matlab model seems to be ever growing til the failure condition is met.

Furthermore, the Matlab model doesn't describe what happens at the end of the plastic regime near failure. At the end of the plastic regime near failure, there is a steep rise in the SCF_t from the DIC experiments. The mid-section stress distributions of the DIC experiments increases significantly and diverges from the results of the Matlab model. The DIC experiments shows a significantly greater stress and strain before failure than the Matlab model. This is best observed from the results of sample D45 and D60. The failure criteria of the Matlab model is set as the fiber failure strain of $0.047\frac{mm}{mm}$. That is when the overall strain of the first yield strip from the SYM at the hole edge has a strain of $0.047\frac{mm}{mm}$. This means that indeed it is possible to have local delamination and fiber bridging mechanism underneath the plastic zone before crack growth or failure. Although, significant warping of the glare plate can be observed, there is no failure of the plate observed. The failure itself is very sudden, and the glare plates breaks in an instant completely through the mid-section. After failure, the dynamic delamination length perpendicular tot the mid-section is observed to be 2.5cm to 3.5cm maximum.

The steep rise in the SCF_t DIC experiments starts even before the fiber failure strain of $0.047\frac{mm}{mm}$. Interestingly, this is also the point where the applied load from the far field is not equal anymore to the net-section load. Load equality for the four samples used can be found in figure 5.7. Since the DIC experiments only observe the surface of the first aluminum layer, delamination must have taken place and the fiber bridging mechanism has kicked in. Since delamination and the fiber bridging mechanism hasn't been build in the model yet, and complex growth and influence of the plastic zone is not taken fully into account, neither the absolute values nor the trend of the Blunt Notch Strength(BNS) of the Matlab Model can be considered correct and doesn't converge with the BNS of the DIC experiments. The BNS results are provided in figure 5.10.

The peak stress profile in the elastic regime was made using Saff's method[11]. It consist of four parameter α, β, γ and C. Since parameter γ and β is bound by the third condition of load equality between the far field load and the net-section load, solving for the peak stress profile must be done iteratively. The main factor for convergence is parameter C. It is to be considered as the finite width correction factor. The finite width correction factor of koiter[11] can be used as a first approximation, but the error of the peak stress is significant. It predict the value of parameter C better for hole diameters below 0.3 D/W. For larger holes the deviance becomes greater. The finite width correction factor C dictates the outcome on α, β, γ in the 2nd and 3d conditions for converging the peak stress profile. For large holes above 0.4 D/W, the increase in β results in a decrease in $\alpha < 0$, because both are bound in the first condition which defines the elastic net-section SCF_t. An $\alpha < 0$ is not possible, because that would mean that the peak stress profile become negative towards the edge of glare plate resulting in a negative stress in that region during elastic loading. More research is needed to find the correct way to define finite width correction factor C. More details on Saff's method, the considered parameters and early iterations of the Matlab model is given in appendix D.

The Strip Yield Model is a great and easy method to create the mid-section geometry by dividing it in small strips and the points of interest to make discrete calculations, without having to deal with the complexity of a Finite Element Model(FEM) or diving deep into complex mathematical calculations. The SYM is promising. The glare material at the mid-section can be modeled through the thickness by creating strip yields through the thickness. This can be beneficial for simulating the onset of delamination by critical shear stress at the interface of two yield strips which coincides with the interface of the pre-preg and metal layer.
Overall the model has proven its benefits and provided the solutions for positive answers to the research questions. The model is not complete, but it is promising and future enhancements can be made in order to describe the behavior and phenomena of a center blunt notch or other stress concentration geometry completely. Further details will be given in section 8 Recommendations.

7

Conclusions

Because of the orthotropic nature of Fiber Metal Laminates, the influence of the geometrical induced stress concentrations cannot be ignored and left out to building trust from empirical data, which needs long term experimental testing and big financial costs. This all can be partially or completely negated by having an analytical solution for the behavior of the material under the geometrical constraints.
The Matlab model is build around the material Glare 2-4/3-0.3 and the geometry of an OHT-specimen, as well as the DIC experiments done for validating the model.
As a first step, questions are made to the literature given in the introduction of this research paper, and more details on the research question is given in section 2.4.2 Research Questions.
Basically, the purpose of this research was to create or develop an analytical model for a center blunt notch, that relates the peak stress profile linear elastically to the net-section stress, and predicts accurately the Blunt Notch Stress(BNS) of a center blunt notch in FML materials.
This would enhance the position of FML's in the aeronautic industry compared to monolithic metal or pure composite(fiber-resin) design.

The results of this research concludes that the energy consideration(conservation) can be used to relate the peak stress profile linear elastically to the net-section stress. Even far in the plastic regime where the model doesn't predict the reality, The results are still quite close to the DIC experiments and strain-gauges. The assumption is made that the strain energy under plastic condition, which is the area under the FML $\sigma'\varepsilon$-curve, is equal to the imaginary elastic energy, when the material was considered to be loaded elastically beyond the elastic limit. As was suggested by Alderliesten[5][2], Neuber's Postulate is indeed valid. Although the complex behavior, growth and influence of the plastic zone formation is not incorporated in the Matlab model. The suggestion of Alderliesten[5] bypasses the causality of the plastic zone formations, but it still gives accurate results far in the plastic regime until delamination beneath the plastic zone came to existence.

Implementing delamination, fiber bridging mechanism and determining the plastic zone size, growth and behavior influencing the mid-sections stress distribution would certainly predicts the BNS of FML's accurately. Because the DIC-experiments en results of the strain-gauges proves that delamination has kicked in before the failure criteria of the glass fiber breakage strain used in the Matlab model, and the material can resist the applied load for a longer duration after. Because of delamination, the fiber bridging mechanism is activated, which mean that the glass fibers in the pre-preg can strain more and the BNS failure is postponed. This is the explanation for the steep increase in strain observed from the surface of the first aluminum layer by the DIC experiments and the strain-gauges.

The analytical solution for the finite width correction factor, parameter C in Saff's method for creating the peak stress profile, has to be made. But the methodology used for developing the Matlab model determines the finite width correction factor C sufficiently for the D/W-ratio below 0.5. Equation 3.21 is used as the finite width correction factor in this research. It seems that this equation can be true for small center D/W-ratio. This equation is close to the results of C-values determined by the matlab model presented in table 5.4. For larger D/W-ratios, there is a significant difference. it seems also that the C-values from the matlab model increases, while equation 3.21 shows that the C-values should decrease for greater hole diameter. As a first estimation, equation 3.21 can be used, but for more precise calculations it is advisable to do more research on this matter The other parameters describing the peak stress profile has a strong dependance on the finite width correction factor C. Because the parameter C is the main independent factor for determining the gradient at the notch root and the absoluut values near the edge of the plate. A higher C-values, results in a steeper gradient at the notch root. For higer D/W-ratios, a higher C-value results in that β is greater than the SCFt, which in turn results in that the α becomes negative. Consequently, the peak stress profile becomes negative towards the edge of the plate, which should not be possible. The parameter C, also assumed to be the finite width correction factor is considered to be the main factor for convergence of the peak stress profile.

8

Recomendations

Although great results has been achieved, there is still much work to be done. The points to be considered for future recommendations are,

- Finite Width Correction factor.
- Determining the plastic zone size and growth.
- Delamination and fiber bridging.
- Methodology for eliminating noise in the elastic regime of the DIC-experiments.
- The Matlab Model

Since the results has proven that delamination does happen, the plastic zone size and growth must be determined at each increment. because there is a causality in plasticity. At the interface between the fiber-resin and metallic layers critical shear stress and strain develops underneath the plastic zone, which would be the main cause of delamination. Though, it is interesting, that the current method does not take causality into account, while still achieving quite good results far in the plastic regime.
The main parameter for convergence of the mid-section stress distribution is considered to be the finite width correction factor C. The finite width correction factor of Koiter[11] is satisfactory to be used as a first estimation for a D/W-ratio below 0.3. For larger hole diameters, the error becomes too great. More research is needed in order to develop a general equation for determining the finite width correction factor, because all parameters that are used for determining the peak stress profile are dependent on the finite width correction factor. In the current method, the finite width correction factor is determined numerically.

The plastic surface determined via the Von-Mises failure criteria for ductile metals, should be used to determine the plastic zone size and growth. This will also take into account the causality of plasticity. It may improve the transition between growth and widening of the plastic zone during the middle stage of plasticity, where the stress concentration factor doesn't increase any more and stays mostly constant before increasing exponentially just before failure. This is also the point where the results of the DIC-experiments and the Matlab model starts to diverge.
It is advisable to have yield strips through the thickness in order to have points, where values of interest can be determined through the thickness. As a first estimation, the First-Ply-Failure method can be used to calculate average stress and strain values for the individual layers. But for determine the plastic

zone size and growth, delamination and fiber bridging, which takes place over a relative wide area and interfaces of the layers, the yield strips can be used as a foundation.
When the stress and strain at the interfaces are known, the Strain Energy Release Rate(SERR) can be used to determine the onset and growth of delamination. After delamination, a redistribution of stress and strain will be observed which is a manifestation of the fiber bridging mechanism.

For future DIC-experiments, a methodology must be made in order to ensure the quality of the results in the elastic regime. A finer speckle pattern and camera with a higher resolution may tackle the problem of the noise in the elastic regime. Sensitive sound equipment and technique could be used to determine delamination underneath the plastic zone. This would make it possible to determine static delamination from the dynamic delamination. Since these processes are very sensitive, consideration on the environmental factors and a decrease in the rate of the applied load must be made.

The matlab model consist of a main file divided in sections. Some examples are the material and geometric section, determining the elastic peak stress profile or data writing and analysis and many more. Additions can be made in these sections in order to define different experimental parameters, such as type of material, geometry, failure mechanisms etc.
In order use the model for a different lay-up and constituent materials, a new directory map would be made for that specific lay-up and FML-material. And all the parameters needed to be changed for that specific type of material and lay-up. This was more enforced due to the addition of uploading specific experimental data for analysis and validating the model.
A major drawback is that it is difficult to track and maintain the input and output data of the process. Therefore it is recommended to use a database software in order to create and edit these parameters with in these section mentioned. A major advantage is the easy way to maintain the database files and records and the automated store, search and extract of the input and output data.
Using a database software would mean that there is only one directory map for the Matlab model. The main file in the matlab model, would be a connection point between the database software and the model. Additions can be made if needed in the matlab model, but input and output is maintained via the database software. It would mean that a complete new setup and FML materials can be modeled, within minutes.

A

Appendix A

The mid-section stress or the peak stress profile for the samples used are presented in this section. For each load increment there are two graphs presented, One for the strain distribution and one for the stress distribution below each other. In the title of the graphs, the load increments are shown as well as whether the sample is in the elastic or the elasto-plastic regime. The first graph in the row of a particular sample that has 'elasto-plastic behavior' in the title, that is the onset of plasticity at the edge of the hole for that particular sample .

A.1. Sample D45

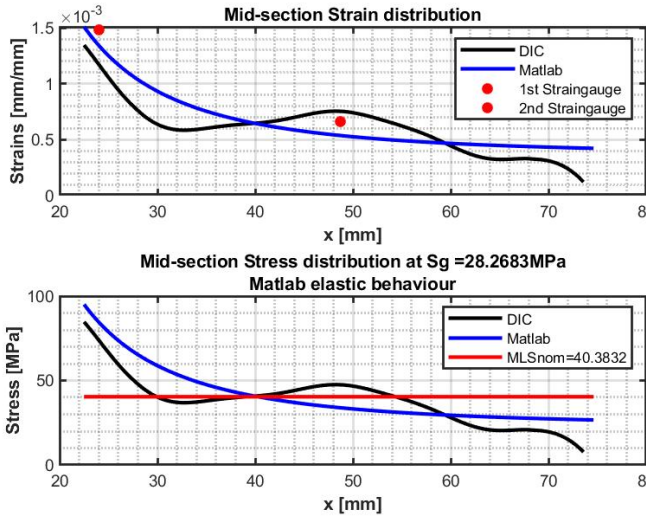

Figure A.1

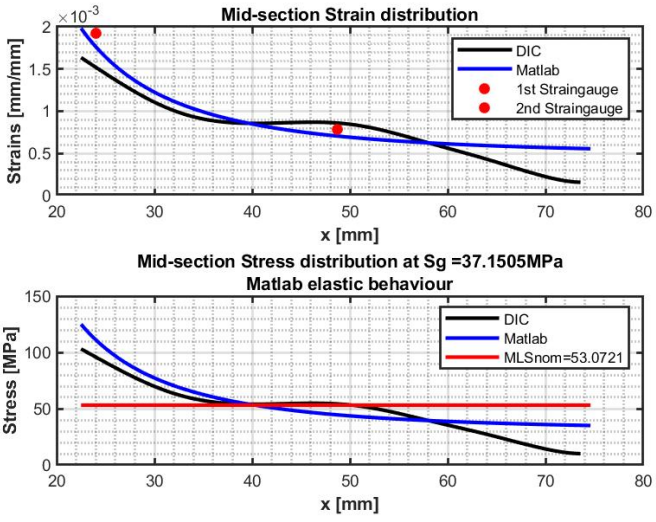

Figure A.2

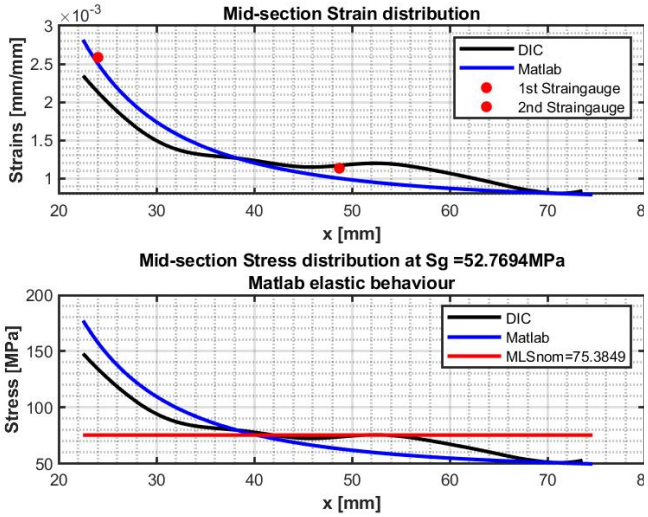

Figure A.3

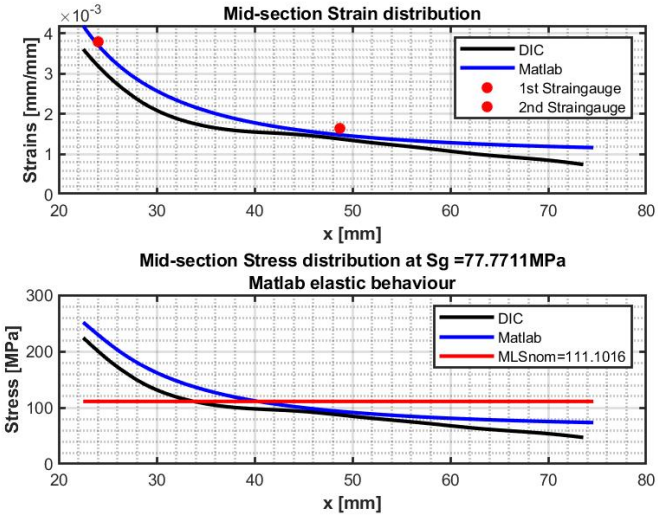

Figure A.4

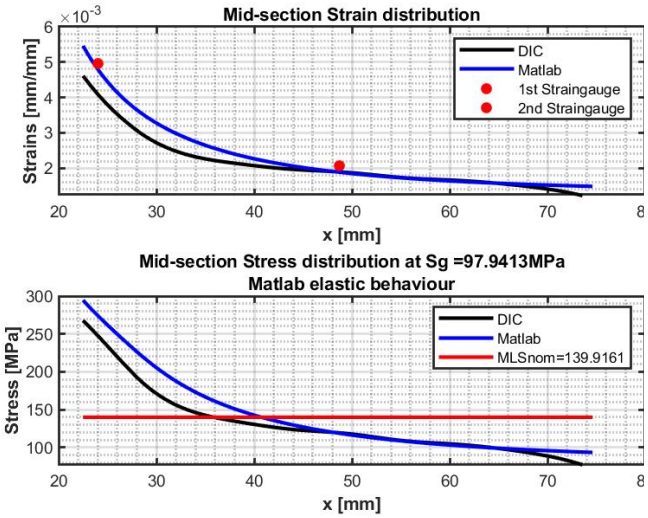

Figure A.5

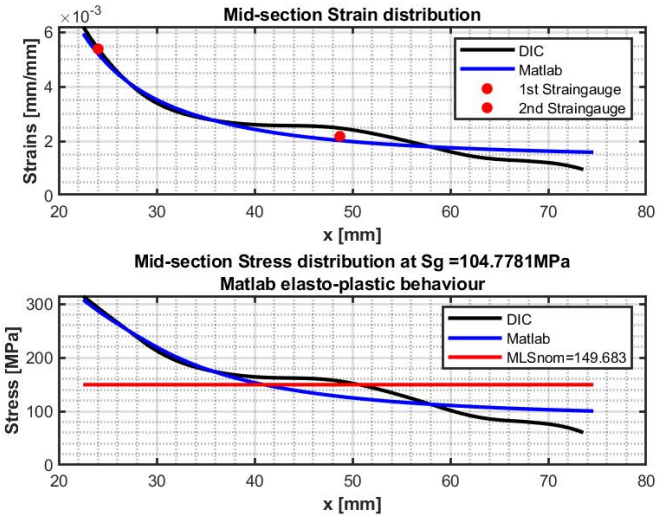

Figure A.6

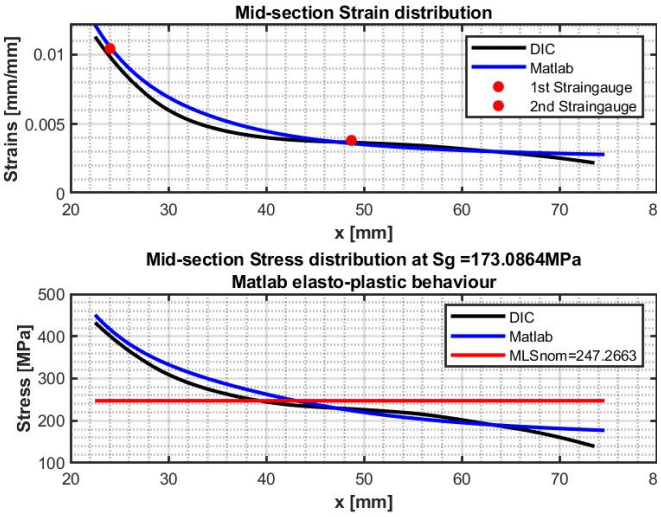

Figure A.7

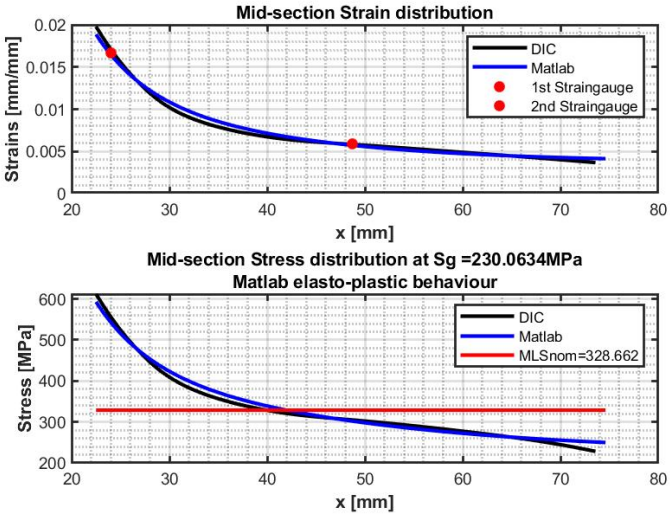

Figure A.8

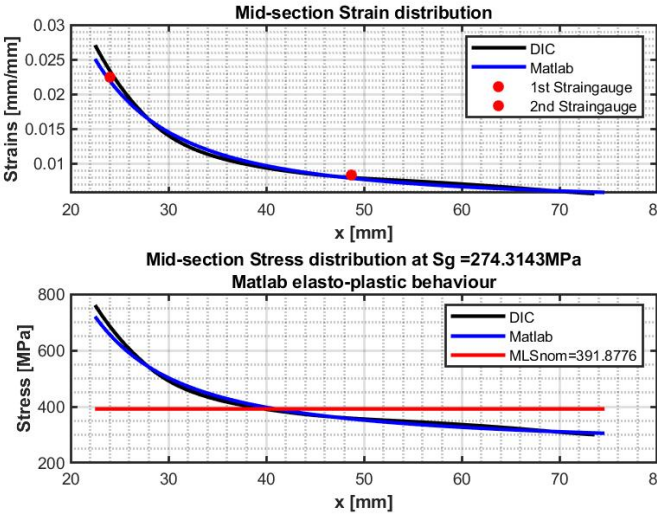

Figure A.9

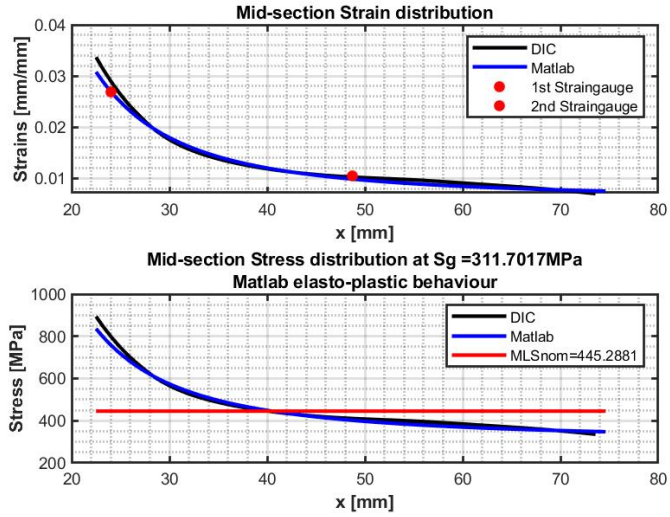

Figure A.10

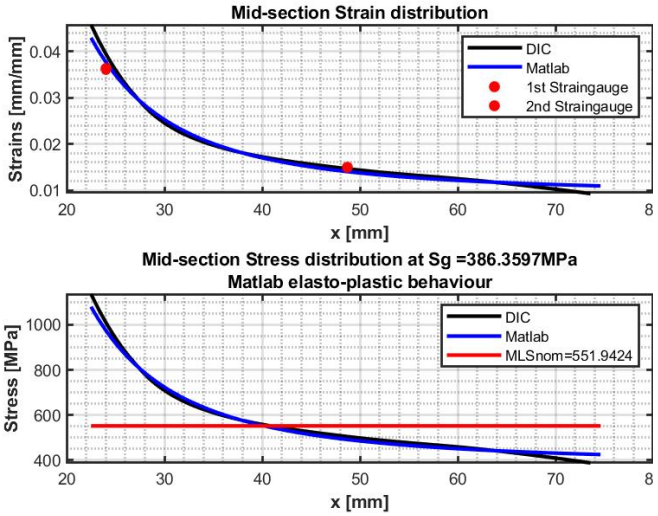

Figure A.11

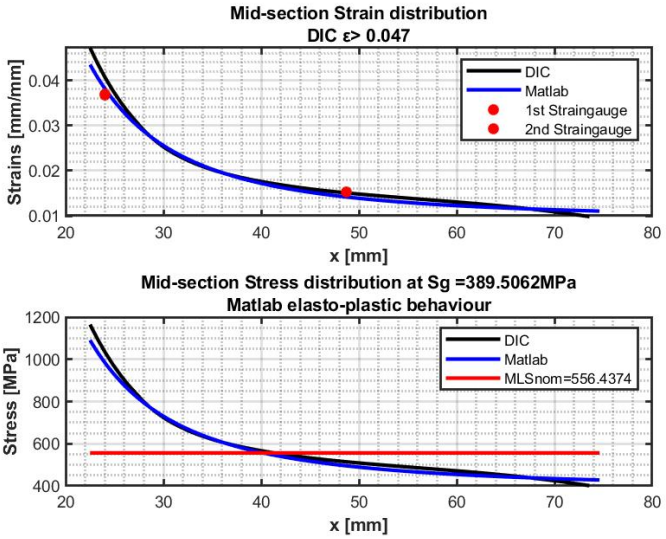

Figure A.12

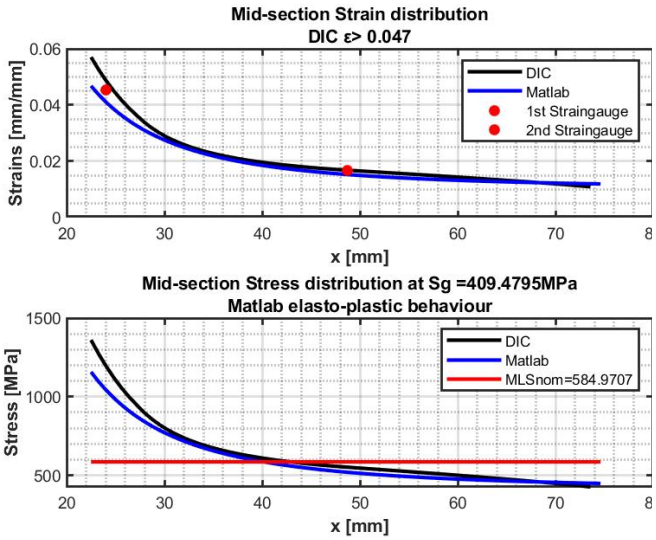

Figure A.13

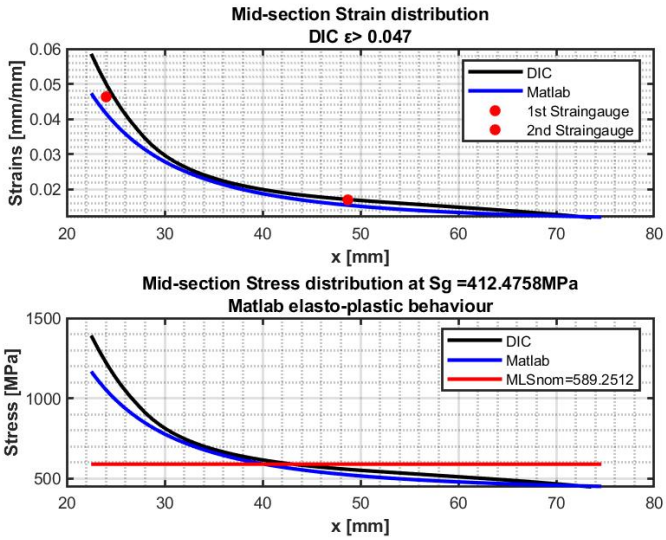

Figure A.14

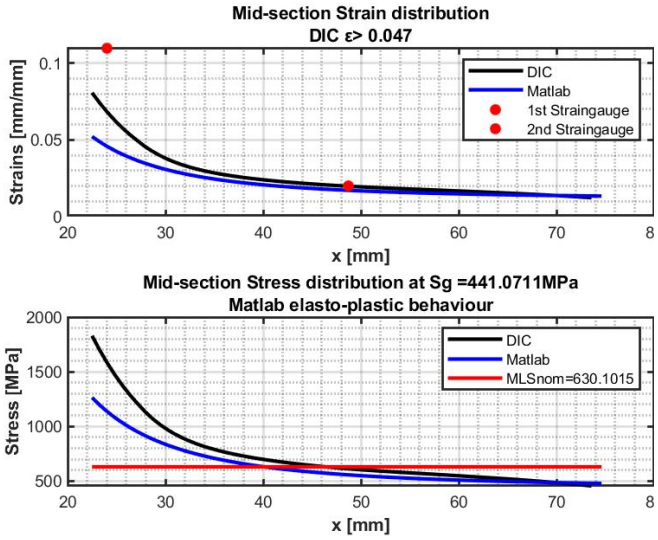

Figure A.15

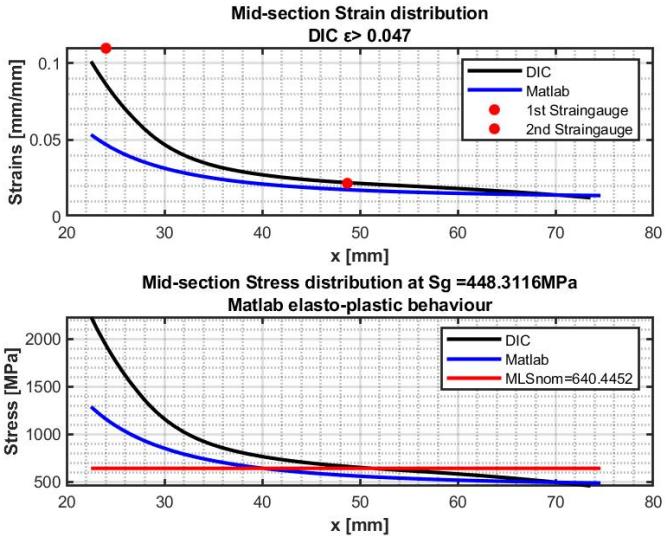

Figure A.16

A.2. Sample D60

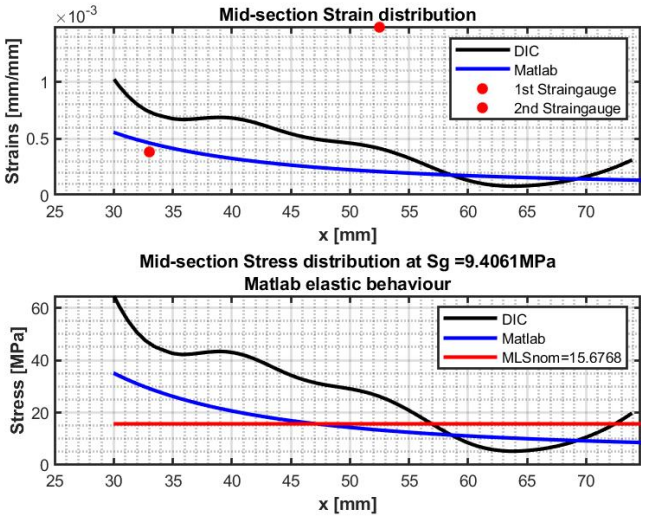

Figure A.17

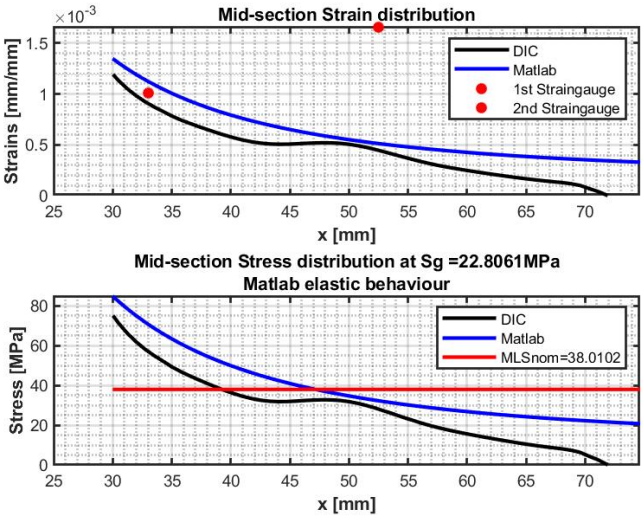

Figure A.18

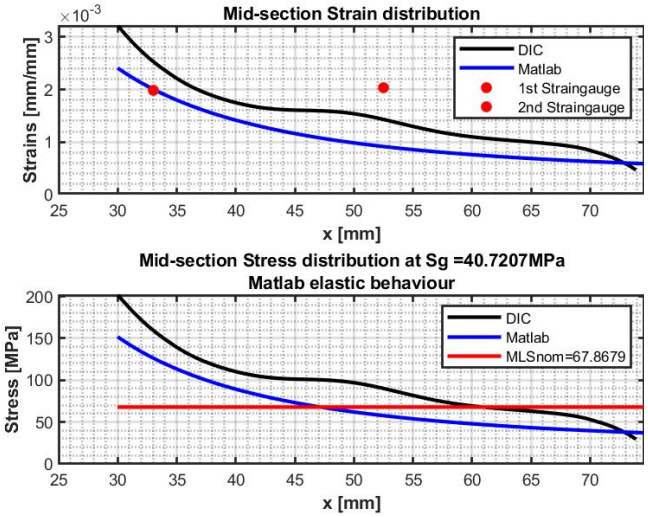

Figure A.19

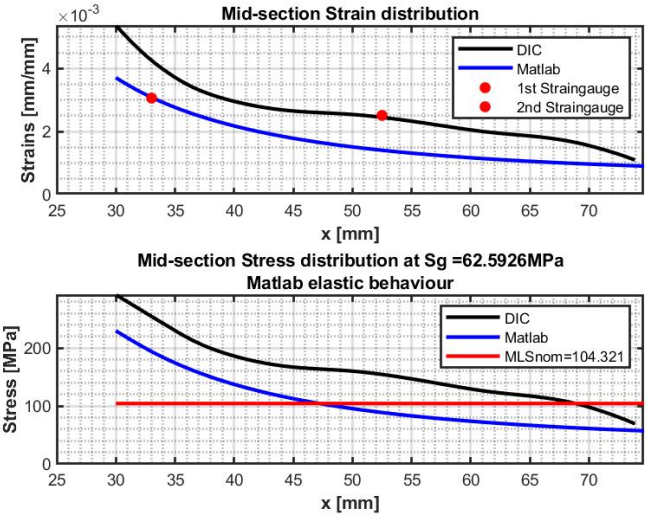

Figure A.20

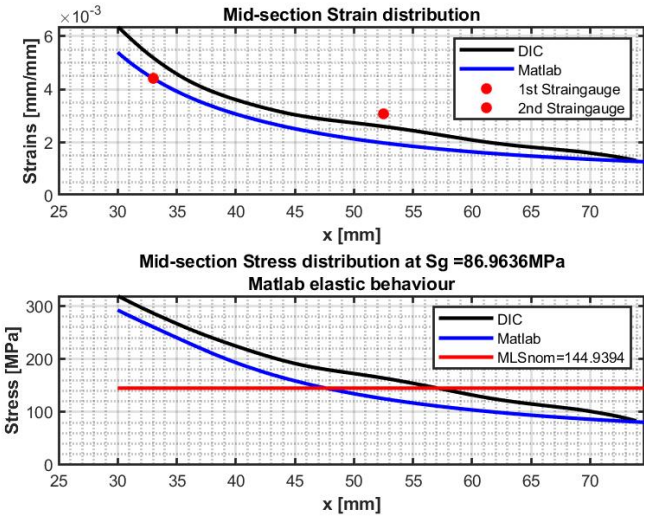

Figure A.21

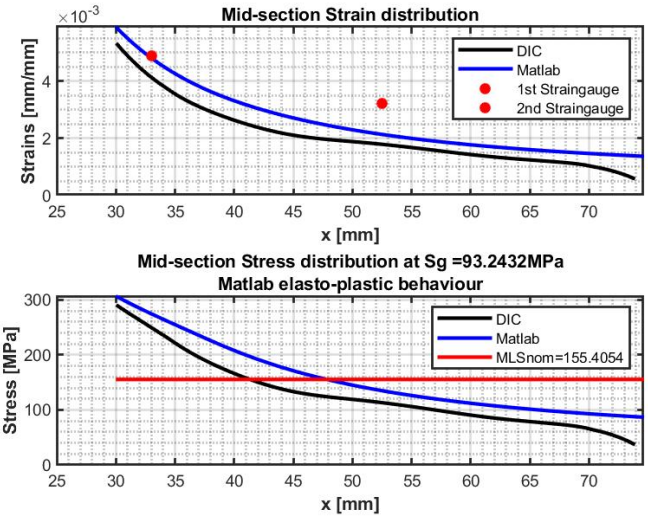

Figure A.22

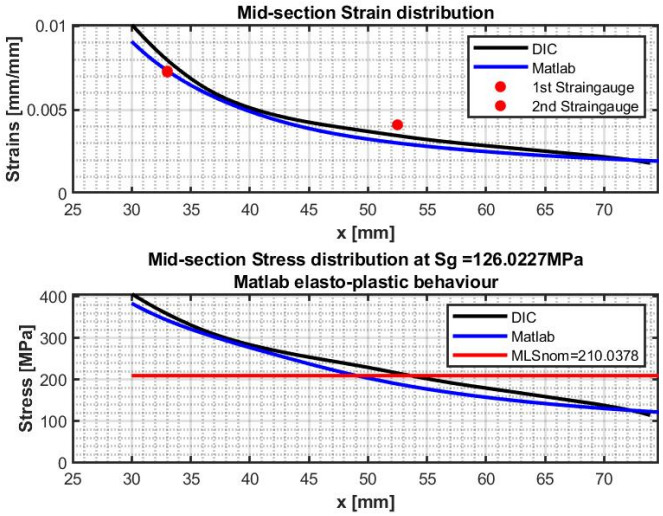

Figure A.23

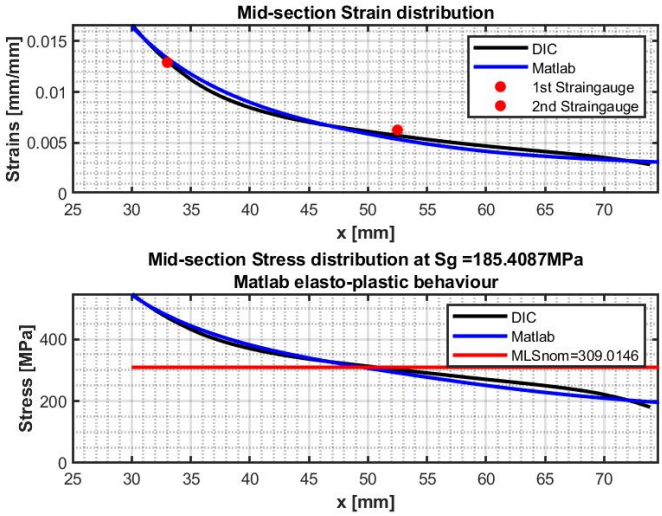

Figure A.24

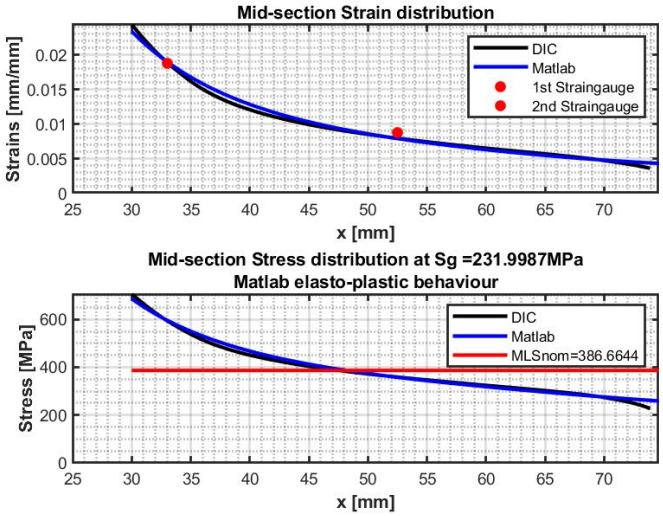

Figure A.25

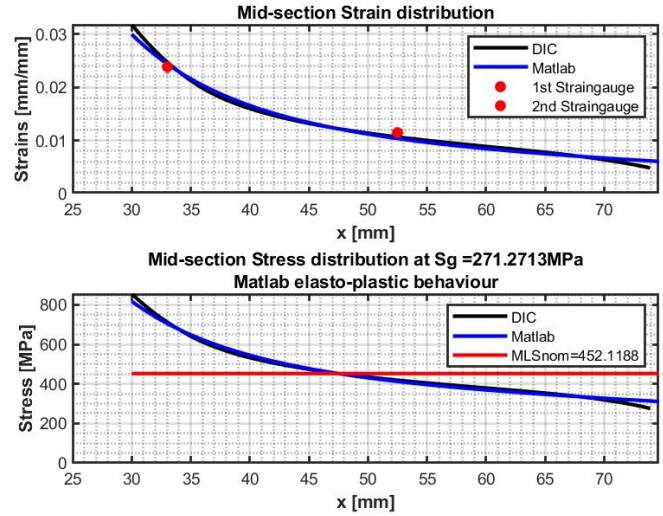

Figure A.26

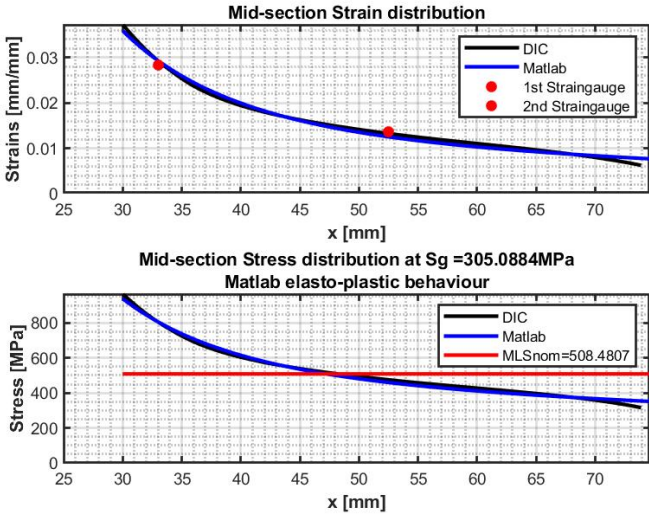

Figure A.27

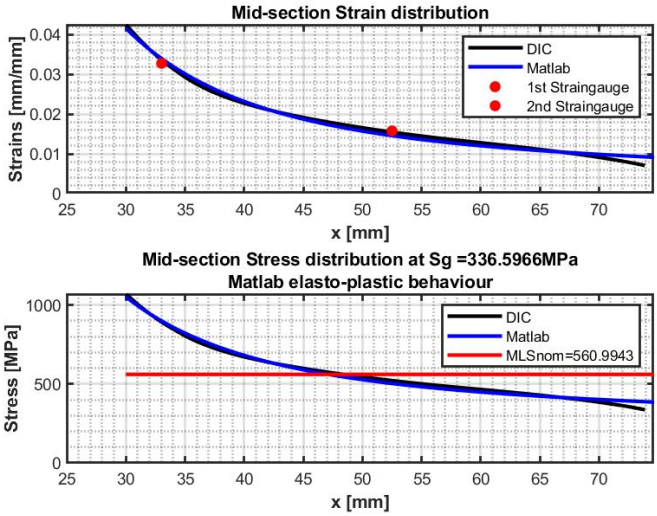

Figure A.28

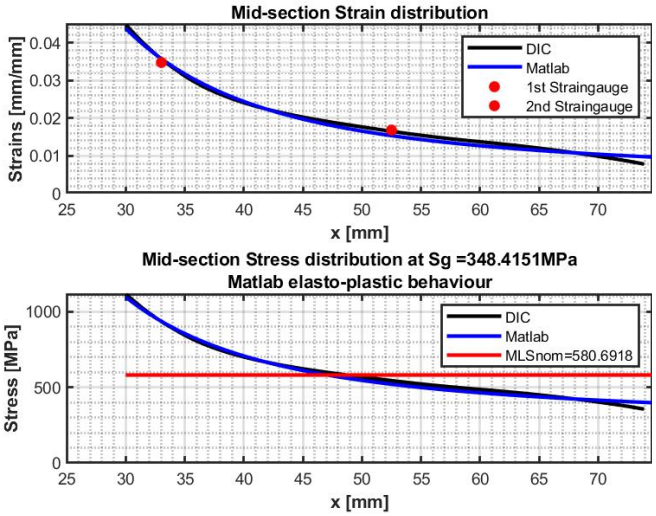

Figure A.29

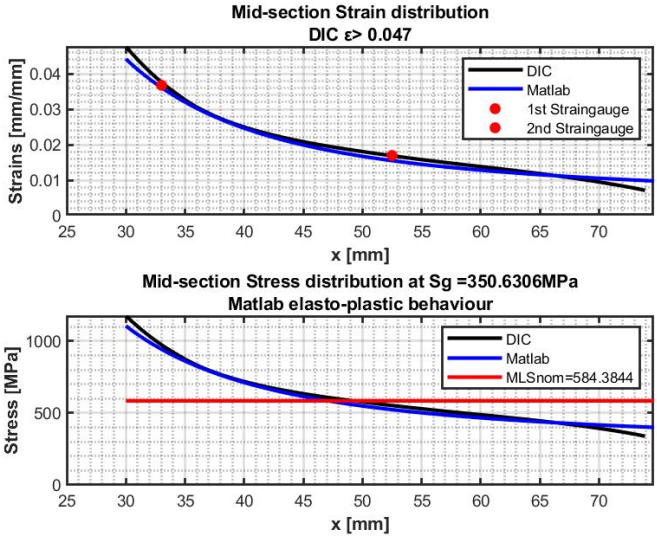

Figure A.30

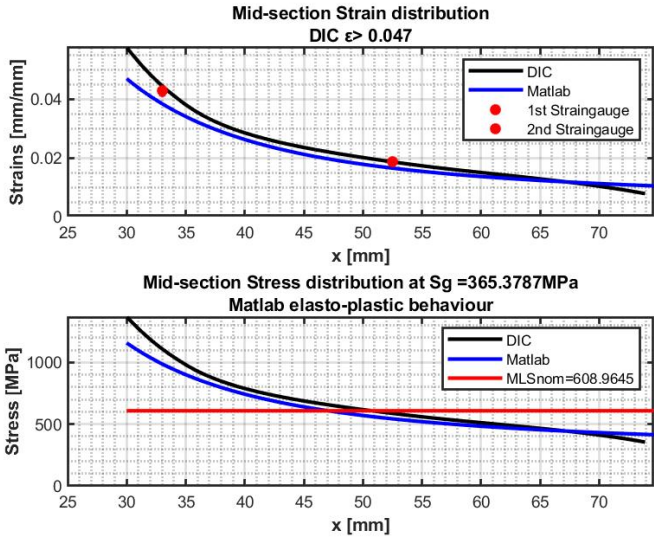

Figure A.31

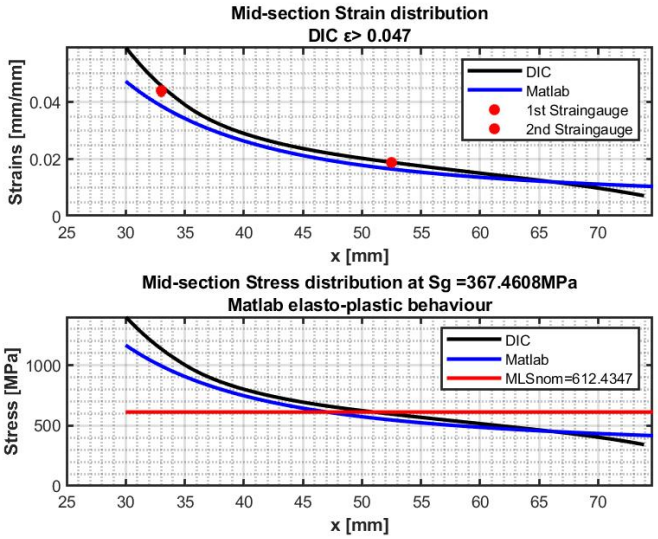

Figure A.32

A.3. Sample D75

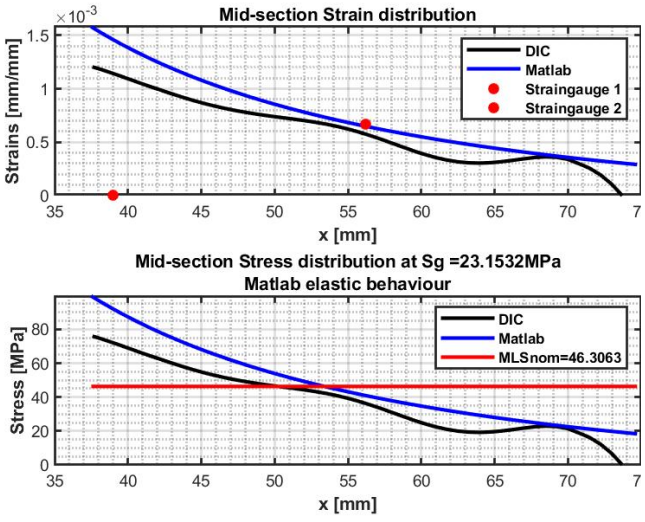

Figure A.33

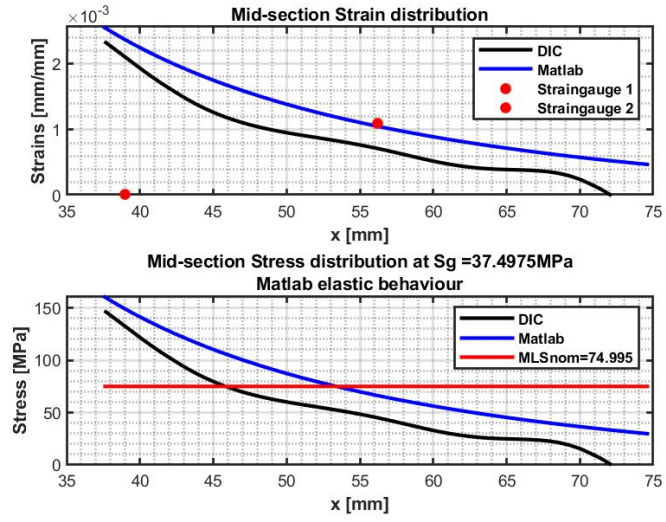

Figure A.34

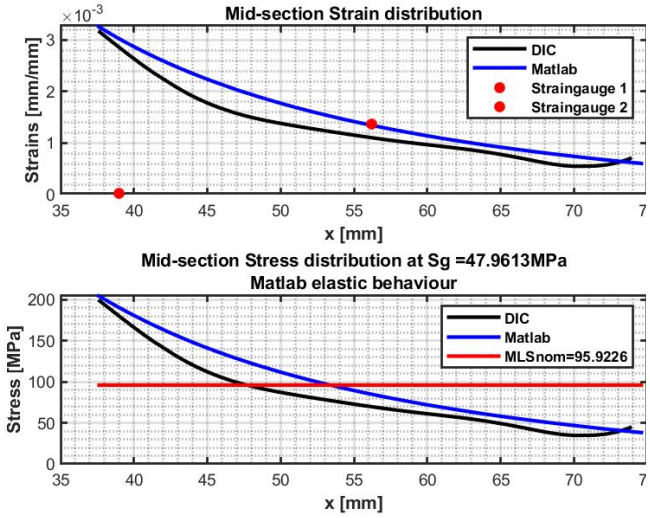

Figure A.35

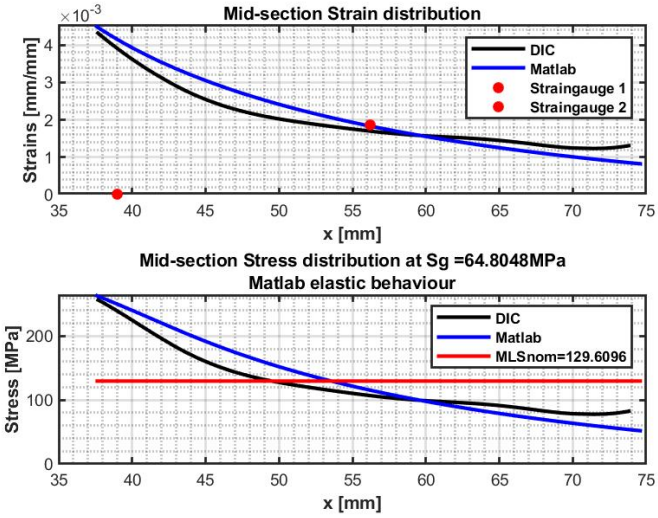

Figure A.36

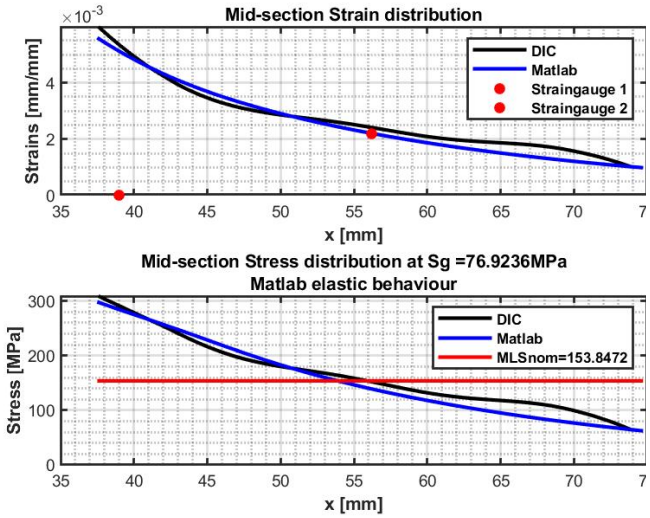

Figure A.37

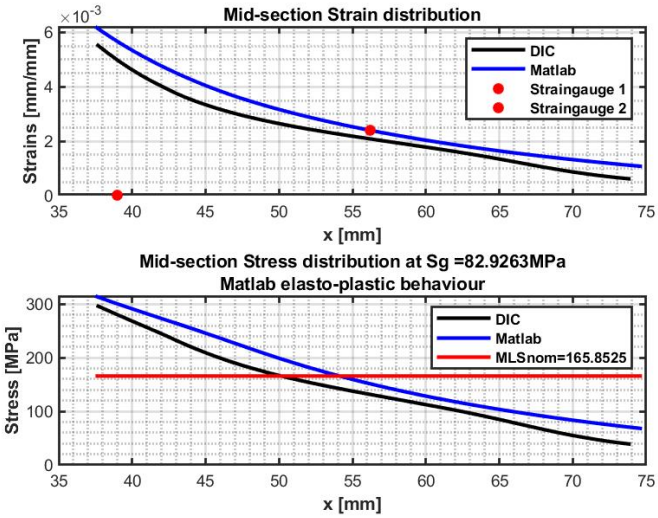

Figure A.38

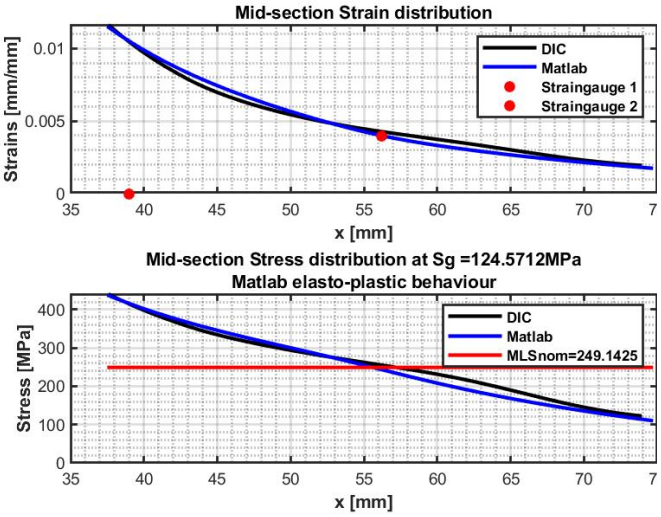

Figure A.39

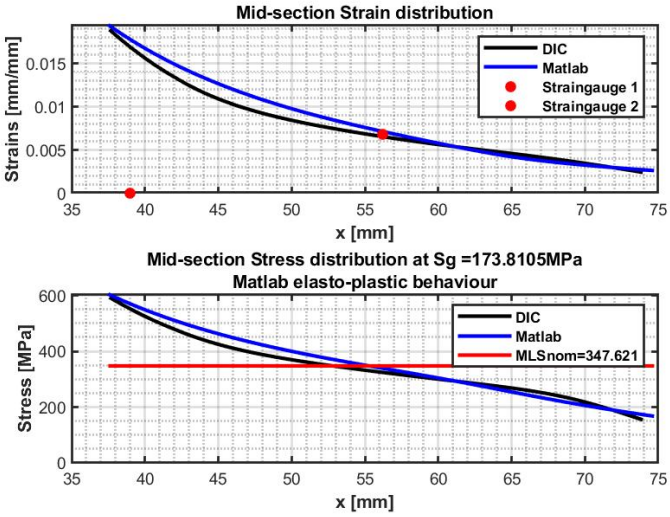

Figure A.40

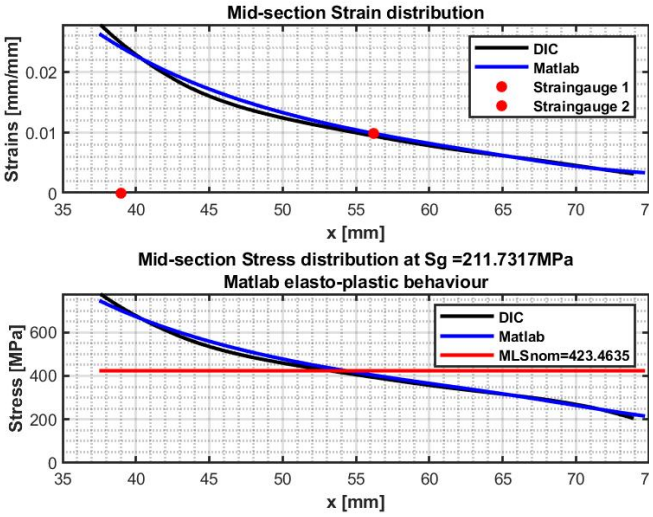

Figure A.41

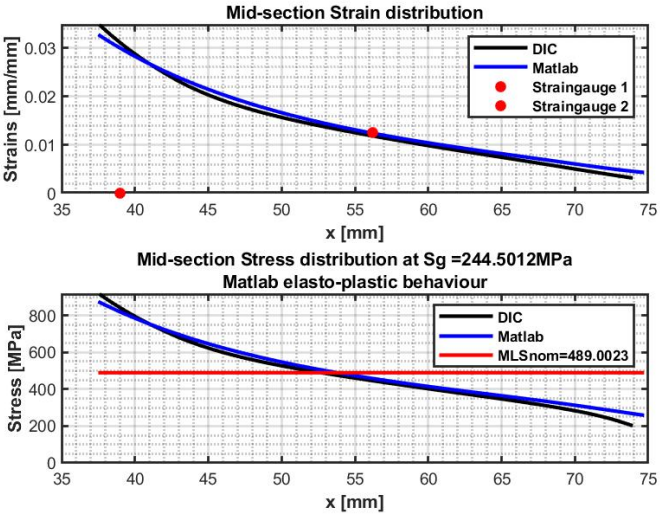

Figure A.42

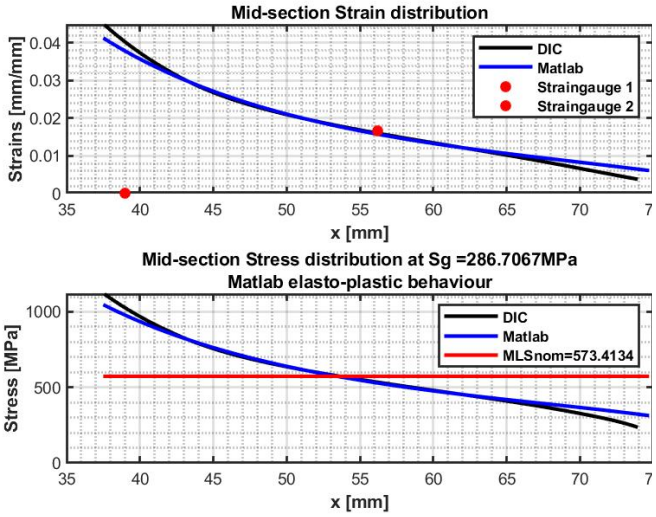

Figure A.43

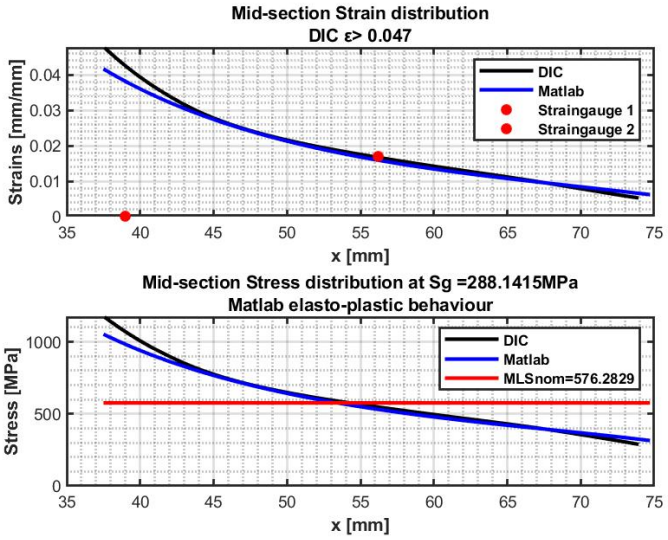

Figure A.44

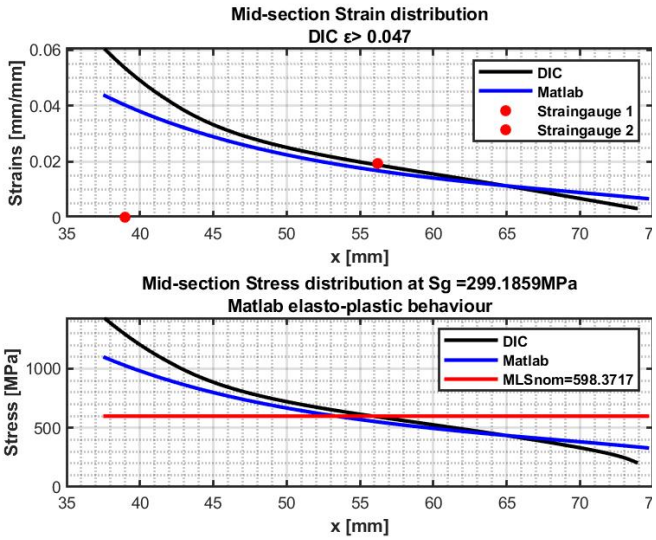

Figure A.45

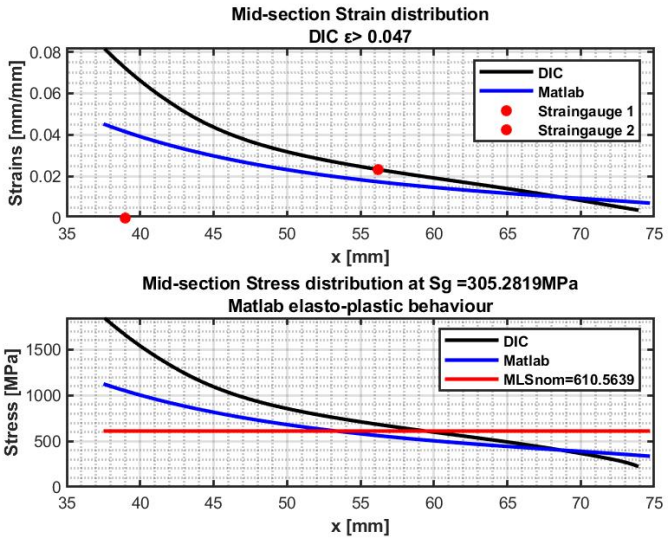

Figure A.46

A.4. Sample D90

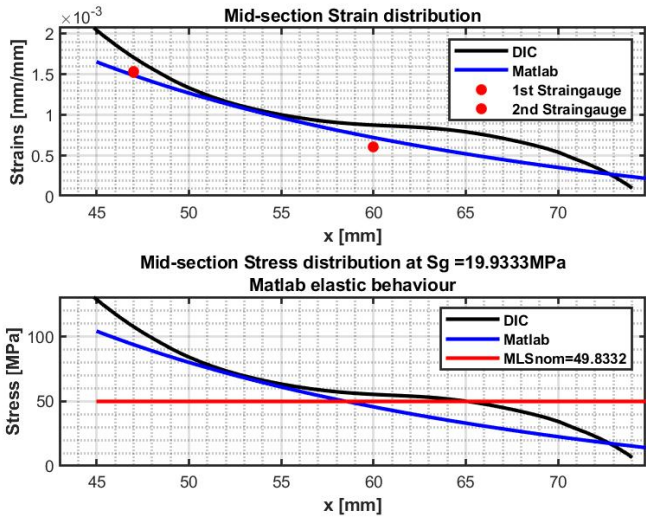

Figure A.47

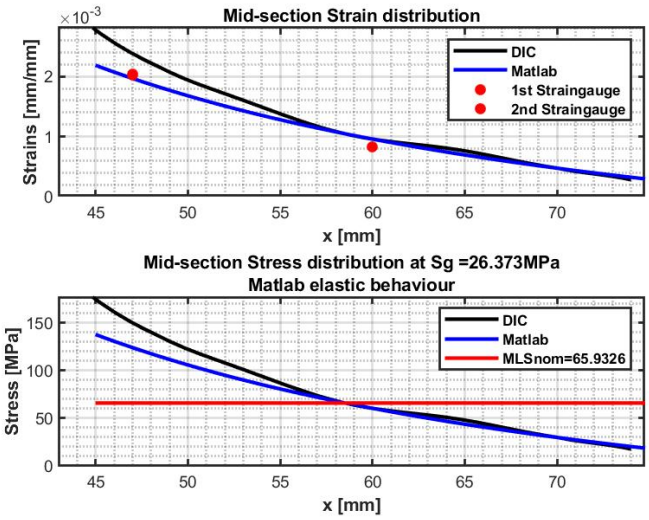

Figure A.48

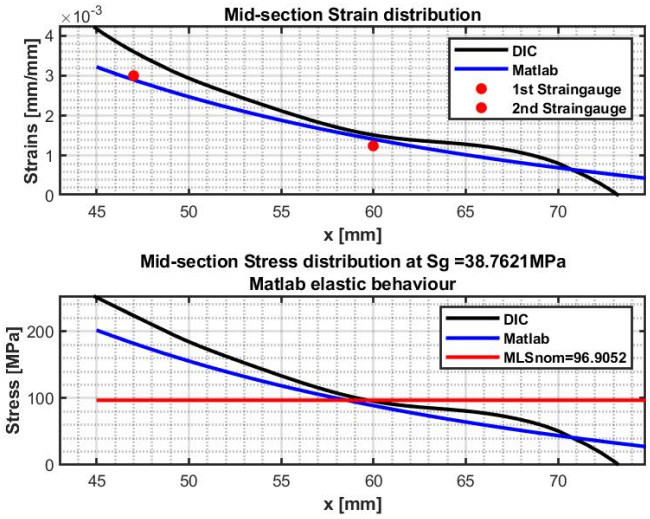

Figure A.49

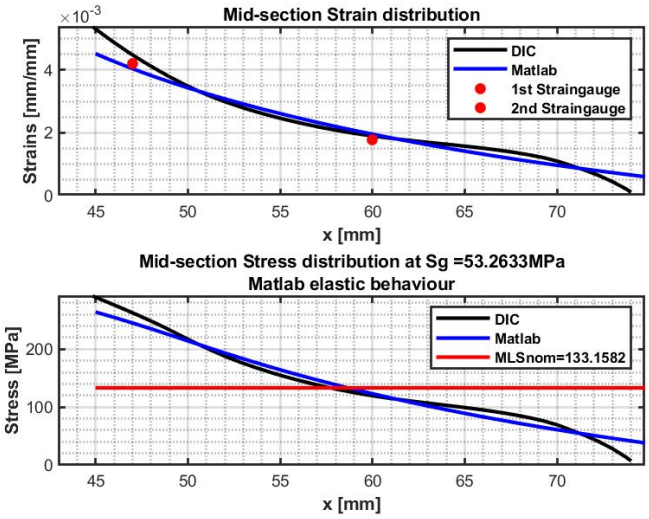

Figure A.50

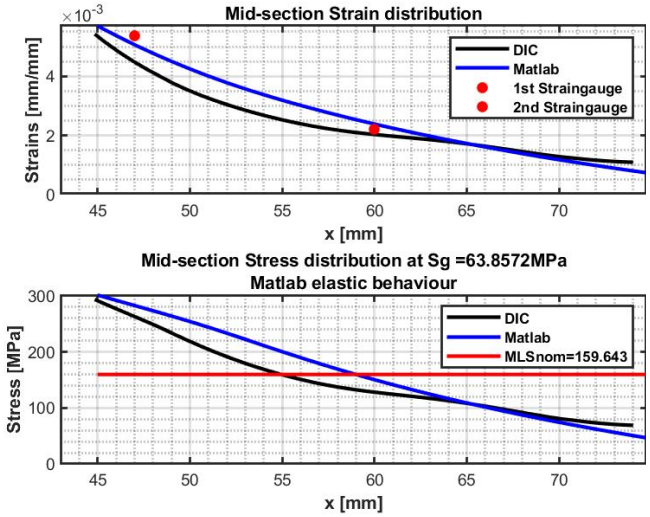

Figure A.51

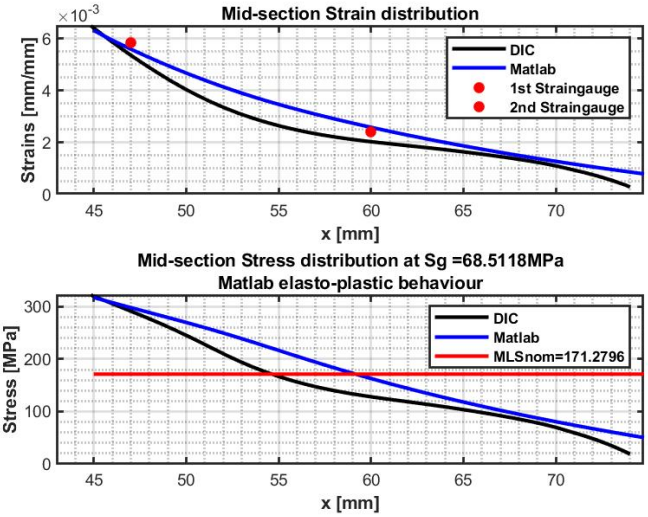

Figure A.52

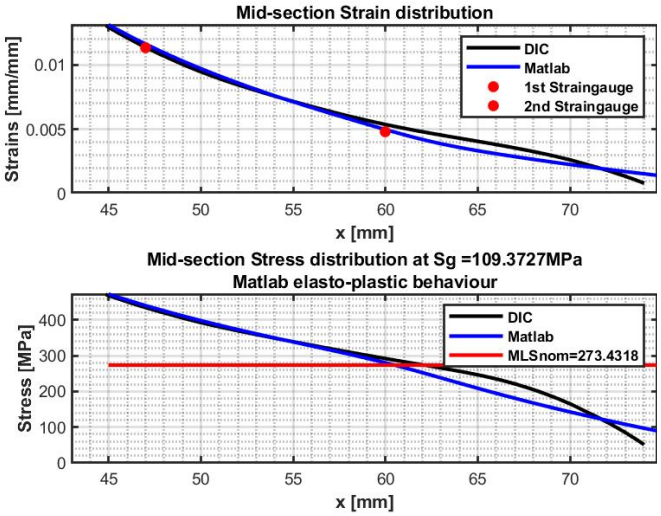

Figure A.53

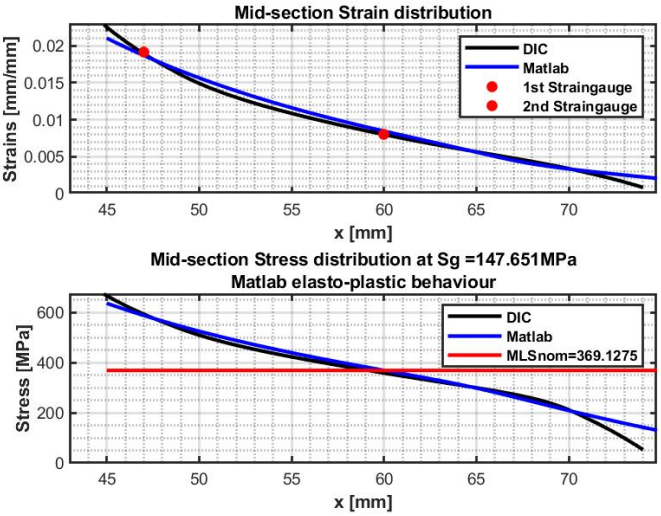

Figure A.54

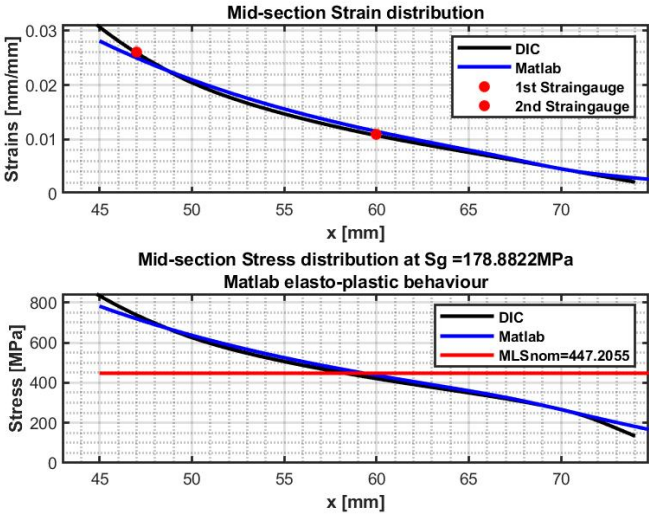

Figure A.55

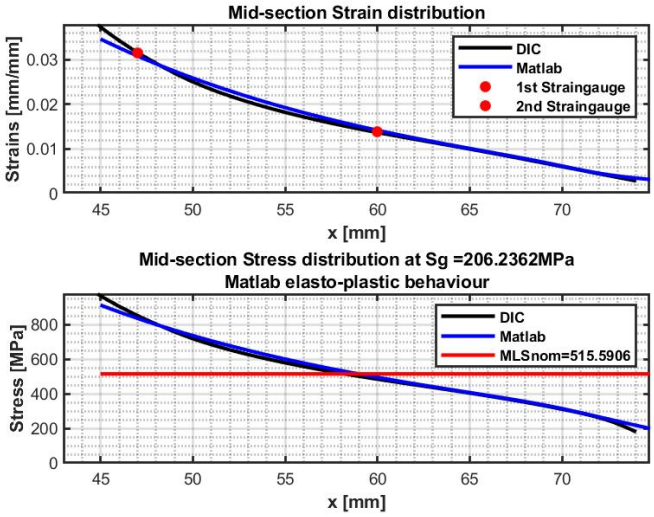

Figure A.56

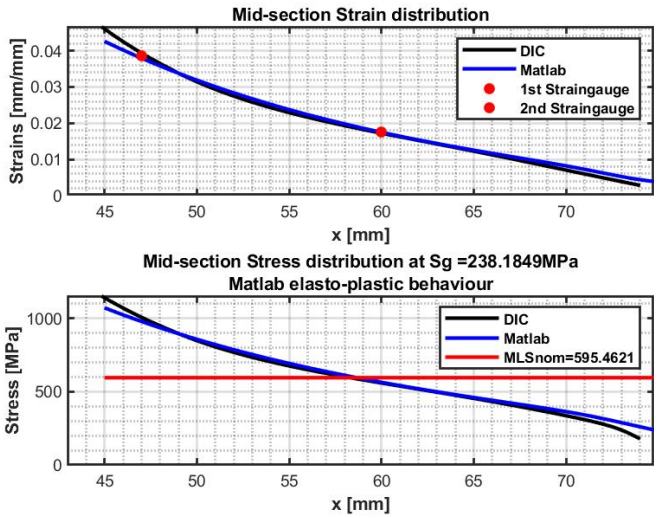

Figure A.57

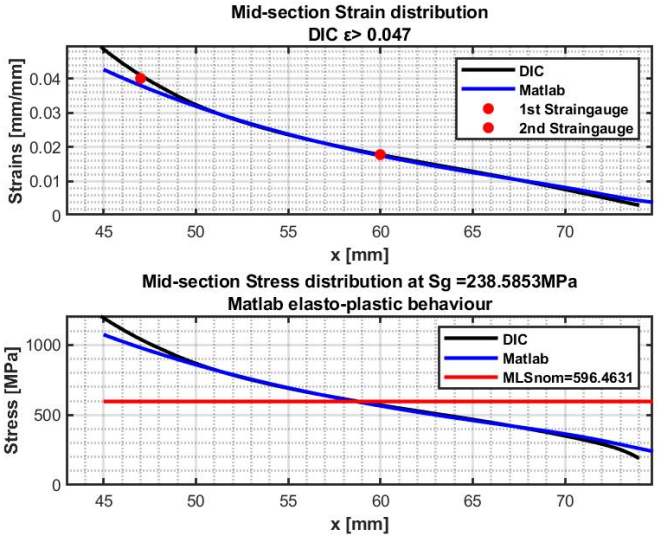

Figure A.58

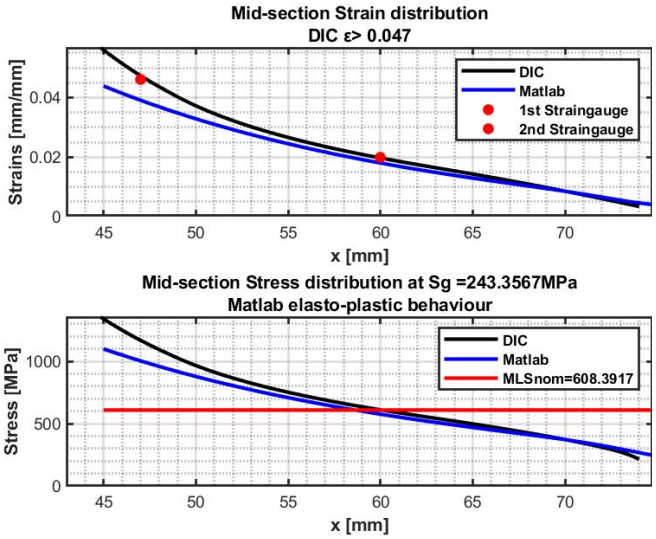

Figure A.59

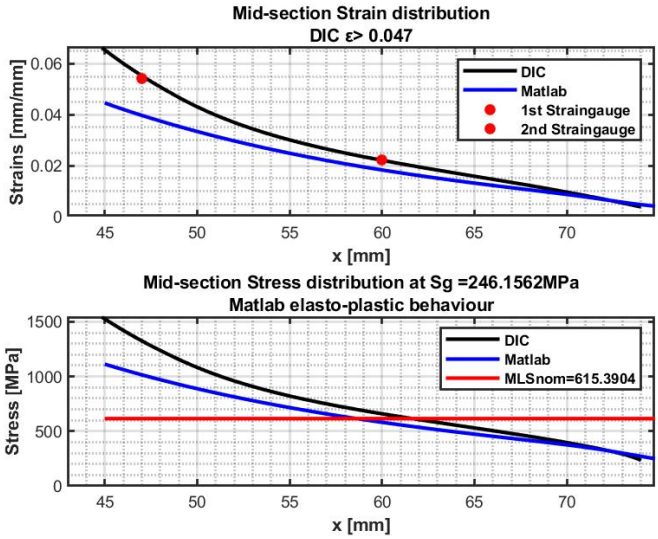

Figure A.60

A.5. DIC pictures of sample D45

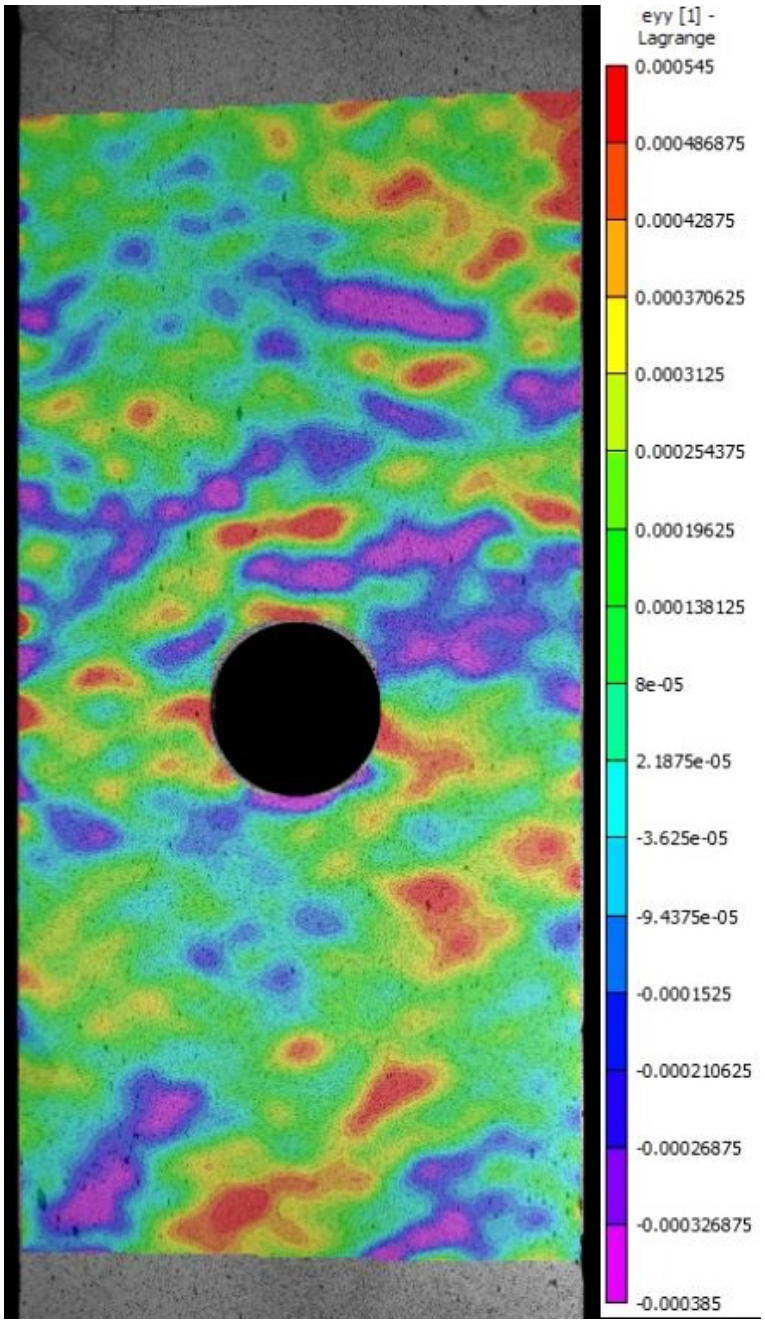

Figure A.61

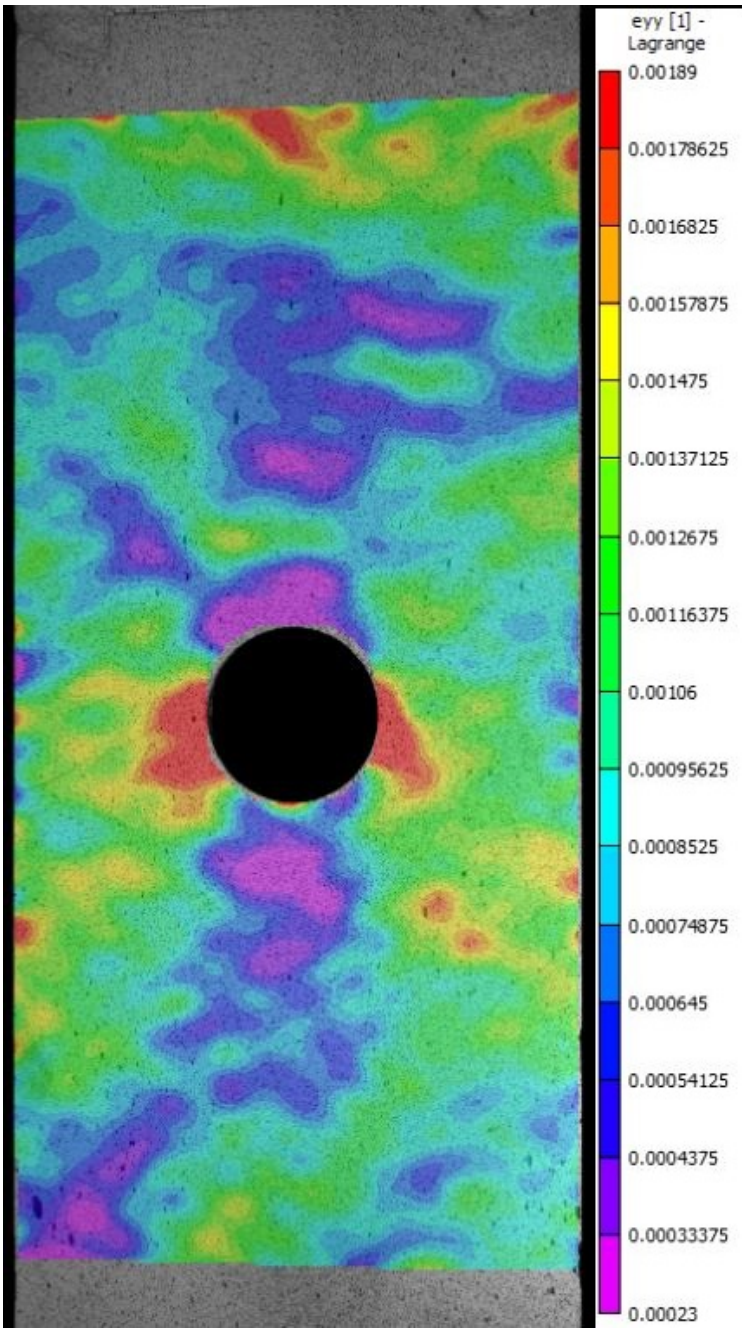

Figure A.62

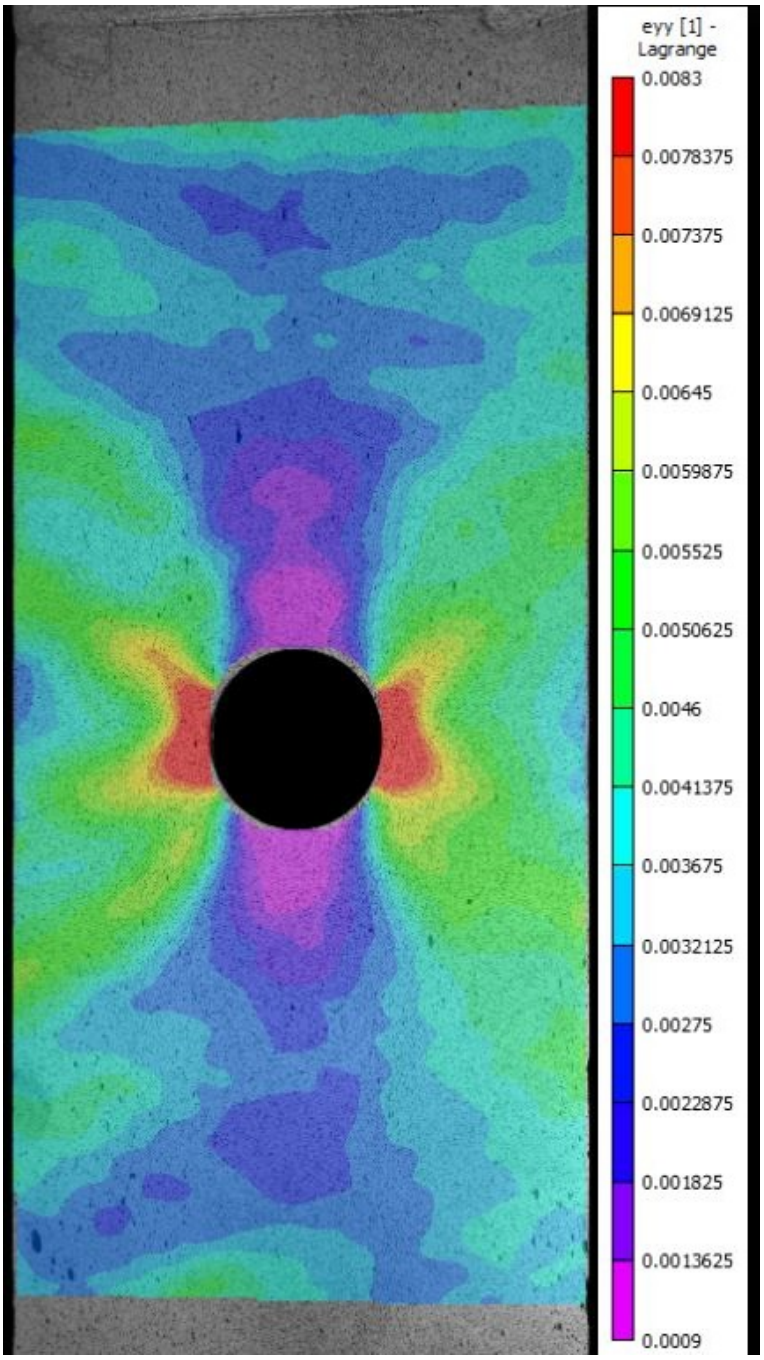

Figure A.63

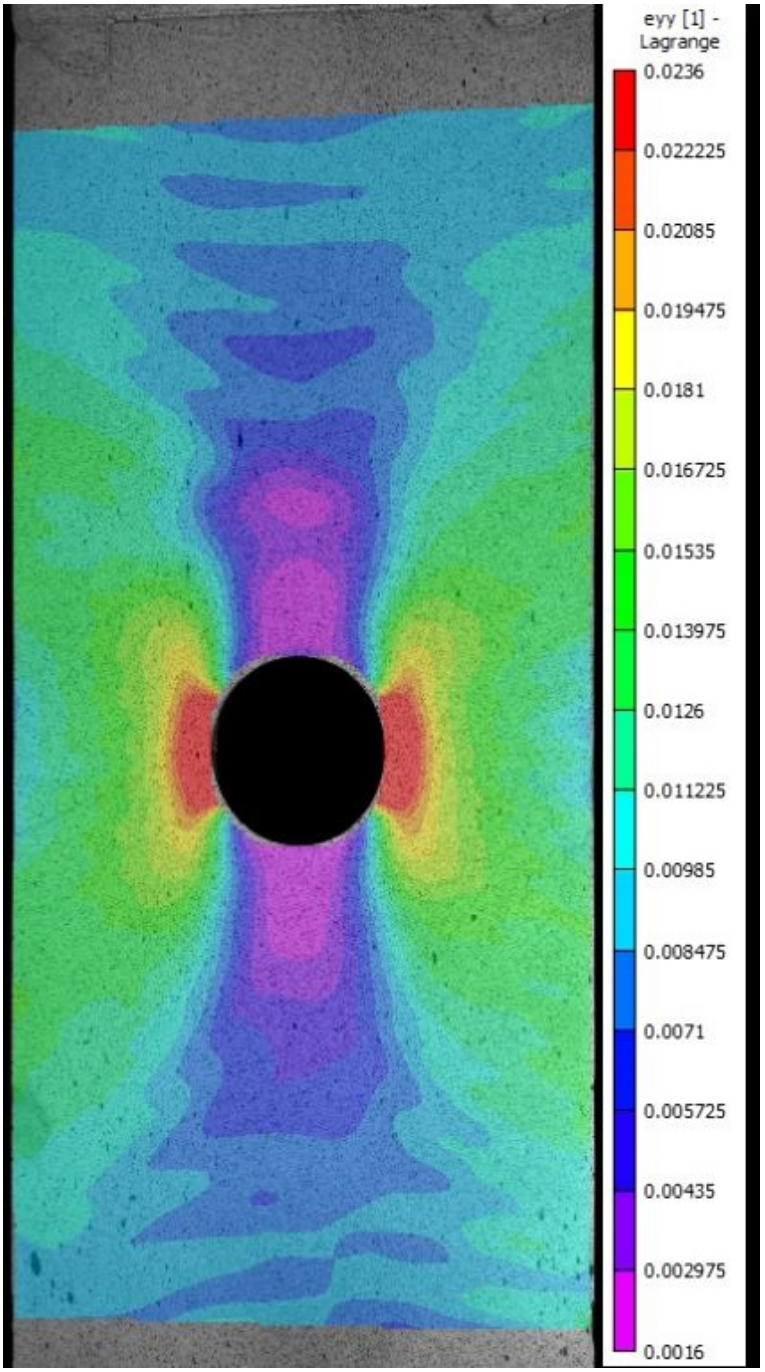

Figure A.64

B

Appendix B

In the first section the CLT is explained and in the second section the Airy stress function considering their mathematical overview.

B.1. Classical Laminate Theory(CLT)

The properties of plate stacked hybrid structure should be a function of the properties of the individual layer with their specific stacking sequence. This is the so called CLT theory. The following assumptions and restrictions are considered when using CLT.

- Displacements are continuous through the whole laminate.
- In-plane displacements **u** and **v** are linear function of the z-coordinate.
- straight lines perpindicular to the mid-surface remains perpendicular to that surface after deformation. This implies that transverse shear strain γ_{xz} and γ_{yz} are zero.
- stress-strain relations are linear.

Stress-Strain relations Since plates and sheets are considered with thickness much smaller than its lateral dimension, the laminate is assumed to be in a plane stress condition. That means out of plane stress σ_z, τ_{yz} and τ_{xz} are negligible in comparison to the in plane stresses. except at its edges. The compliance **S** of a single orthotropic layer with uni-direction of the fibers is as follow;

$$\mathbf{S} = \begin{bmatrix} \frac{1}{E_1} & \frac{-\nu_{21}}{E_2} & 0 \\ \frac{-\nu_{12}}{E_1} & \frac{1}{E_2} & 0 \\ 0 & 0 & \frac{1}{G_{xy}} \end{bmatrix} \tag{B.1}$$

For the isotropic metal layers of FML $E_1 = E_2$ and $\nu_{12} = \nu_{21}$ can be used. In order to get stiffness **Q** of a single layer the compliance **S** is inversed accordingly, this results in;

$$Q_{ij} = S_{ij}^{-1} = \begin{bmatrix} \frac{E_1}{1-\nu_{21}\nu_{12}} & \frac{\nu_{21}E_1}{1-\nu_{21}\nu_{12}} & 0 \\ \frac{\nu_{12}E_2}{1-\nu_{21}\nu_{12}} & \frac{E_2}{1-\nu_{21}\nu_{12}} & 0 \\ 0 & 0 & G_{xy} \end{bmatrix} \tag{B.2}$$

In The CLT the stiffness matrix Q of single layer is also called the reduced stiffness matrix. A this point the reduced stiffness matrix is valid for layer with uni-directional fibers in the x-direction. In order to get the reduced stiffness of a layer with fibers in θ-direction in the XY-plane, the transformation matrix T is introduced.

$$\mathbf{T} = \begin{bmatrix} m^2 & n^2 & 2mn \\ n^2 & m^2 & -2mn \\ -mn & mn & m^2 - n^2 \end{bmatrix} \tag{B.3}$$

In equation B.3, 'm' and 'n' stands for $cos(\theta)$ and $sin(\theta)$. The reduced stiffness matrix is then rotated according to equation B.4. The rotation angle θ coincides with fiber angle alignment.

$$\mathbf{Q}^{\theta} = \mathbf{T}^{-1} \begin{bmatrix} \frac{E_1}{1-\nu_{21}\nu_{12}} & \frac{\nu_{21}E_1}{1-\nu_{21}\nu_{12}} & 0 \\ \frac{\nu_{12}E_2}{1-\nu_{21}\nu_{12}} & \frac{E_2}{1-\nu_{21}\nu_{12}} & 0 \\ 0 & 0 & G_{xy} \end{bmatrix} \mathbf{T} \tag{B.4}$$

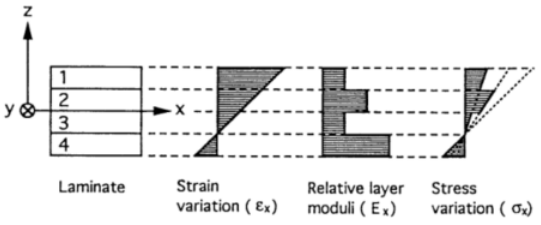

Figure B.1: Illustration of linear strain variation and discontinuous stress variation[12].

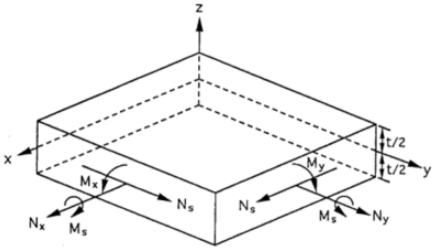

Figure B.2: A single layer with force and moment resultants[12].

Because of the orthotropic nature of the laminated structure the Young's moduli varies discontinuous from layer to layer, as a consequence the stress varies also discontinuous through the thickness of the laminate as shown in B.1. In order to get the stress-strain relation of a FML laminate, a close approximation can be made by integrating the stresses through the thickness of the FML laminate. Integration of the stresses results in resultant forces and moments as shown in equations B.5 and B.6 and figure B.2. Note that the forces and moment resultants are in units per width.

$$N_x^k = \int_{-h/2}^{h/2} \sigma_x dz \qquad M_x^k = \int_{-h/2}^{h/2} \sigma_x z dz$$

$$N_y^k = \int_{-h/2}^{h/2} \sigma_y dz \tag{B.5} \qquad M_y^k = \int_{-h/2}^{h/2} \sigma_y z dz \tag{B.6}$$

$$N_{xy}^k = \int_{-h/2}^{h/2} \tau_{xy} dz \qquad M_{xy}^k = \int_{-h/2}^{h/2} \tau_{xy} z dz$$

From the CLT assumptions the strains of a FML laminate is a superposition of the membrane strains and curvature. The overall laminate strains are equal to the mide-plane strains and are constant through the thickness of the laminate. The in-plane stresses are defined by Hooks Law and Kirchoffs pure bending assumptions as;

$$\begin{bmatrix} \sigma_x \\ \sigma_y \\ \tau_{xy} \end{bmatrix} = \begin{bmatrix} Q_{xx} & Q_{xy} & Q_{xs} \\ Q_{yx} & Q_{yy} & Q_{ys} \\ Q_{sx} & Q_{sy} & Q_{ss} \end{bmatrix} \begin{bmatrix} \epsilon_x^0 \\ \epsilon_y^0 \\ \gamma_s^0 \end{bmatrix} + \begin{bmatrix} Q_{xx} & Q_{xy} & Q_{xs} \\ Q_{yx} & Q_{yy} & Q_{ys} \\ Q_{sx} & Q_{sy} & Q_{ss} \end{bmatrix} \begin{bmatrix} z\kappa_x^0 \\ z\kappa_y^0 \\ z\kappa_s^0 \end{bmatrix} \tag{B.7}$$

Substituting equation B.7 into equation B.5 and B.6 results in;

$$\mathbf{N} = \left[\sum_{k=1}^{n} \mathbf{Q}^k \int_{z_{k-1}}^{z_k} dz\right] [\boldsymbol{\epsilon}^0] + \left[\sum_{k=1}^{n} \mathbf{Q}^k \int_{z_{k-1}}^{z_k} z dz\right] [\boldsymbol{\kappa}] = [\mathbf{A}] [\boldsymbol{\epsilon}^0] + [\mathbf{B}] [\boldsymbol{\kappa}] \tag{B.8}$$

$$\mathbf{M} = \left[\sum_{k=1}^{n} \mathbf{Q}^k \int_{z_{k-1}}^{z_k} z dz\right] [\boldsymbol{\epsilon}^0] + \left[\sum_{k=1}^{n} \mathbf{Q}^k \int_{z_{k-1}}^{z_k} z^2 dz\right] [\boldsymbol{\kappa}] = [\mathbf{B}] [\boldsymbol{\epsilon}^0] + [\mathbf{D}] [\boldsymbol{\kappa}] \tag{B.9}$$

Where

$$\begin{aligned} A_{ij} &= \sum_{k=1}^{n} Q_{ij}^k (z_k - z_{k-1}) \\ B_{ij} &= \tfrac{1}{2} \sum_{k=1}^{n} Q_{ij}^k (z_k^2 - z_{k-1}^2) \\ D_{ij} &= \tfrac{1}{3} \sum_{k=1}^{n} Q_{ij}^k (z_k^3 - z_{k-1}^3) \end{aligned} \tag{B.10}$$

with i,j = x,y,s. z_k and z_{k-1} are upper and bottom surface of the k^{th} layer. This is visualised in figure B.3. Matrix A and D are the in-plane stiffness and bending stiffness of the laminate respectively. Matrix B is coupling stiffness matrix which couples the in-plane with the outer-plane properties.

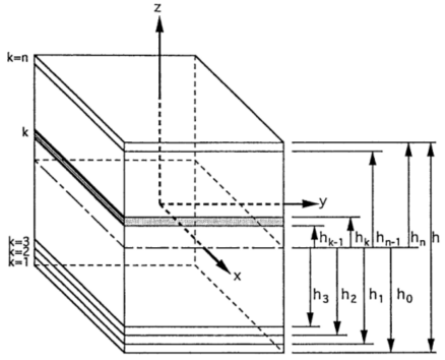

Figure B.3: A multi layer stacked laminate[12].

$$\begin{aligned} A_{ij} &= \sum_{k=1}^{n} Q_{ij}^k (z_k - z_{k-1}) \\ B_{ij} &= \tfrac{1}{2} \sum_{k=1}^{n} Q_{ij}^k (z_k^2 - z_{k-1}^2) \\ D_{ij} &= \tfrac{1}{3} \sum_{k=1}^{n} Q_{ij}^k (z_k^3 - z_{k-1}^3) \end{aligned} \tag{B.11}$$

The constitutive relation of a orthotropic thin plate is defined by equation B.12 and B.13;

$$\begin{bmatrix} N \\ M \end{bmatrix} = \begin{bmatrix} A & B \\ B & D \end{bmatrix} = \begin{bmatrix} \epsilon^0 \\ \kappa \end{bmatrix} \tag{B.12}$$

$$\begin{bmatrix} \epsilon^0 \\ \kappa \end{bmatrix} = \begin{bmatrix} a & b \\ b & d \end{bmatrix} = \begin{bmatrix} N \\ M \end{bmatrix} \tag{B.13}$$

B.2. Airy's stress function

Assuming plane strain condition, $\varepsilon_{13} = \varepsilon_{23} = \varepsilon_{33} = 0$. From Hook's Law the constitutive relations are given as:

$$\varepsilon_{11} = \frac{1}{E}\left[\sigma_{11} - \nu\left(\sigma_{22} + \sigma_{33}\right)\right] \tag{B.14}$$

$$\varepsilon_{22} = \frac{1}{E}\left[\sigma_{22} - \nu\left(\sigma_{11} + \sigma_{33}\right)\right] \tag{B.15}$$

$$\varepsilon_{33} = \frac{1}{E}\left[\sigma_{33} - \nu\left(\sigma_{11} + \sigma_{22}\right)\right] = 0 \tag{B.16}$$

$$\sigma_{33} = \nu\left(\sigma_{22} + \sigma_{33}\right) \tag{B.17}$$

$$2\varepsilon_{12} = \frac{1+\nu}{2}\sigma_{12} \tag{B.18}$$

σ_{13} and σ_{13} is set to be zero assuming ε_{13} and ε_{13} are zero.

Substituting equation B.17 into equation B.14 and B.15. Afterward differentiate the new ε_{11} w.r.t. y twice and differentiate the new ε_{22} w.r.t. x twice;

$$\varepsilon_{11,22} = \frac{1}{E}\left(1-\nu^2\right)\sigma_{11,22} - (1+\nu)\,\nu\sigma_{22,22} \tag{B.19}$$

$$\varepsilon_{22,11} = \frac{1}{E}\left(1-\nu^2\right)\sigma_{22,11} - (1+\nu)\,\nu\sigma_{11,11} \tag{B.20}$$

$$2\varepsilon_{12,12} = \frac{2\sigma_{12,12}\,(1+\nu)}{2} = \gamma_{12,12} \tag{B.21}$$

Substitute equation B.19 B.20 B.21 into the strain-compatibility equation B.34. The following derivation is made;

$$(1-\nu)\left[\sigma_{11,22} + \sigma_{22,11}\right] - \nu\left[\sigma_{22,22} + \sigma_{11,11}\right] - 2\sigma_{12,12} = 0 \tag{B.22}$$

Equation B.32 and B.33 are force equilibrium equations including the influence of the body forces. Assuming and elastic solid with no body force, differentiate both equilibrium equations w.r.t. x and y respectively. the following equations are made;

$$\sigma_{11,11} = -\sigma_{12,12} \tag{B.23}$$

$$\sigma_{22,22} = -\sigma_{12,12} \tag{B.24}$$

$$2\sigma_{12,12} = -\sigma_{11,11} - \sigma_{22,22} \tag{B.25}$$

Substitute equation B.25 into equation B.22, after simplifying the stress-compatibility equation is made;

$$\sigma_{11,22} + \sigma_{22,11} + \sigma_{11,11} + \sigma_{22,22} = 0 \tag{B.26}$$

Defining the 2D Laplacian operator as $\nabla^2 = \frac{\partial^2}{\partial x^2} + \frac{\partial^2}{\partial y^2}$, equation B.26 becomes;

$$\nabla^2 (\sigma_{11} + \sigma_{22}) = 0 \tag{B.27}$$

The relation between the Caushy-stresses en the Airy-stress function is defined as;

$$\begin{aligned} \sigma_{11} &= U_{,22} \\ \sigma_{22} &= U_{,11} \\ \sigma_{12} &= -U_{,12} \end{aligned} \tag{B.28}$$

Taking into account equation B.25 and the relation between the Caushy- and Airy's stress function, The stress-compatibility equation B.26 can be redefined as;

$$U_{,1111} + U_{,2222} + 2U_{,1122} = 0 \tag{B.29}$$

When defining the biharmonic operator as, $\nabla^4 = \left(\nabla^2\right)^2$, How the conditions of the Airy's stress function need to be satisfied, becomes more clear.

$$\left(\nabla^2\right)^2 U\left(x,y\right) = \left(\frac{\partial^2}{\partial x^2} + \frac{\partial^2}{\partial y^2}\right)\left(\frac{\partial^2}{\partial x^2} + \frac{\partial^2}{\partial y^2}\right) U\left(x,y\right) = \frac{\partial^4 U(x,y)}{\partial x^4} + 2\frac{\partial x^2 \partial y^2 U(x,y)}{\partial x^4} + \frac{\partial^4 U(x,y)}{\partial y^4} = 0 \tag{B.30}$$

$$\nabla^4 U\left(x,y\right) = 0 \tag{B.31}$$

B.3. Lekhnitskii Theory; Predicting stress on a round boundary.

In this section a possible solution for an infinite plate with a circular hole and a first order edge loading is explained. In principle we assume that there is a plate without a disturbance(e.g. a hole). The stress field induced by loading the plate is called a homogeneous solution of the particular differential equation B.40. The second step is solving of the stress field or the change of the stress field when somewhere in that field is a disturbance(e.g. a hole).
In essence the strain-compatibility equation B.34 is a differential equation. For the problem of interest, there is the need of finding an equation which is a solution to this differential equation.
Assuming plane-strain condition, a derivation of the strain-compatibility equation can be made in terms of stresses.
Using the relation between Caushy- and Airy-stresses, the stress-compatibility, which is a second order differential equation can made into fourth order biharmonic differential equation. For these sets of problems closed form analytical solution are still a luxury in Solid Mechanics, but there is the possibility of near field solutions which can be more than satisfactory.

Basic Equations
Considering an elastic body under plane stress conditions with free body diagram given in figure B.4, the force equilibrium equations are given as;

$$\frac{\partial \sigma_x}{\partial x} + \frac{\partial \tau_{xy}}{\partial y} + X = 0 \tag{B.32}$$

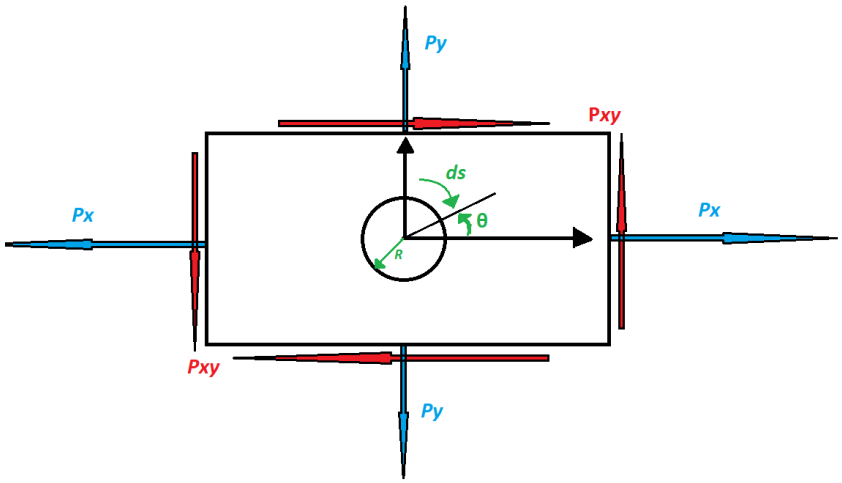

Figure B.4: A multi layer stacked laminate.

$$\frac{\partial \tau_{xy}}{\partial x} + \frac{\partial \sigma_y}{\partial y} + Y = 0 \tag{B.33}$$

The strain-compatibility equation is given by;

$$\frac{\partial^2 \epsilon_x}{\partial y^2} + \frac{\partial^2 \epsilon_y}{\partial x^2} - \frac{\partial^2 \gamma_{xy}}{\partial x \partial y} = 0 \tag{B.34}$$

The applied stress on the contour of interest(e.g. hole) are given by;

$$\sigma_x cos(\theta) + \tau_{xy} cos(\theta) = X(\theta)(MPa) \tag{B.35}$$
$$\sigma_y cos(\theta) + \tau_{xy} cos(\theta) = Y(\theta)(MPa) \tag{B.36}$$

And the Biharmonic equation that need to be satisfied is given by,

$$\nabla^4 U(x,y) = 0 \tag{B.37}$$

The Solution of the basic plate problem under plane stress/strain conditions

In this section the foundation are layed for a possible function which could satisfy the Airy's stress function.

Substituting the Caushy-stresses in equation B.28 as function of the Airy's stresses, into the constitutive relations given by equation B.14 and B.15, While taking into account the plane stress condition, then for an orthothropic unbalanced laminate, the compatibility in term of the Airy's stress function is defined as;

$$a_{22}\frac{\partial^4 U}{\partial x^4} + (2a_{12} + a_{66})\frac{\partial^4 U}{\partial x^2 \partial y^2} - 2a_{16}\frac{\partial^U}{\partial x \partial y^3} + 2a_{26}\frac{\partial^4 U}{\partial x^3 \partial y} + a_{11}\frac{\partial^4 U}{\partial y^4} = 0 \tag{B.38}$$

Or one could also simply use equation B.13, and not taking into consideration the coupling effects of matrix B and assuming no out-of-plane deformations, The in-plane strains are define by;

$$\begin{aligned}\varepsilon_{11} &= a_{11}\sigma_{11} + a_{12}\sigma_{22} + a_{16}\sigma_{12}\\ \varepsilon_{22} &= a_{21}\sigma_{11} + a_{22}\sigma_{22} + a_{26}\sigma_{12}\\ \gamma_{12} &= a_{61}\sigma_{11} + a_{62}\sigma_{22} + a_{66}\sigma_{12}\end{aligned} \tag{B.39}$$

Using equation B.28, Substituting the Airy's stress function into equation B.39, Differentiate ε_{11} and ε_{22} w.r.t. y and x twice repectively, and differentiate γ_{12} w.r.t. x and y. Afterward substitute the calculated $\frac{\partial^2\varepsilon_{11}}{\partial y^4}$, $\frac{\partial^2\varepsilon_{22}}{\partial x^4}$ and $\frac{\partial^2\gamma_{12}}{\partial x\partial y}$ into the strain-compatibility equation B.34. The same equation B.38 can be deduced.

For a Balanced laminate the terms a_{16} and a_{26} are zero. Equation B.38 can be rewritten as equation B.40. The 'r' stands for the directionality and the 'a' stand for the angularity, not to be confused with the compliance terms a_{ii}.

$$r^2U_{,xxxx} + 2\alpha U_{,xxyy} + U_{,yyyy} = 0 \tag{B.40}$$

$$\begin{aligned} r &= \sqrt{\tfrac{a_{22}}{a_{11}}}\\ \alpha &= \tfrac{1}{2}\tfrac{2a_{12}+a_{66}}{a_{11}}\end{aligned} \tag{B.41}$$

Note that for isotropic material $r = 1$ and $\alpha = 2$. Thus solving stress/strain problems for isotropic materials, the function U(x,y) becomes in principal independent of the material properties a_{ii}, if the boundary is given in forces/stresses.

Using the laplacian transformation of $s^nH(s) = \frac{\partial^n h(x)}{\partial x^n}$, and introducing a new function F(z) and substituting into equation B.40, where $U(x,y) = F(z)$. Decomposing this new partial differential equation into differential operator product, afterward rewrite the product terms as vector inner products, it becomes clear that $z = x + sy$.
Lekhnitskii[13] proved on the basis of energy consideration that equation B.38 when written in laplacian form, it can not have real roots.
Since there is a need for a non trivial solution, where $F''''(z) \neq 0$, The characteristic equation is obtained as;

$$r^2 + 2\alpha s^2 + s^4 = 0 \tag{B.42}$$

Solving the characteristic equation for the laplacian variable s, four complex root are to be found;

$$\begin{aligned} s_1 &= +\sqrt{\tfrac{r-a}{2}} + i\sqrt{\tfrac{r+a}{2}}\\ s_2 &= -\sqrt{\tfrac{r-a}{2}} + i\sqrt{\tfrac{r+a}{2}}\\ s_3 &= +\sqrt{\tfrac{r-a}{2}} - i\sqrt{\tfrac{r+a}{2}}\\ s_4 &= -\sqrt{\tfrac{r-a}{2}} - i\sqrt{\tfrac{r+a}{2}}\end{aligned} \tag{B.43}$$

The complex variable $z = x + s_k y$, with $k = 1,2,3,4$ in the complex function F(z). Thus, the general solution of the partial differential equation is;

$$U(x,y) = F_1(z_1) + F_2(z_2) + F_3(z_3) + F_4(z_4) \tag{B.44}$$

Complex functions are convenient for solving differential equations as shown in the work of Muskhelishvili, Kolosov, and Lekhnitskii[13]. Analyzing the roots, it can be seen that when the directionality 'r' is greater than the angularity 'α', $s_3 = \bar{s_1}$ and $s_4 = \bar{s_2}$.
When the angularity 'α' is greater than or equal to the directionality 'r', $s_4 = \bar{s_1}$ and $s_3 = \bar{s_2}$.
Since the stress and strain are a real thing to be calculated, the function U(x,y) must be real. Hence the function of U(x,y) must always consist of two pairs of complex conjugates. The general solution becomes;

$$U(x,y) = F_1(z_1) + F_2(z_2) + \overline{F_1(z_1)} + \overline{F_2(z_2)} \tag{B.45}$$

Or,

$$U(x,y) = 2\Re e\left[F_1(z_1) + F_2(z_2)\right] \tag{B.46}$$

With the function given by equation B.47 the stresses at the edge of the hole can be calculated.

$$\begin{gathered}\sigma_{xx} = 2\Re e\left[s_1^2\phi_1'(z_1) + s_2^2\phi_2'(z_2)\right] \\ \tau_{xy} = 2\Re e\left[s_1\phi_1'(z_1) + s_2\phi_2'(z_2)\right] \\ \sigma_{yy} = 2\Re e\left[\phi_1'(z_1) + \phi_2'(z_2)\right]\end{gathered} \tag{B.47}$$

In equation B.47 $\phi_k(z_k) = \frac{dF_k(z_k)}{dz_k}$. And the displacements can be calculated, thus also the strains.

$$\begin{gathered}u = 2\Re e\left[u_1\phi_1(z_1) + u_2\phi_2(z_2)\right] + C_1 y + C_2 \\ v = 2\Re e\left[v_1\phi_1(z_1) + v_2\phi_2(z_2)\right] + C_3 x + C_4\end{gathered} \tag{B.48}$$

In equation B.48 $u_k = a_{11}s_k^2 + a_{12}$ and $v_k s_k = a_{11}s_k^2 + a_{12}$. u_k and v_k should not be confused with the displacement term u and v.

Using the fact that every analytical function can be written as a series in positive and negative Laurent powers.

$$\begin{gathered}\phi_k'(z_k) = \Sigma_{n=-\infty}^{+\infty}\left[g_n^k z_k^n\right] \\ \phi_k'(z_k) = ... + g_2^k z_k^2 + g_1^k z_k + g_0^k + g_{-1}^k z_k^{-1} + g_{-2}^k z_k^{-2} + ...\end{gathered} \tag{B.49}$$

Since the stresses are finite, only g_0^k and the terms with negative power has meaning. After integration an equation for ϕ_k can be deduced.

$$\begin{gathered}\phi_k(z_k) = g_0^k z_k + g_{-1}^k ln(z_k) - g_{-2}^k z_k^{-1} - \tfrac{1}{2}g_{-3}^k z_k^{-2} - \tfrac{1}{3}g_{-4}^k z_k^{-3} - ... \\ \phi_k(z_k) = h_k z_k + A_k ln(z_k) + \Sigma_{n=1}^{\infty} g_n^k z_k^{-n} + const.\end{gathered} \tag{B.50}$$

In equation B.50 the terms h_k and A_k represents the homogeneous stress field and the effect of the force resultant respectively. The disturbance field is given by g_k^n. The next thing to do is to solve the coefficient which are included in the Laurent power series. When ϕ_k is known, then the stresses and strains on the boundary of the hole can be calculated. This method in the elastic regime can be used in order to calculate Stress Concentration Factors(SCF) on the contour of the center hole. Next step is to solve the problem in plastic regime. Next section will deal with that.

Solving plasticity in the complex domain.
In this section plasticity beyond the elastic limit will be considered. Some problems and possible solution for predicting the plastic zone near a hole are discussed.

An ideal plastic material is defined by, that it cannot endure any stresses beyond the elastic yield limit. For these materials there is a defined function $F(\sigma_{ij}) = 0$, which is also used as a critical condition for plasticity. Using non-ideal plastic materials, when the plasticity occurs, it is known that some hardening takes place. This could be predicted by the Ramberg-Osgood equation. Do note that unlike in the elastic regime, in the plastic regime load history must be taken into account.

The total deformation increments is given by adding the elastic- and the plastic strain increments given by;

$$d\varepsilon_{ij} = d\varepsilon^{el}_{ij} + d\varepsilon^{pl}_{ij} \tag{B.51}$$

Assumption is made that the elastic deformation in plastic range are still related to the stresses by Hook's law given as;

$$\varepsilon^{el}_{ij} = \frac{1}{2G}\left[\sigma_{ij} - \delta_{ij}\sigma\right] + [1-2\nu]\,\delta_{ij}\frac{\sigma}{E} \tag{B.52}$$

In equation B.52, E, G and ν are the Young's modulus, shear modulus and the poison ratio. δ_{ij} is the Kronecker delta and σ is the average stress. When the problem regarding ideally plastic material, only if the boundary conditions are given in stresses(contour of interest), only those problems can be statistically defined. Then, the problem consist only of three equation. These are two equilibrium equation plus the critical condition when plasticity starts.

The condition of plasticity for an anisotropic(metallic) body is given as;

$$f(\Sigma_2, \Sigma_3) \tag{B.53}$$

In which, Σ_2 and Σ_3 are the second and third invariants respectively. These invariants are from the deviatoric stress(also known as the volumetric stress).

When $\varepsilon_{33} = 0$, then stress in the z-direction(out of plane) is given by equation B.17. Usually it is possible to limit the analysis of a statistically defined elasto-plastic problems, to the assumption of in-compressibility of material in order to determine the deformations. In-compressibility means $\nu = \frac{1}{2}$. Then the third invariant of the deviatoric stress $\Sigma_3 = 0$, and the plasticity conditions given in equation B.53 reduces to,

$$\left[\sigma_{xx} - \sigma_{yy}\right]^2 + 4\tau^2_{xy} = 4k^2 \tag{B.54}$$

Savin states that according to the theory of greatest tangential stresses, $k = \frac{\sigma_{yield}}{2}$, And according to the theory of octahedral tangential stresses, $k = \frac{\sigma_{yield}}{\sqrt{3}}$. Where σ_{yield} is the yield point while the material is under uni-axial tension.

The equation system that is needed for elasto-plastic analysis is given in appendix C.

It is assumed that the stress function U_1 in the plastic regime satisfies some hyperbolic function. In this hyperbolic function the boundary conditions and the plasticity conditions are included. Solving

these equations for the given elasto-plastic regime, boils down to determining of a biharmonic function U_2 outside of some unknown contour L, which surrounds the hole. U_1 and U_2 are related to each other by conditions that are valid on contour L. The difficulty of this problem is the determination of contour L, which separates the 'plastic' zone from the elastic zone. If this contour is known, the determination of function U_2 is equivalent to the solution of the elastic problem from section B.3. Savin[13] states that, if the stress components in the plastic range is known, then the solution of the stated problem can be found in some cases. Displacements that are made previously with only taken elasticity into account, plays the part of the initial Caushy stresses needed for the equation system C.3. The displacements in the plastic range is solved after the stresses are determined. The range of applied stresses need to be defined, otherwise local relaxation of the material while operating in the plastic range makes the equations B.54 and C.3 invalid. The boundary of the elastic zone will be determined by an ellipse. The boundary of this ellipse will be contour L.

As mentioned in section 2.1, at initialization of the plasticity at the hole edge to some extent of the applied load, the plastic zone does not encompasse the hole completely. The plastic zone grows at the hole edge as can be seen in figure 2.13, 2.14 and C.4. In order to use the Lekhnitskii model for the purpose of the MSc thesis, the contour L must be defined as shown in figure C.4. The growth of the plastic zone can then be related to the change of the peak stress profile.

C

theory of plasticity

In this section the system equation for a plane state deformation will be given for an ideally plastic body.

The increment of the plastic deformation given in equation B.51 is defined by the flow rule given as

$$d\varepsilon_{ij}^{pl} = d\lambda \frac{\partial F}{\partial \sigma_{ij}} \tag{C.1}$$

where $d\lambda$ is the constant that refers to the hardening rule. and $F(\sigma_{ij})$ is the yield function that characterizes the the relation between the plastic strain and the stress state. Materials such as metals has hardening potential which is defined by the characteristic curve beyond the elastic limit. For these materials the yield surface expands according to the history of the loading. In equation C.1, when $F(\sigma ij) < 0$ then $d\lambda = 0$. This mean that when there is no plasticity, there is no hardening taking place inside the material. Thus there is no expansion of the yield surface.

Using equation B.51, B.52 and C.1 together with the deduced plasticity condition given in equation B.54, the system equation for an ideal plastic body under plane state deformation is then given by,

$$\begin{gathered} \frac{\partial \sigma_x}{\partial x} + \frac{\partial \tau_{xy}}{\partial y} = 0 \qquad \frac{\partial \tau_{xy}}{\partial x} + \frac{\partial \sigma_y}{\partial y} = 0 \\ \left(\sigma_x - \sigma_y\right)^2 + 4\tau_{xy}^2 = 4k^2 \quad k = constant \end{gathered} \tag{C.2}$$

$$\begin{gathered} \frac{2d\varepsilon_x^{pl}}{\sigma_x - \sigma_y} = \frac{2d\varepsilon_y^{pl}}{\sigma_y - \sigma_x} = \frac{d\varepsilon_{xy}^{pl}}{2\tau_{xy}} \\ \varepsilon_x = \varepsilon_x^{pl} + \frac{\sigma_x - \sigma_y}{4G} \quad \varepsilon_y = \varepsilon_y^{pl} + \frac{\sigma_y - \sigma_x}{4G} \qquad \varepsilon_{xy} = \varepsilon_{xy}^{pl} + \frac{\tau_{xy}}{G} \\ \varepsilon_x = \frac{\partial u_x}{\partial x} \qquad \varepsilon_y = \frac{\partial u_y}{\partial y} \qquad \varepsilon_{xy} = \frac{1}{2}\left(\frac{\partial u_x}{\partial y} + \frac{\partial u_y}{\partial x}\right) \end{gathered} \tag{C.3}$$

The normal and the tangential forces on the contour of the hole is given as,

$$\sigma_n = f_1(s,\mu) \quad \tau_{nt} = f_2(s,\mu) \tag{C.4}$$

where 's' is the contour parameter and μ is the stress parameter. The stresses in the elastic regime at infinity is given as,

$$\sigma_x^\infty = P_1(x,y,\mu) \quad \sigma_y^\infty = P_2(x,y,\mu) \quad \tau_{xy}^\infty = -P_3(x,y,\mu) \tag{C.5}$$

$U_1(x,y,\mu)$ is the biharmonic equation used in the plastic range. U_1 is then given as a function,

$$f\left(x,y,\frac{\partial^2 U_1}{\partial x^2},\frac{\partial^2 U_1}{\partial y^2},\frac{\partial^2 U_1}{\partial x \partial y},\frac{\partial U_1}{\partial x},\frac{\partial U_1}{\partial y}\right) = 0 \tag{C.6}$$

This function satisfies the boundary conditions and the condition of plasticity given in equation B.54.

In principle, it can be assumed that during plasticity, there exist two type of disturbances. the first disturbance is the round hole. The second disturbance is the plastic zone with a shape that is defined by contour L. The second disturbance encompasses the first disturbance. Then two biharmonic equations are implemented, one inside of contour L(e.g. U_1) and one outside of contour L(e.g. U_2). In order to have valid compatibility between the plastic region(inside of contour L) and elastic region(outside of contour L) the following conditions must need to be satisfied on contour L,

$$\frac{\partial^2 U_1}{\partial x^2} = \frac{\partial^2 U_2}{\partial x^2}, \quad \frac{\partial^2 U_1}{\partial y^2} = \frac{\partial^2 U_2}{\partial y^2}, \quad \frac{\partial^2 U_1}{\partial x \partial y} = \frac{\partial^2 U_2}{\partial x \partial y} \tag{C.7}$$

For coordinates x and y at infinity, the stresses are defined as,

$$\frac{\partial^2 U_2}{\partial x^2} = P_2(x,y,\mu), \quad \frac{\partial^2 U_2}{\partial y^2} = P_1(x,y,\mu), \quad \frac{\partial^2 U_2}{\partial x \partial y} = P_3(x,y,\mu) \tag{C.8}$$

The main difficulty is to determine contour L. When Contour L is known then determining U_2 will be done in the same matter as in the elastic problem explained in section B.3.

The figures below gives a illustration of solutions made for some cases, by Muskhelishvili, Savin and others[13].

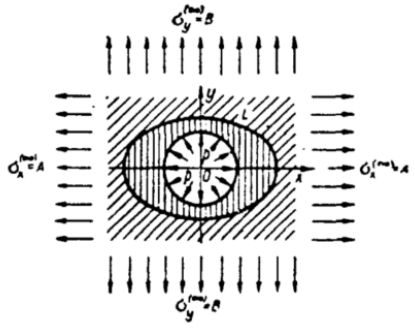

Figure C.1: Illustration of a plastic zone under normal pressure on the contour of a hole in an infinite plate[13].

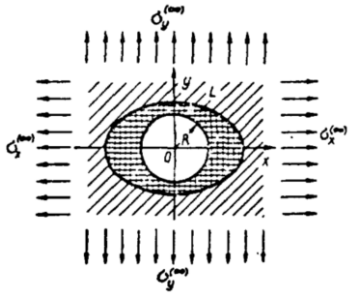

Figure C.2: Illustration of a plastic zone arround the contour of a hole in an infinite plate under biaxial tension[13].

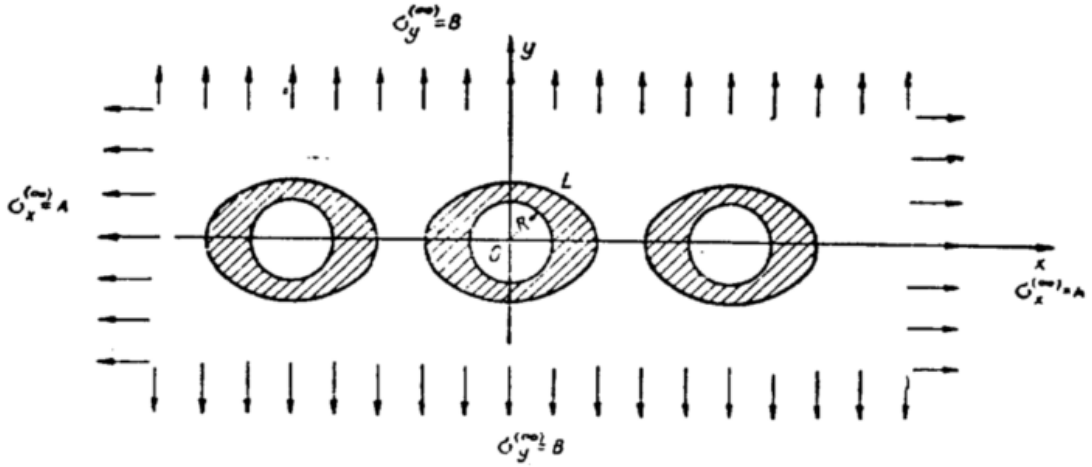

Figure C.3: Illustration of plate with infiinite row of identical holes[13].

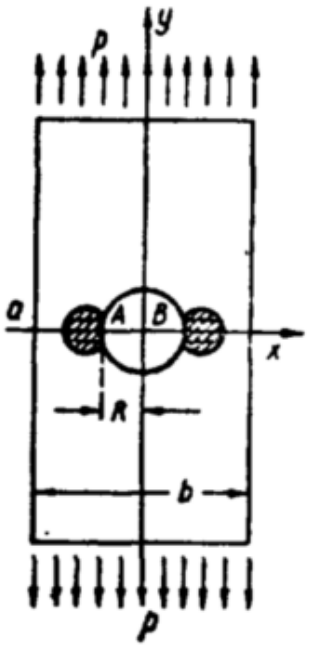

Figure C.4: Illustration of an infinite plate under uni-axial tension with small plastic zones at the edges of the hole[13].

D

Variation and implimentation of the Methods

D.1. Saff's method

Saff[11] presented a couple of graphs, which is made using his method in the presented paper. Two of his graphs are presented below including with the results made using the method discussed in this research.

These graphs are figure D.1 and D.2. The net-section stress gradient for a blunt notch in an isotropic infinite plate is presented in figure D.1. As suggested by Saff[11], The gross SCF_{tg} is calculated using equation 3.11. Saff's parameters are determined as,

$$\alpha = 1 \tag{D.1}$$

$$\beta = SCFtg - 1 = 2.0633 \tag{D.2}$$

$$\gamma = C\frac{SCFtg}{SCtg - 1} = 3.2167 \tag{D.3}$$

$$C = \left(\frac{1}{2} + \frac{5}{3} + \sqrt{\frac{b}{a}}\right) = 2.1666 \tag{D.4}$$

The net-section stress gradient for a blunt notch in an isotropic infinite plate are determined by substituting the paramaters α, β, γ into equation 3.17. The results are presented as graph 'fig78 SDF C=koiter' in figure D.6. 'SDF' stands for Saff's Deduced Formula presented as equation,

$$\beta = \frac{1 - SCF_t\left(1 - \frac{2a}{W}\right)}{\left(\frac{2a}{W} - 1\right) + \frac{2b^2}{Wa(1-\gamma)}\left[\left(1 - \frac{a}{b}^2 + \frac{a}{b}\frac{2W}{2a}\right)^{1-\gamma} - 1\right]} \tag{D.5}$$

Equation D.5 is made by integrating equation D.7, which defines equilibrium between the load applied and the net-section load in the elastic regime known as condition 3 in section 3.3. For the isotropic infinite case, Saff's method correlates well with the Timoshenko-Goodier equation,

$$\frac{\sigma_y(x,y=0)}{S_{gross}} = 1 + \frac{1}{2}\left(\frac{r}{x}\right)^2 + \frac{3}{2}\left(\frac{r}{x}\right)^4 \tag{D.6}$$

Saff's method for the infinite isotropic case results in a bit greater stress concentration than $SCFtg = 3$ at the edge of the hole due to using equation 3.12. Although equation 3.12 is a quite good fit, this could result in a different BNS than would be expected when using finite or orthotropic cases. Saff suggests that for the circular hole in an infinite isotropic plate $C = 3.25$ was found to give a good correlation with the classical stress gradient solution, but this is not case seeing the graph in figure D.1. Furthermore, the stress concentration factor at the edge of the hole in saff's method are for both values of C, greater than the solution of Timoshenko-Goodier with a stress concentration of 3.

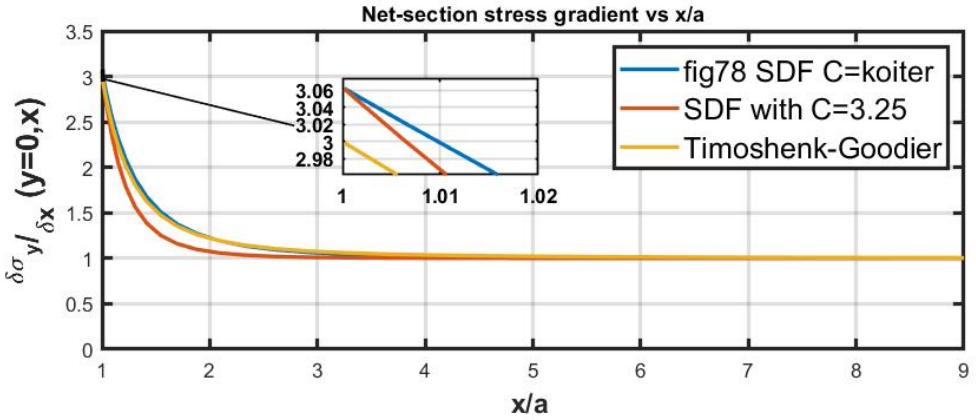

Figure D.1: Net-section stress gradient for an isotropic infinite case. Saff vs. Timoshenko-Goodier

The net-section stress gradient for a blunt notch in an isotropic finite plate is presented in figure D.2. In figure D.2 the two graphs in black are taken from the research of saff[11], for D/W-ratio of 0.3 and 0.5. Since this research only considers round holes/blunt notches in a plate, assumption are made for integrating equation D.7.

$$1 = \frac{2a}{W}\int_1^{\frac{W}{2a}} \alpha + \beta\left(1 + \frac{x-a}{\rho}\right)^{-\gamma} d\left(\frac{x}{a}\right) \tag{D.7}$$

For a blunt notch, $\rho = \frac{b^2}{a}$, with $a = b$. Therefore equation D.7 can be written as,

$$1 = \frac{2a}{W}\int_1^{\frac{W}{2a}} \alpha + \beta\left(\frac{x}{a}\right)^{-\gamma} d\left(\frac{x}{a}\right) \tag{D.8}$$

$$1 = \frac{2a}{W}\left(\left[\left(SCF_t - \beta\right)\left(\frac{W}{2a}\right) + \frac{\beta}{1-\gamma}\left(\frac{W}{2a}\right)^{1-\gamma}\right] - \left[\left(SCF_t - \beta\right) + \frac{\beta}{1-\gamma}\right]\right) \tag{D.9}$$

$$1 = SCF_t\left(1 - \frac{2a}{W}\right) + \beta\left(-1 + \frac{1}{1-\gamma}\left(\frac{W}{2a}\right)^{-\gamma} + \left(\frac{2a}{W}\right) - \frac{1}{1-\gamma}\left(\frac{2a}{W}\right)\right) \tag{D.10}$$

$$\beta = \frac{1 - SCF_t\left(1 - \frac{2a}{W}\right)}{\frac{1}{1-\gamma}\left[\left(\frac{W}{2a}\right)^{-\gamma} - \frac{2a}{W}\right] + \frac{2a}{W} - 1} \tag{D.11}$$

Equation D.11 is used to make the graphs in figure D.2 with 'ODF' in their name. Figure D.2 present the variation on the net-section stress gradient made for different values of C.
C=koiter means that the parameter C is determined using equation 3.21.

For a D/W-ratio of 0.3, although there are some minor variations using different values for C, The graphs correlates well with the black graph 'Saff fig81 D/W=0.3. interestingly, using Saff's Deduced Formula(SDF) of equation D.5 with parameter C determined by equation 3.21, which includes the finite width correction factor of koiter, has a quite large divergence in comparison with the Own Deduced Formula(ODF). For a D/W-ratio of 0.3, the best results are made by using the SDF with a C-value of 2.2 and an ODF with a C-value of 2.0. This could mean that SDF equation D.5 and ODF equation D.11 are not similar for blunt notches.

For a D/W-ratio of 0.5, the SDF equation D.5 would not converge for any β in terms of γ implenting the third condition from section 3.3. Therefore, the two graphs that are made for a D/W-ratio of 0.5, are determined using the ODF equation D.11. Again calculating the parameter C with equation 3.21 gives a quite large divergence from the black graph for D/W-ratio of 0.5. In figure D.2, parameter C=original, means that the finite width correction of Koiter is used.

All the graphs starts on a similar point at the edge of the hole, that is because the same SCF_{tg} is defined for them all. Furthermore, only in this section, the SCF_{tg} is used for defining the stress gradient at the edge of the hole. In all other section of this research paper, the net-section SCF_{tn} is used for further calculations.

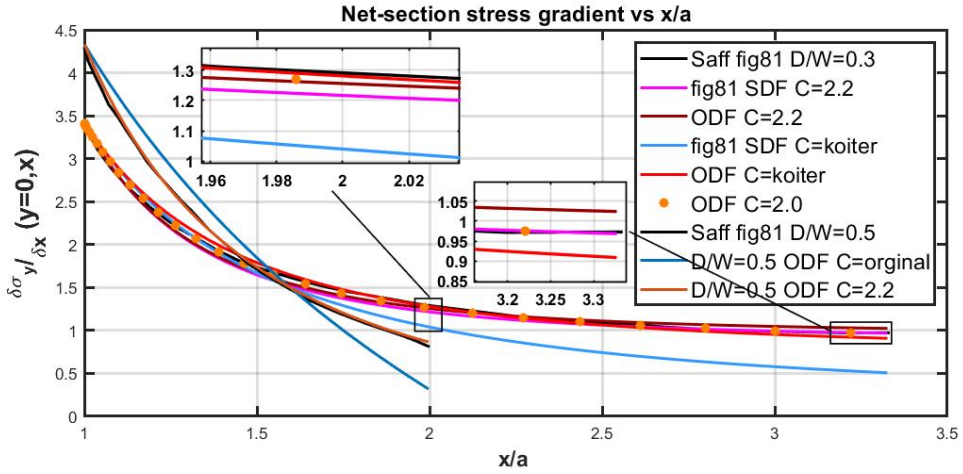

Figure D.2: Net-section stress gradient for an isotropic infinite case. WD2 wd3333

D.2. Saff's method results for the samples

A specific input for the calculation of the BNS in a glare plate is the net-section stress gradient. Section 3.3 explains how to create the net-section stress gradient. Following the 3rd condition results in an equation that consists of β in terms of γ. These are equations D.5 and D.11. The results of these equations are presented as SDF and ODF in the figures presented in this section with a variation on parameter C.
Furthermore, results of two other methods are shown, namely the 'Guessing Alpha and the Numerical methods. The numerical method is explained in section 3.3. The Guessing Alpha method is a previous iteration used before implementing the numerical method, though the results are almost similar for all four glare samples used in this research.

The Guessing Alpha method explained
The Guessing Alpha method, as name suggests, is based on that in order to run the matlab algorithm, The parameter alpha need to be guessed. This is done by analyzing the stress en strain results of the DIC-experiments. The stress and strain results of the DIC-experiments are shown in appendix A. The parameter α is determined only from the elastic increments of the DIC-experiments. The parameter C is determined using the finite width correction of Koiter. Afterward, the β and γ is calculated using equation 3.18 and 3.19. Since the parameters α, β and γ are known, the net-section stress gradient can be determined using equation 3.17. This would result in a close estimation for the stresses en strain at the edge of the hole and at the edge of the plate compared to the DIC results. But there would be no equilibrium between the applied and the net-section load. Therefore another parameter C1 is introduced. The values of C1 for the four samples can be seen in table D.1.
Since the parameter C, which includes the finite width correction of Koiter, is known, C1 can not deviate much more. The parameter C defines the exponent γ in equation 3.17. Since the net-section stress gradient is depended on the exponent γ in equation 3.17, it is choesen to multiply C1 with γ as in,

$$\frac{\sigma_y(x, y=0)}{S_{nom}} = \alpha + \beta \left[1 + \frac{x-a}{\rho}\right]^{-\gamma C1} \tag{D.12}$$

Thus a vector C1 is created around the parameter C. In order to determine C1, the net-section load and the applied load are compared only under elastic conditions.
The stress and strain results of equation 3.17 is integrated over the net-section in order to determine the net-section load. The net-section load is then compared with the applied load, which normally results into a non-equilibrium. Then, for each load increment, equation D.12 with all the values in vector C1 is used, to calculate the net-section load and compare it with the applied load. The value of C1 is chosen, when the net-section load converges with the applied load.

D.2.1. Results of the discussed methods

In this section the results of the methods in the previous section are discussed. These were the SDF, ODF, Guessing Alpha and the Numerical method. The SDF and The ODF are done using the finite width correction of koiter and with the finite witdth correction determined using the Numerical method. For each sample used in this research, there are five graphs. These are the net-section stress gradient, the net-section or nominal stress concentration factor SCFt, The r1 graphs and the two load equilibrium graphs. More details on the value of the parameters used are given in table D.1.

Sample D45 with D/W=0.3
The results for Sample D45 are shown in figure D.3 till D.7. Because the stress values at the edge of the hole are governed by the SCF_t, all the net-section stress gradient starts at the same point shown in figure D.3. Because of change in the parameters, they have different gradient and different values at the edge of the plate. Interestingly, the SDF and the ODF functions gives similar results. This should also be the case, since the ODF function should be a simpler form of the SDF function. The SDF function would be applicable to round and ellipse notches, while the ODF function is limited to round notches. Furthermore, the finite width correction of Koiter is determined as 1.81, which is quite close to the 1.84 determined for the Numerical method.

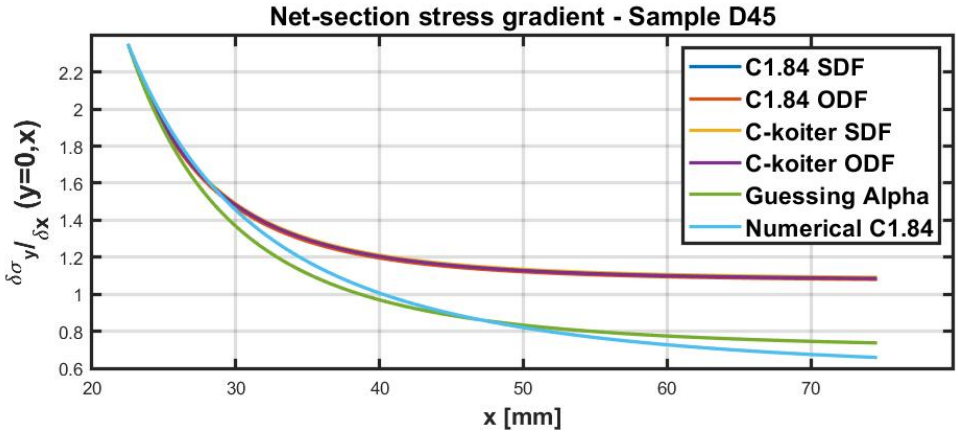

Figure D.3: Net-section stress gradient for sample D45.

The SCF_t as function of the applied load is presented in figure D.4. In the elastic regime, the SCF_t is constant. Thou, it should be possible to observe small changes, when there is a change in sample geometry due to contraction of the plate. But this is not taken into account. All calculations are done using the nominal width of the glare plate. There is a gradual change when at higher loads, plasticity is induced at the edge of the hole. All the methods shows a sharp decrease and afterward a gradual increase during the first part of the plastic regime.
Although at different absolute values, all methods shows a similar trend. Analyzing the net section stress gradient, the results of the SCF_t as function of the gross stress S_g was expected.
Though the mid-section stress would be a derived by a multiplication factor(net-section stress gradient) on the nominal stress, caused by a discontinuity in a FML plate like a blunt notch, the applied load must be equal to the net-section load. Therefore, since the $SCF_t > 1$ at the edge of hole, the net-section stress gradient must reaches a value < 1 close to the edge of the plate. The only exception would be that the discontinuity is very small compared to the width of the Glare plate due to the load distribution from the far field through the net-section geometry of the plate.
The net-section stress gradient of the ODF and SDF methods are all > 1 close to the edge of the plate as can be seen in figure D.3. These net-section stress gradients will result in that even in the elastic regime there is no load equilibrium between the applied and the net-section load.

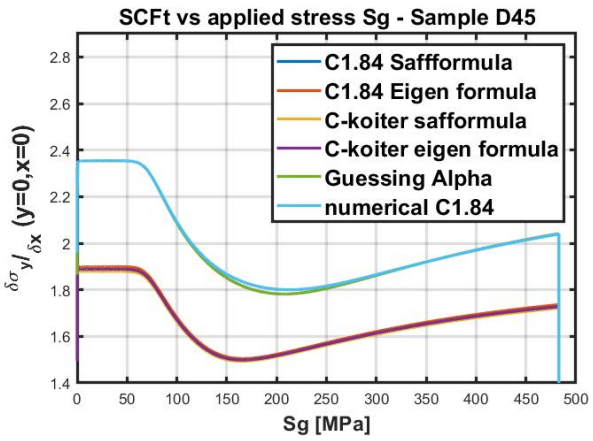

Figure D.4: The SCF_t at the edge of the hole for the methods used.

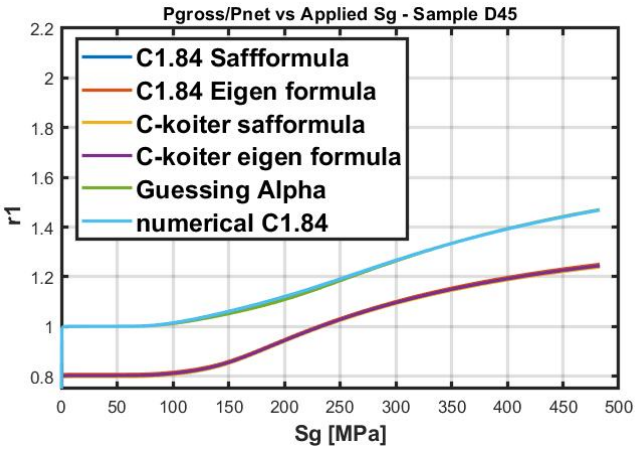

Figure D.5: The r1 factor for the methods used.

The r1 graphs in figure D.5 is best explained through figure 2.8. Above the onset of plasticity, The imaginary strain energy defined by the elastic modulus and the applied deformation, is set equal to the actual strain energy defined by the $\sigma'\varepsilon$-curve of the FML.
Assuming that Neuber's Postulate[2] is correct and applicable, the stress on the Yield Strips can be determined in the plastic regime. Consequently, that would imply that there is no load equilibrium between the applied load and the net-section load anymore. In order to have load equilibrium the factor r1 is introduced.

$$r1 = \frac{P_{gross}}{P_{net}} \tag{D.13}$$

The factor r1 is multiplied with the net-section load P_{net} in order to enforce load equilibrium between the applied and the net-section load in the plastic regime.
Since there is no load equilibrium between the net-section load P_{net} and the applied P_{gross} in the elastic regime due to the chosen net-section stress gradient using the ODF and SDF methods, the mechanism of the factor r1 in the MATLAB model is also introduced in the elastic regime. Therefore the SCF_t at the edge of the hole as function of the applied S_g is lower compared to the Guessing Alpha and Numerical method.
In the elastic regime r1 must always be $r1 = 1$ as presented by the results of the Guessing alpha and the Numerical method.

The load equilibrium for the method discussed are presented in figure D.6 and D.7. In figure D.6 are the results of the SDF and ODF method stacked on top of each other. This is the same for the load equilibrium of the Guessing Alpha and the Numerical methods presented in figure D.7.
The MLP and Pnetel are the applied gross load and the elastic net-section load from the Matlab model respectively. These graphs should always coincide as can be seen from the results of the Guessing Alpha and the Numerical methods. The Pnetel in the elastic regime can be considered as the real elastic net section load, and it can be considered as the imaginary load in the plastic regime.
The Pnetplb is the plastic load before the r1 factor is applied, and the Pnetpla is the plastic load after the r1 factor is applied. Since there is a load inequality in the elastic regime using the SDF and the ODF method, the r1 factor is activated by the model in order to enforce the load equilibrium. Thus the r1 factor is activated and will be determined to have a value of $r1 < 1$. The Difference in gradient or the observable small horizontal shift of the graphs in figure D.4 and D.5 is due to the difference in the change of the area between the Pnetplb and MLP, when comparing the load equilibrium results of the methods presented in figure D.6 and D.7.

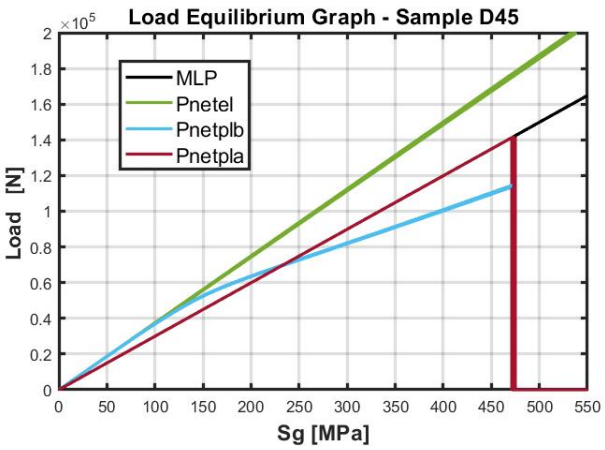

Figure D.6: Load equilibrium of the SDF and ODF method.

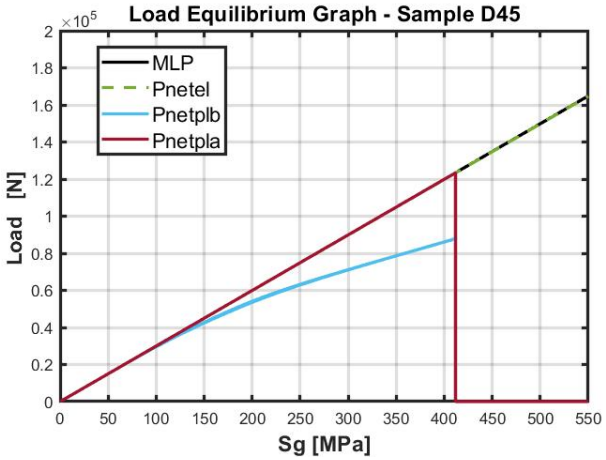

Figure D.7: Load equilibrium of the Guessing Alpha and Numerical method.

The other samples can be interpreted in the same manner as sample D45. Considering how the methods discussed are implemented, the major differences between the results of the samples and the methods used seems to be influenced by the parameter C. A greater value for C leads to a sharper net-section stress gradient. because the parameter C determined by the finite width correction factor decreases with increasing D/W-ratio, resulting in a decrease in value of γ due to compliance with condition 2 in section 3.3. The parameter C1 is introduced in the Guessing Alpha method and implemented as in equation D.12 in order to have sharp decrease of the net-section stress gradient near the hole edge.
The parameter γ increases for increasing D/W-ratio using the SDF and ODF method. Overall the net-section stress gradient must decrease with an increase of D/W-ratio. Therefore the Guessing Alpha method and the Numerical method are considered much better. And because the values determined for the parameters are much more agreeable, although the negative values for α using the Numerical method is questionable. The parameters determined for the method used are presented in table D.1.

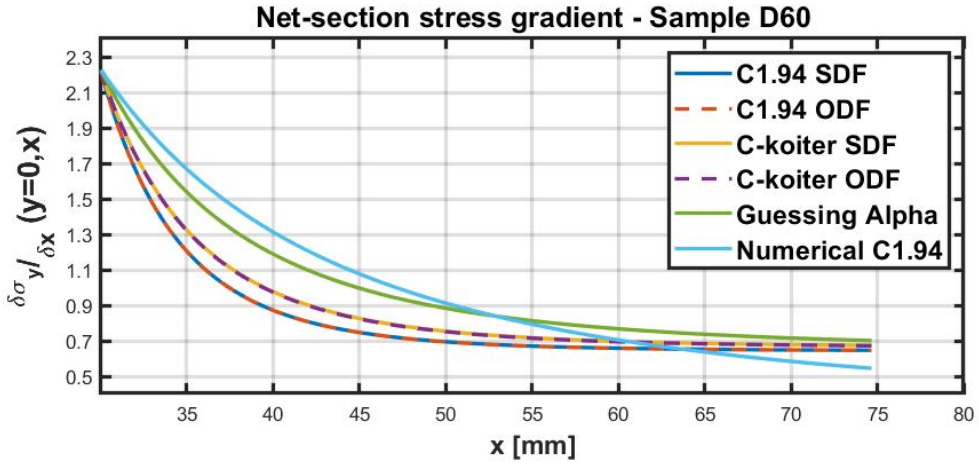

Figure D.8: Net-section stress gradient for sample D60.

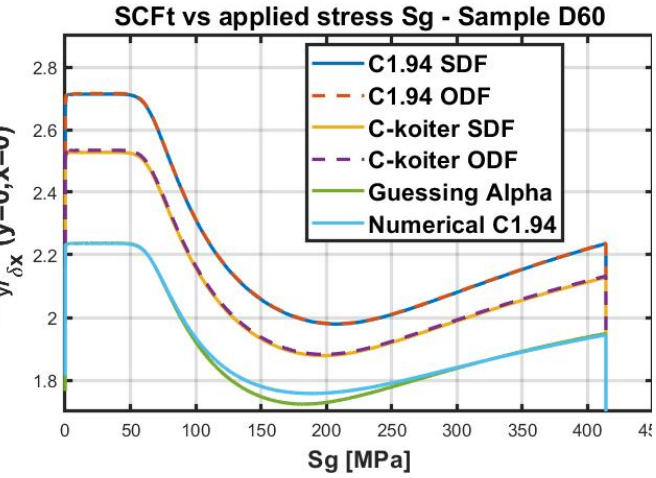

Figure D.9: The SCF_t at the edge of the hole for the methods used.

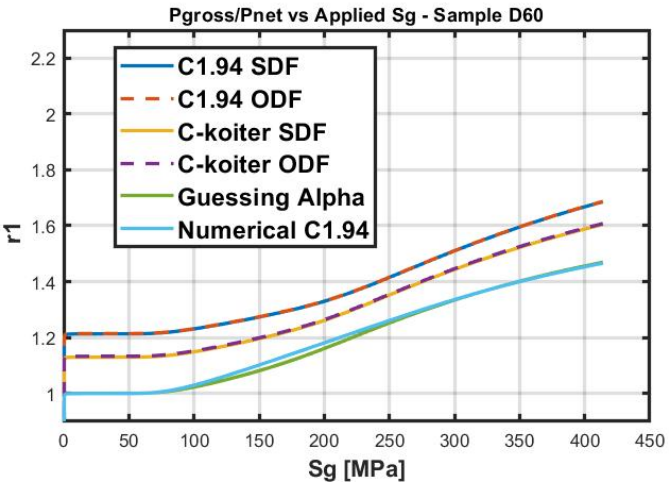

Figure D.10: The r1 factor for the methods used.

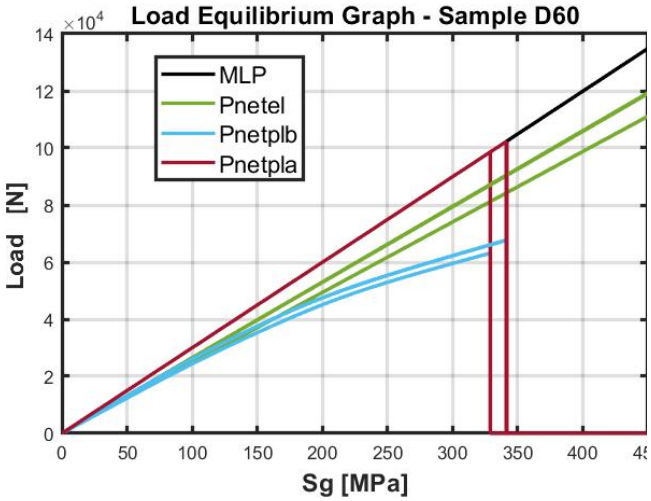

Figure D.11: Load equilibrium of the SDF and ODF method.

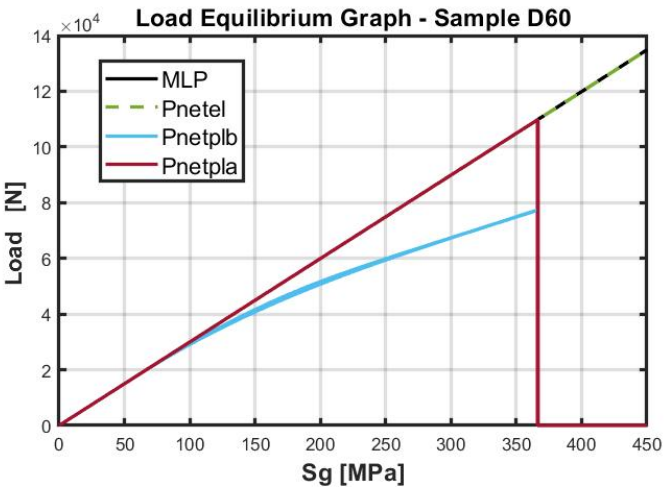

Figure D.12: Load equilibrium of the Guessing Alpha and Numerical method.

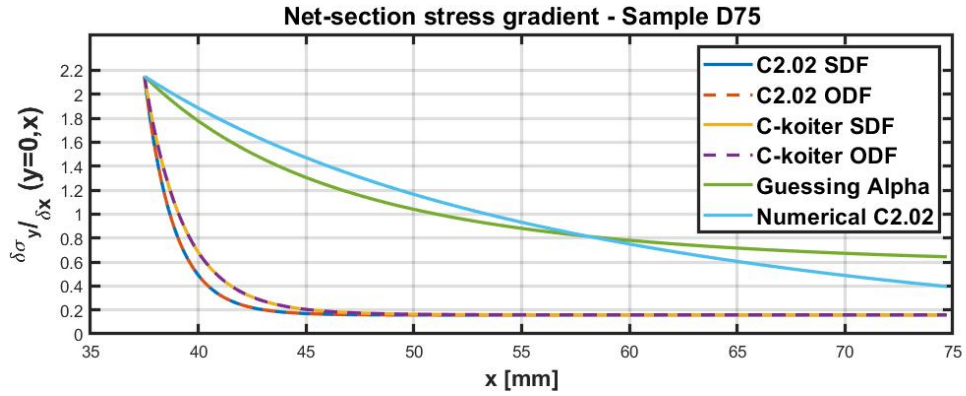

Figure D.13: Net-section stress gradient for sample D75.

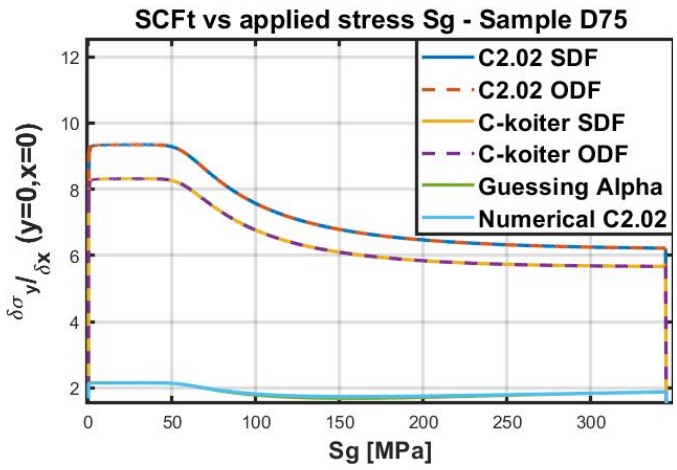

Figure D.14: The SCF_t at the edge of the hole for the methods used.

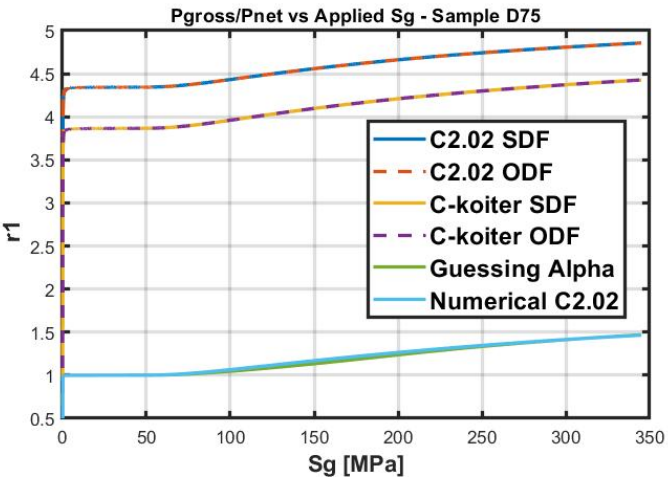

Figure D.15: The r1 factor for the methods used.

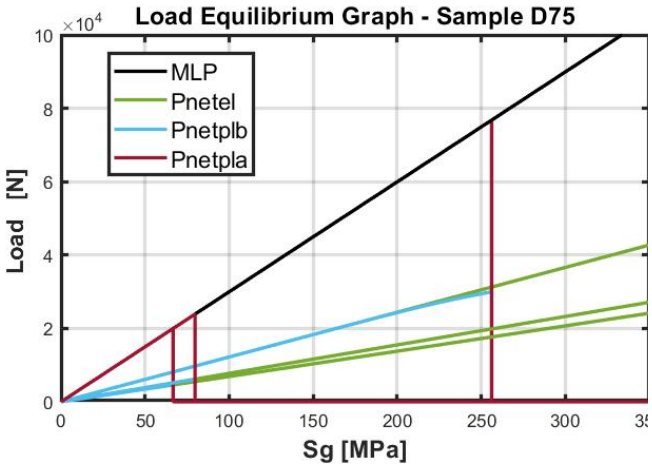

Figure D.16: Load equilibrium of the SDF and ODF method.

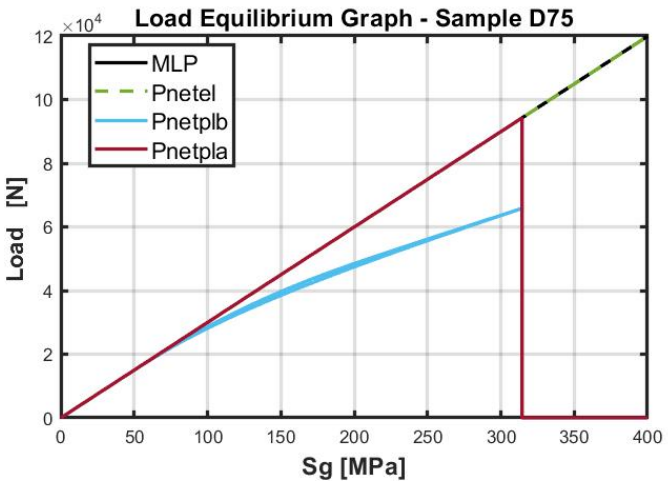

Figure D.17: Load equilibrium of the Guessing Alpha and Numerical method.

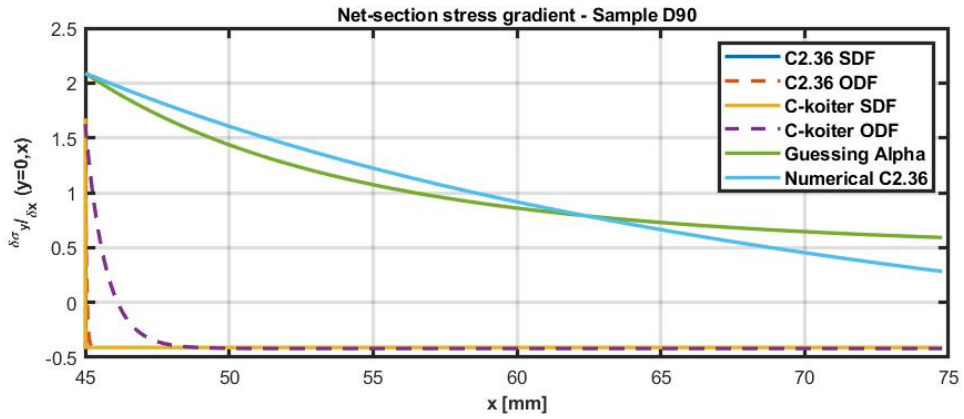

Figure D.18: Net-section stress gradient for sample D90.

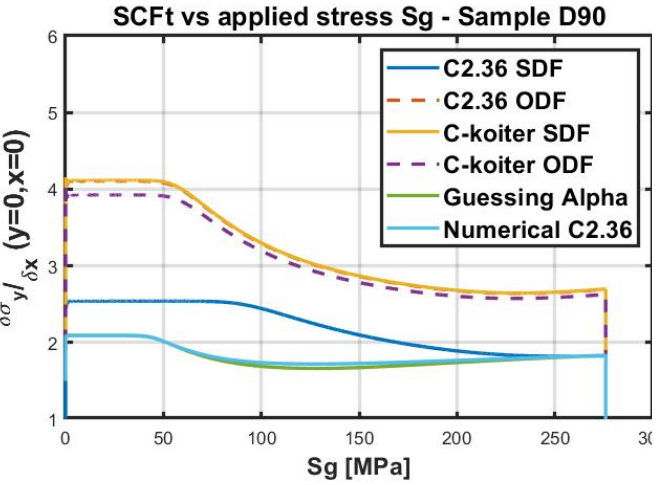

Figure D.19: The SCF_t at the edge of the hole for the methods used.

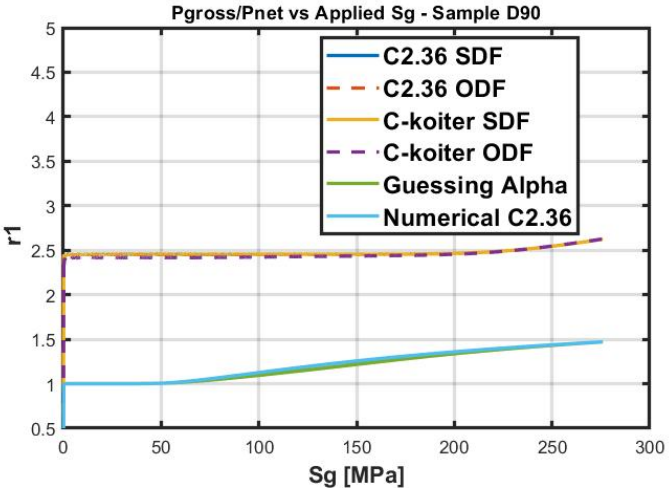

Figure D.20: The r1 factor for the methods used.

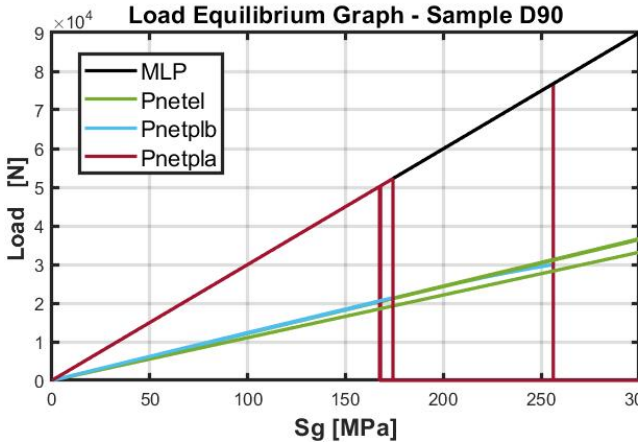

Figure D.21: Load equilibrium of the SDF and ODF method.

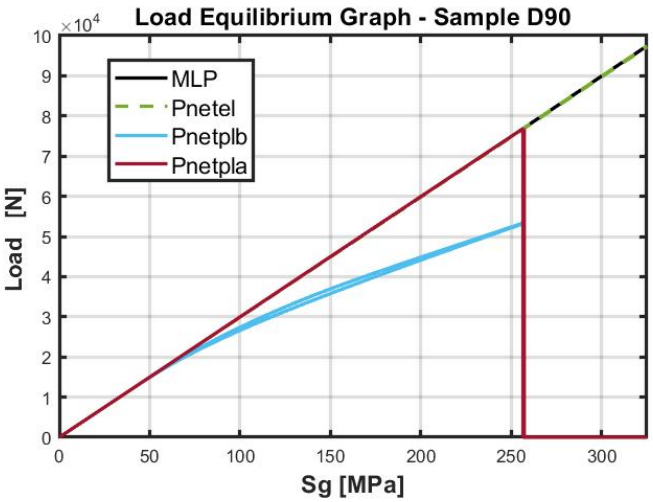

Figure D.22: Load equilibrium of the Guessing Alpha and Numerical method.

		α	β	γ	C	BNS	C1
D45	SDF	1.076	1.277	4.023	1.84	675.40	
	ODF	1.071	1.282	4.042	1.84	673.38	
	SDF	1.080	1.272	3.947	1.81	678.42	
	ODF	1.075	1.278	3.968	1.81	676.13	
	Guessing Alpha method	0.7	1.652	2.581	1.81	588.08	1.22
	Numerical method	0.560	1.792	2.415	1.84	588.42	
D60	SDF	0.644	1.592	6.730	1.94	548.31	
	ODF	0.644	1.592	6.735	1.94	548.09	
	SDF	0.666	1.570	5.608	1.67	569.44	
	ODF	0.664	1.572	5.624	1.67	568.59	
	Guessing Alpha method	0.65	1.586	2.366	1.67	610.39	1.580
	Numerical method	0.292	1.944	2.231	1.94	611.12	
D75	SDF	0.157	1.994	27.72	2.02	133.4	
	ODF	-	-	-	-	-	
	SDF	0.159	1.991	20.74	1.53	159.47	
	ODF	-	-	-	-	-	
	Guessing Alpha method	0.55	1.601	2.058	1.53	628.84	2.00
	Numerical method	-0.378	2.529	1.718	2.02	628.92	
D90	SDF	-0.410	2.090	8.856e6	2.36	640.42	
	ODF	-0.411	2.85	1.047e3	2.36	419.75	
	SDF	-0.410	2.089	1.943e4	1.37	418.56	
	ODF	-0.420	2.045	64.12	1.37	635.60	
	Guessing Alpha method	0.45	1.640	1.746	1.37	642.93	2.76
	Numerical method	-1.527	3.617	1.364	2.36	641.28	

Table D.1: The values of the parameters determined for the methods discussed.

Bibliography

[1] J. Schijve. *Fatigue of Structures and Materials*. Springer, 2009.

[2] R. Alderliesten. *Fatigue and Fracture of Fibre Metal Laminates*. Springer, 2017.

[3] T.J. De Vries. Blunt and sharp notch behavior of glare laminate, April 2001.

[4] A. Vlot and J.W. Gunnink. *Fibre Metal Laminate: An introduction*. Springer, 2011.

[5] (Restricted)R. Alderliesten. Theory to calculate the blunt notch strength of isotropic ductile materials, 2019.

[6] R. Rodi. The residual strength failure sequence in fibre metal laminates. TuDelft Repository, March 2012.

[7] A. Hassani and R.T. Faal. Dugdale's model for platic zone size of interacting crack under antiplane deformation. *Elsevier*, 2016.

[8] G.L.G. Gonzales, L. D. Rodrigues, and J.L.F. Freire. Accurate measurements of high strain gradients near notches using a feature-based dic algorithm. *Journal of Mechanics Engineering and Automation*, 7, 2017.

[9] J. Schwinn, E. Breitbarth, T. Beumler, and G. Requena. Blunt notch strength of aa2024 3-3/2-0.4 fiber metal laminate under biaxial tensile loading. *metals*, 2019.

[10] S. Pourhassan, P.J. Tavares, and P.M.G.P. Moreira. Material properties of 2024-t3 alclad and 2124-t851 aluminium alloys using 2d and 3d digital image correlation techniques. *Procedia Structural Integrity*, 5, 2017.

[11] C.R. Saff, D.M. Harmon, and Dr. C.T. Sun. Durability of continuous fiber reinforced metal matrix composites, Oktober 1987.

[12] I.M. Daniel and O. Ishai. *Engineering Mechanics of Composite Materials*. Oxford University Press,Inc, New York, 2nd edition, 2006.

[13] G.N. Savin. Stress distribution around holes. IEEE, November 1970. NASA TECHNICAL TRANSLATION:Raspredeleniye Napryazheniy Okolo Otversitiy, 'Naukova Dumbka' Press, Kiev, 1968.

[14] S. Timoshenko and J.N. Goodier. *Theory of Elasticity*. McGraw Hill, 1987.

[15] M. Hagenbeek, C. Van Hengel, O.J. Bosker, and C.A.J.R. Vermeeren. Static properties of fiber metal laminates. *Applied Composite Material*, 10, 2003.

[16] G.N. Savin. Stress concentration around holes. IEEE, 1961. NASA TECHNICAL TRANSLATION:Raspredeleniye Napryazheniy Okolo Otversitiy, 'Naukova Dumbka' Press, Kiev, 1968.

[17] D.K. Yi, Z.M. Xiao, and S.K. Tan. Elastic and plastic fracture analysis of a crack perpendicular to an interface between dissimilar materials, 2012.

[18] C.T. Sun and Z.H. Jin. *Fracture Mechanics*. Academic Press, 2012.

[19] S.G. Lekhnitskii. *Theory of Elasticity of an Anisotropic Elastic Body*. Holden Day Inc., San Francisco, CA, 1963.

[20] O. Bosker. Determining of optimum blunt notch strength specimen geometry. TuDelft Repository, 1998.

[21] R.C.J. Howland. On the stresses in the neighborhood of a circular hole in a strip under tension. *Philosophical Transaction of the Royal Society of London*, 229, 1930.

[22] A. Shimamoto and Susumu Takahashi. Plastic strain concentration by means of photoplasticity at a circular hole edge in a finite sheet subjected to uniaxial tension. *JSME International Journal*, 34, 1991.

[23] W. Ramberg and W.R. Osgood. Description of stress and strain curves by three parameters. IEEE, July 1943. Technical Note No. 902.

[24] F.B. Seely and J.O. Smith. *Advanced Mechanics of Materials.* Wiley and Sons, 1952.

[25] W.T. Koiter. Quarterly journal of applied mathematics. 15.

[26] W.D. Pilkey. *Peterson's Stress Concentration Factors.* Wiley and Sons, 1997.

[27] M.M.I. Hammouda and M.H. Seleem. Elastic- plastic analysis of notch root stress-strain and deformation fields under cyclic loading. In Mohamed F. HASSAN and Said M. MEGAHED, editors, *Current Advances in Mechanical Design and Production VII*, pages 215–222. Pergamon, Oxford, 2000.

[28] Alice M. Agogino. Notch Effects, Stress State, and Ductility. *Journal of Engineering Materials and Technology*, 100(4):348–355, 10 1978.